AD NUMBER
ADB020287
LIMITATION CHANGES

TO:

Approved for public release; distribution is unlimited.

FROM:

Distribution authorized to U.S. Gov't. agencies only; Test and Evaluation; JUN 1977. Other requests shall be referred to Air Force Weapons Laboratory, Kirtland AFB, NM 87117.

AUTHORITY

AFWL ltr, 7 Nov 1986

AD _Bo 20287_

AUTHORITY:
AFWL etc.
7 NOV 86

ADB020287

POSTTEST, TWO-DIMENSIONAL, FREE-FIELD CALCULATION OF HARD PAN I, EVENT 3: CALCULATION HPI-3.4

Eric H. Wang Civil Engineering Research Facility
University of New Mexico
Albuquerque, NM 87131

June 1977

Final Report

Distribution limited to US Government agencies only because of test
and evaluation of military systems/equipment (Jun 1977). Other
requests for this document must be referred to AFWL (DES), Kirtland
AFB, NM 87117.

D D C

AUG 2 1977

C
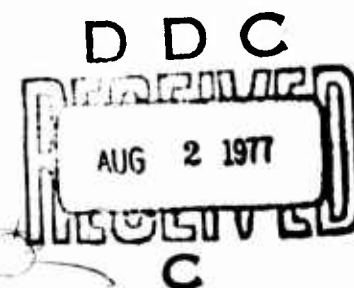
Prepared for
SPACE AND MISSILE SYSTEMS ORGANIZATION
P.O. Box 90009, WWPC
Los Angeles, CA 90009

AIR FORCE WEAPONS LABORATORY
Air Force Systems Command
Kirtland Air Force Base, NM 87117

AD No.
DDC FILE COPY

This final report was prepared by the Eric H. Wang Civil Engineering Research Facility, University of New Mexico, Albuquerque, New Mexico, under Contract F29601-76-C-0015, Job Order 133B1307 with the Air Force Weapons Laboratory, Kirtland Air Force Base, New Mexico. Lt James D. Shinn (DES) was the Laboratory Project Officer-in-Charge.

When US Government drawings, specifications, or other data are used for any purpose other than a definitely related Government procurement operation, the Government thereby incurs no responsibility nor any obligation whatsoever, and the fact that the Government may have formulated, furnished, or in any way supplied the said drawings, specifications, or other data, is not to be regarded by implication or otherwise, as in any manner licensing the holder or any other person or corporation, or conveying any rights or permission to manufacture, use, or sell any patented invention that may in any way be related thereto.

This technical report has been reviewed and is approved for publication.

JAMES D. SHINN
Lt, USAF
Project Officer

FOR THE COMMANDER

JAMES M. WARREN
Lt Colonel, USAF
Chief, Survivability Branch

FRANK J. LEECH
Lt Colonel, USAF
Chief, Civil Engineering Research
Division

DO NOT RETURN THIS COPY. RETAIN OR DESTROY.

REPORT DOCUMENTATION PAGE	READ INSTRUCTIONS BEFORE COMPLETING FORM

1. REPORT NUMBER AFWL-TR-77-63	2. GOVT ACCESSION NO.	3. RECIPIENT'S CATALOG NUMBER

4. TITLE (and Subtitle) POSTTEST, TWO-DIMENSIONAL, FREE-FIELD CALCULATION OF HARD PAN I, EVENT 3: CALCULATION HPI-3.4	5. TYPE OF REPORT & PERIOD COVERED Final Report
	6. PERFORMING ORG. REPORT NUMBER CERF-DP/EM-8

7. AUTHOR(s) Glenn T. Baird David K. Rudeen Cornelius J. Higgins	8. CONTRACT OR GRANT NUMBER(s) F29601-76-C-0015

9. PERFORMING ORGANIZATION NAME AND ADDRESS Eric H. Wang Civil Engineering Research Facility University of New Mexico, Box 25, University Sta. Albuquerque, NM 87131	10. PROGRAM ELEMENT, PROJECT, TASK AREA & WORK UNIT NUMBERS 11213F 133B1307

11. CONTROLLING OFFICE NAME AND ADDRESS Space and Missile Systems Organization P. O. Box 92960, WWPC Los Angeles, CA 90009	12. REPORT DATE June 1977
	13. NUMBER OF PAGES 76

14. MONITORING AGENCY NAME & ADDRESS(if different from Controlling Office) Air Force Weapons Laboratory (DES) Kirtland Air Force Base, NM 87117	15. SECURITY CLASS. (of this report) Unclassified
	15a. DECLASSIFICATION/DOWNGRADING SCHEDULE

16. DISTRIBUTION STATEMENT (of this Report)

Distribution limited to US Government agencies only because of test and evaluation of military systems/equipment (Jun 1977). Other requests for this document must be referred to AFWL (DES), Kirtland AFB, NM 87117.

17. DISTRIBUTION STATEMENT (of the abstract entered in Block 20, if different from Report)

18. SUPPLEMENTARY NOTES

19. KEY WORDS (Continue on reverse side if necessary and identify by block number)

HARD PAN
Wave propagation
Ground motions
TOODY II Code
Nuclear simulation

20. ABSTRACT (Continue on reverse side if necessary and identify by block number)

The results of the pretest calculations of HARD PAN I Event 3 were analyzed and compared with experimental data to evaluate the accuracy of the input (pressure functions, geology, material properties) and output (computed velocity waveforms). Seismic velocities for a recommended geology were developed from contours of experimental times-of-arrival of first motion and incorporated into new material properties as the initial loading and unloading slope of the hydrostat. Lock-up strain values and shear failure   (over)

DD FORM 1473 1 JAN 73   EDITION OF 1 NOV 65 IS OBSOLETE

ABSTRACT (cont'd)

envelopes were consistent with previous material properties and laboratory test results. The analysis indicated that the BLEST pressure function was satisfactorily modeled based on the impulse delivered to the soil. However, a new HEST pressure function which would accurately reflect the experimental pressure/time history was developed for the posttest calculations. Posttest calculation HPI-3.4 was performed with the new input and compared with experimental data. This comparison indicated fairly good agreement. Adjustment factors to modify the data for input to the Three-Dimensional, Structure/Media Interaction (SMI3D) Code were then recommended.

CONTENTS

ILLUSTRATIONS

TABLES

2

SECTION 1
INTRODUCTION

BACKGROUND

The results of an analysis of two pretest calculations of HARD PAN I, Event 3, HPI-3.1 and 3.2 (ref. 1) were presented at a meeting on 23 and 24 June 1976 at the Air Force Weapons Laboratory, with representatives from the Air Force Weapons Laboratory (AFWL), the Space and Missile Systems Organization (SAMSO), TRW Systems (TRW), the Waterways Experiment Station (WES), Weidlinger Associates, and the Civil Engineering Research Facility (CERF) in attendence. The purpose of this meeting was to review the analytical results and to establish the best available material properties, geology, and BLEST/HEST pressure functions for posttest calculations of HARD PAN I Event 3. The following is a summary of the conclusions and recommendations reached at the end of this two-day meeting:

(1) The BLEST pressure function is accurately modeled based on the limited number of experimental stress records.

(2) HEST pressure records indicate that the pressure/time history should be changed to accurately reflect the experimental data, and new HEST pressure equations should be developed.

(3) New material models and geology which would emphasize laboratory tests performed on undisturbed samples, field boring logs, seismic field investigations, and WES recommendations should be established.

These recommendations were incorporated into a posttest calculation designated HPI-3.3 (ref. 2). This calculation was then compared to the experimental data. Some of the calculated data correlated better, but overall quality did not significantly improve over the pretest predictions. CERF then undertook an analysis

---

1. Baird, Glenn T., Rudeen, David K., and Higgins, Cornelius J., *Pretest, Two-Dimensional, Free-Field Calculation of HARD PAN I, Event 3: Calculations HPI-3.1 and 3.2*, DE-TN-77-002, Air Force Weapons Laboratory, Kirtland Air Force Base, New Mexico (to be published).

2. Rudeen, David K., *Post-Test, Two-Dimensional, Free-Field Calculation of HARD PAN I, Event 3: Calculation HPI-3.3*, DE-TN-77-003, Air Force Weapons Laboratory, Kirtland Air Force Base, New Mexico (to be published).

of the experimental data stressing time-of-arrival of first motion to derive seismic properties and a geology for a second posttest calculation (HPI-3.4).

OBJECTIVE

The purpose of posttest calculation HPI-3.4 was two-fold: (1) to generate free-field boundary input to the Three-Dimensional, Structure/Media Interaction (SMI3D) Code used to calculate structural response, and (2) to improve the capability and accuracy of calculating the free-field environments of actual experimental tests.

SCOPE

The input for the two pretest calculations (ref. 1) was based on experimental design impulse loadings, geology and seismic velocities determined by boring logs and seismic refraction and uphole surveys (ref. 3), and material models from one-dimensional iterations (ref. 4). A comparison of the pretest predicted response and the actual field response was necessary to determine the accuracy of the pretest information and how the code input could be modified to better reflect the field conditions to improve the posttest calculation. Preliminary analysis of the experimental data and pretest calculations, HPI-3.1 and 3.2 (section 2), indicated that the input HEST pressure/time history was poorly modeled in the pretest calculations and the first posttest calculation (HPI-3.3) was performed with a more accurate pressure/time history input and some revised material properties. Comparison of the HPI-3.3 results with the experimental data indicated that the new input did not significantly improve the calculated responses. A detailed analysis was then performed on geologic profile data, material properties, field seismic data, and experimental data to determine the most accurate and most representative input for calculation

3. Pinker, Robert W., Capt., *HARD PAN I-3 Geologic and Seismic Profiles*, memorandum, Air Force Weapons Laboratory, Kirtland Air Force Base, New Mexico, 17 January 1975.

4. Dzwilewski, Peter T., Lt., *Stress-Strain Relationships for Hard Pan Soils and Rocks*, DE-TN-75-022, Air Force Weapons Laboratory, Kirtland Air Force Base, New Mexico, December 1975.

HPI-3.4 (section 3). Section 4 presents the results of the HPI-3.4 calculation and the adjustment factors used to modify the calculated velocity/time histories to improve their accuracy for input to the soil island of the SMI3D Code.

Calculations of HARD PAN I Event 3 were performed with TOODY II, a finite-difference code that uses Lagrangian equations-of-motion to calculate two-dimensional wave propagation in layered media (ref. 5). The code was developed at Sandia Laboratories and modified by AFWL to calculate ground motions resulting from surface airblast loading. The constitutive relationship consists of an incrementally elastic, ideally plastic equation-of-state, which is input in the form of a hydrostatic stress/strain curve, yield criteria in terms of the square root of the second invariant of deviator stress tensor versus mean normal stress, and Poisson's ratio.

5. Bertholf, L. D., and Benzley, S. E., *TOODY II - A Computer Program for Two-Dimensional Wave Propagation*, SC-RR-68-41, Sandia Laboratories, Albuquerque, New Mexico, November 1968.

SECTION 2
ANALYSIS OF PRETEST CALCULATIONS

AIRBLAST PRESSURE FUNCTIONS

In the pretest calculations, the airblast pressure/time history and propagation velocity were designed to represent 30 msec of a 125-kt nuclear detonation at a 210-ft height-of-burst. Triangular pulses with an instantaneous initial stress rise were used to model the BLEST pressure/time history. These pulses matched the estimated impulse delivered to the soil and they were in approximate agreement with the few available BLEST stress records from previous experiments. The HEST region was modeled in more detail, with peak pressure and impulse designed to match the nuclear detonation and an exponential decay. A polynomial equation determined by a best-fit, fourth-degree curve through nuclear times-of-arrival and ranges was used to define the airblast time-of-arrival at the surface for the BLEST and HEST regions. This equation is as follows:

$$t_a = 1.763E-3 + 3.8247E-6R + 2.8387E-8R^2 + 6.3368E-11R^3 - 1.974E-14R^4$$

where

t_a = airblast time-of-arrival, sec
R = range from theoretical ground zero, ft

Analysis of the experimental data indicated that this equation was accurate for the BLEST region, but that the HEST times-of-arrival would be better modeled by a constant propagation velocity of 10,277 ft/sec (fig. 1). Therefore, for the posttest calculations, the following equation was used to define the airblast time-of-arrival in the HEST region:

$$t_a = 0.02324 + \frac{R - 575}{10277}$$

A comparison of input pressure functions in the BLEST region and a limited number of available uncorrected BLEST pressure records is shown in figure 2. It can be seen that a triangular pulse roughly approximates the actual pressure/time history, but sufficient BLEST pressure records were not available to dictate a new pressure function. Figure 3 shows experimental design impulse zones
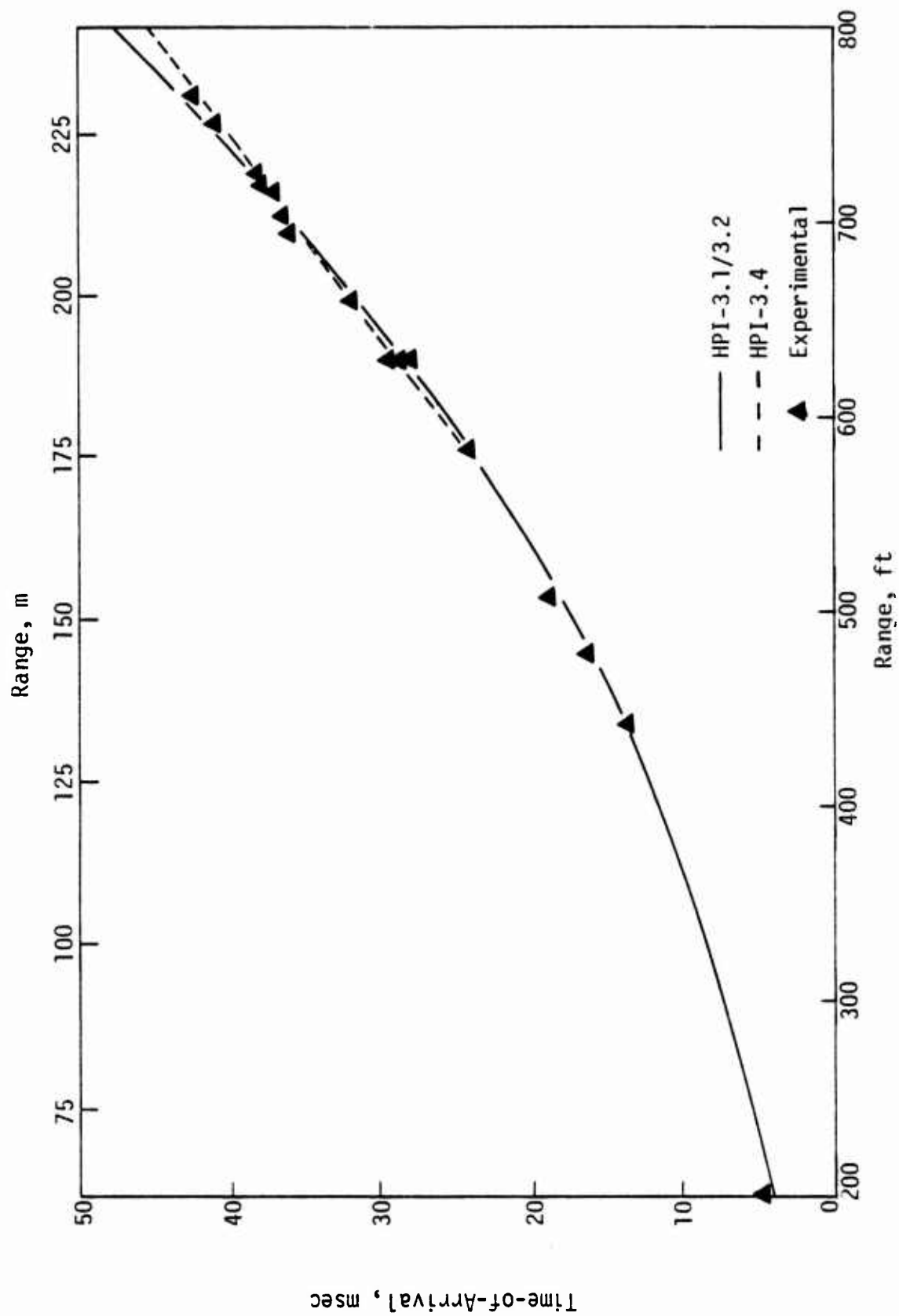
6

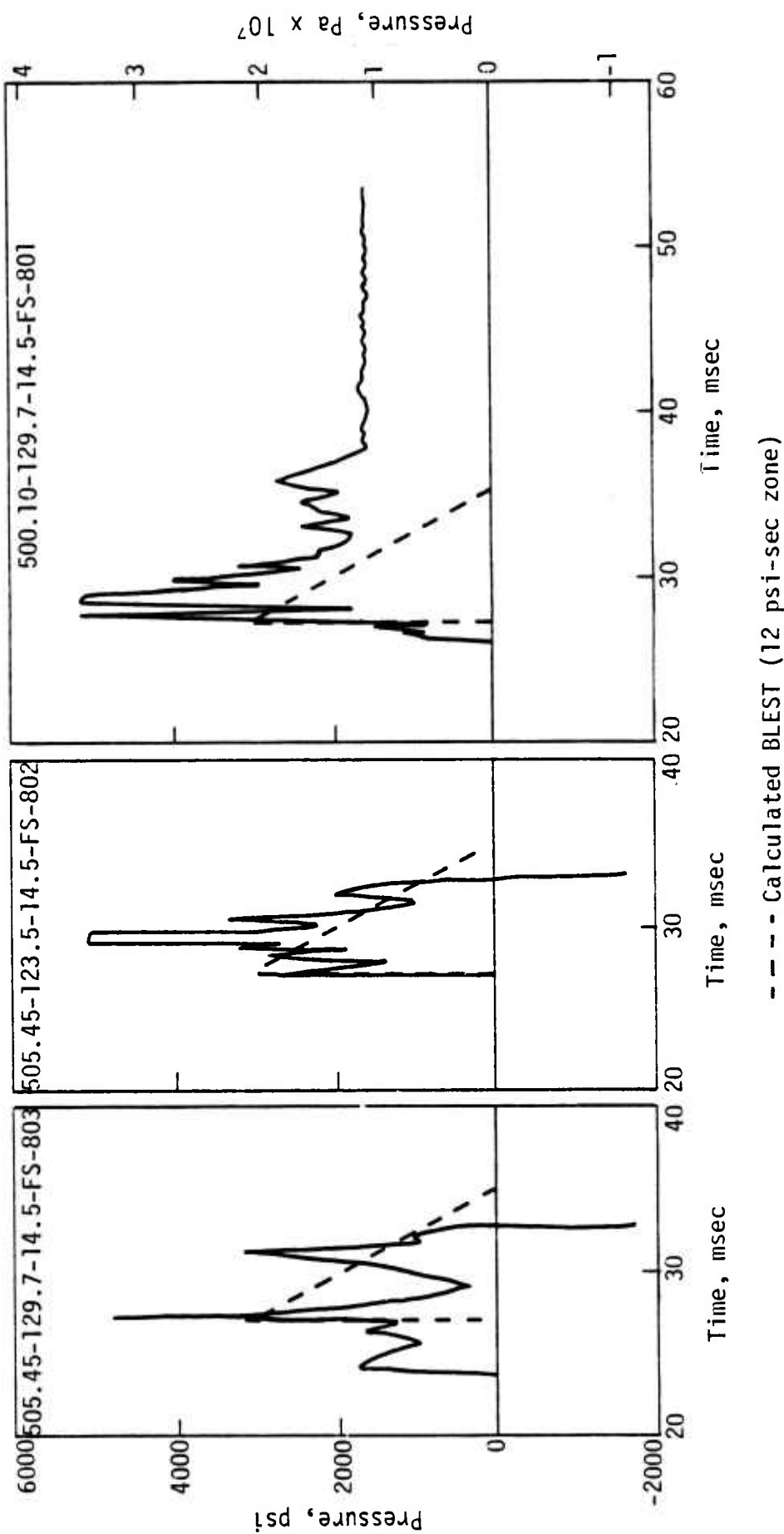Figure 1. Calculated and Experimental BLEST/HEST Times-of-Arrival

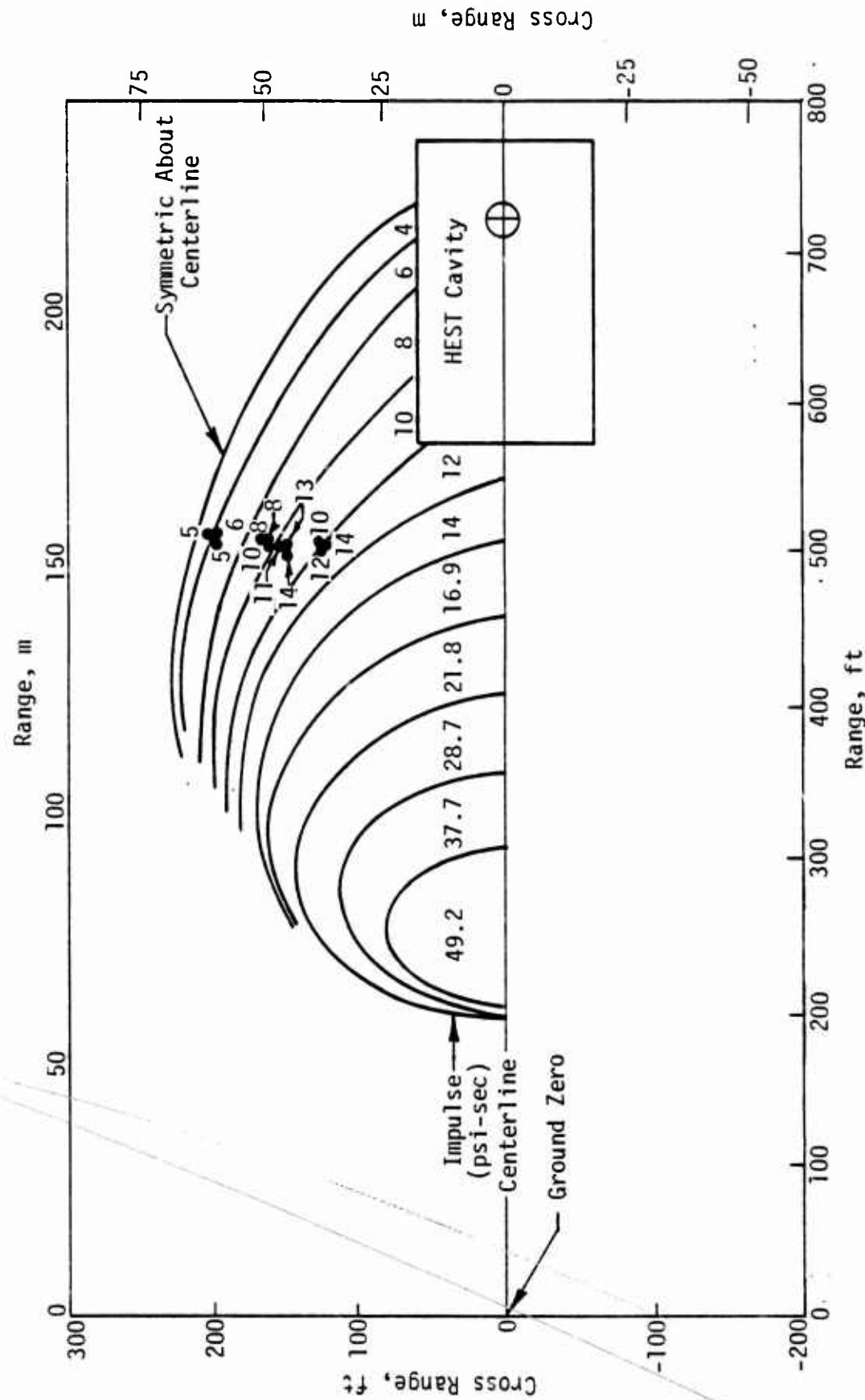Figure 2. Calculated and Experimental BLEST Pressure/Time Histories

8

Figure 3. BLEST Impulse Design and Experimental Data

and impulses calculated from the uncorrected BLEST pressure records. The agreement between experimental and design impulse is good, and based on impulse criteria no changes were made to the BLEST time histories for the posttest calculations. The parameters describing the BLEST triangular pulses (table 1) are used with the following equation to define the BLEST pressure function:

$$P = P_o(1.0 - T)$$

where

P_o = peak pressure (varies with range; see table 1.)
$T = (t - t_a)/t_d$
t = time from detonation, sec
t_a = airblast time-of-arrival, sec
t_d = duration, sec

In the HEST region 13 pressure records were available for analysis and comparison with the input HEST pressure function. Representative comparisons of experimental, pretest, and posttest HEST pressure/time histories are shown in figure 4. The pretest pressure function has a lower peak pressure and a slower initial decay than the experimental record; therefore, a new HEST pressure function was developed for the posttest calculations. This new pressure

Table 1. BLEST Pressure/Time History Parameters

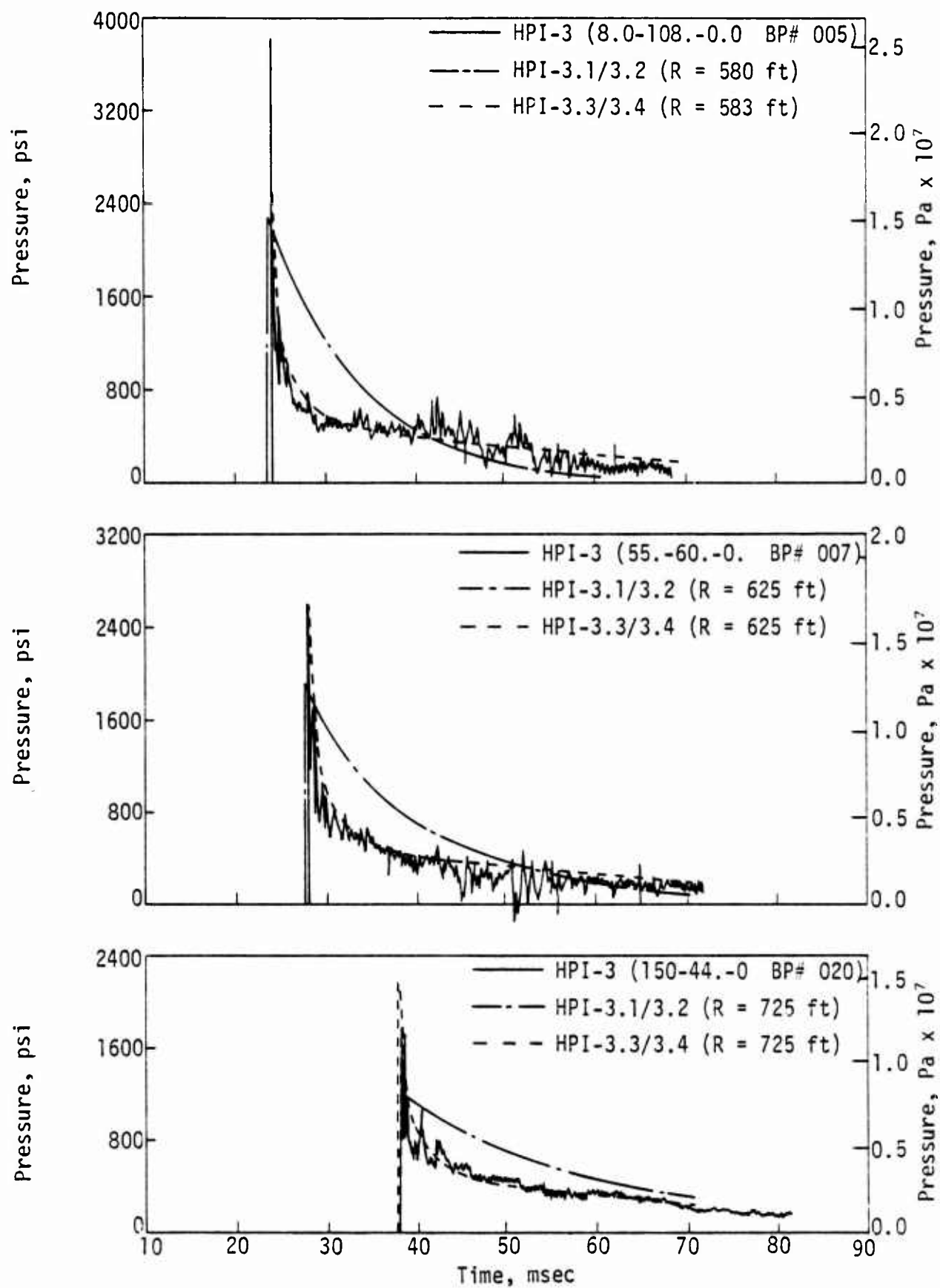| Range (R), ft	Peak Pressure (P_o), psi	Duration (t_d), sec	Design Impulse (I), psi-sec
190-305	4700	0.021	49.2
305-350	3600	0.021	37.7
350-415	2750	0.021	28.7
415-460	2625	0.017	21.8
460-510	2575	0.013	16.9
510-545	2125	0.013	14.0
545-575	2900	0.008	12.0

Figure 4.   Calculated and Experimental HEST Pressure/Time Histories

function is defined by two equations--one for the first millisecond after the
arrival of the airblast, the second for later times. These equations are as
follows: For $t_a \leq t \leq t_a + 0.001$

$$P = P_0 \left[0.185 + 0.815 \exp(KT_0) \right] \left[1.0 - T_0 \right]$$

where

$P_0 = -4R + 5100$, psi

$K = 0.25R - 293.75$

$T_0 = (t - t_a)/0.125$

t = time from detonation, sec

t_a = airblast time-of-arrival, sec

and for $t_a + 0.001 < t < t_a + 0.066$

$$P = P_1 \left[0.425 + 0.575 \exp(-25T_1) \right] \left[1.0 - T_1 \right]$$

where

$P_1 = -0.5R + 1487.5$, psi

$T_1 = (t - t_a - 0.001)/0.065$

t = time from detonation, sec

t_a = airblast time-of-arrival, sec

Peak pressure relationships for the BLEST and HEST regions are shown for the
centerline cross section in figure 5 for the pretest and post-test calculations.
The BLEST peak pressures are identical for the pretest and posttest calcula-
tions. The two pretest calculations (HPI-3.1 and 3.2) were identical, except
for the shear failure envelope used to define the material properties. The
results of these two calculations were similar, despite major differences
in the failure envelope, and thus only the HPI-3.2 results were compared with
the experimental data from this point.

FIRST-ARRIVAL CONTOURS

In using time-of-arrival contours as an analytical tool, it must be realized
that exact location of contours is very sensitive to the times selected from
the waveforms; first-arrival times, in particular, are sensitive to waveform
interpretation. For calculated waveforms the first motion is due to artificial
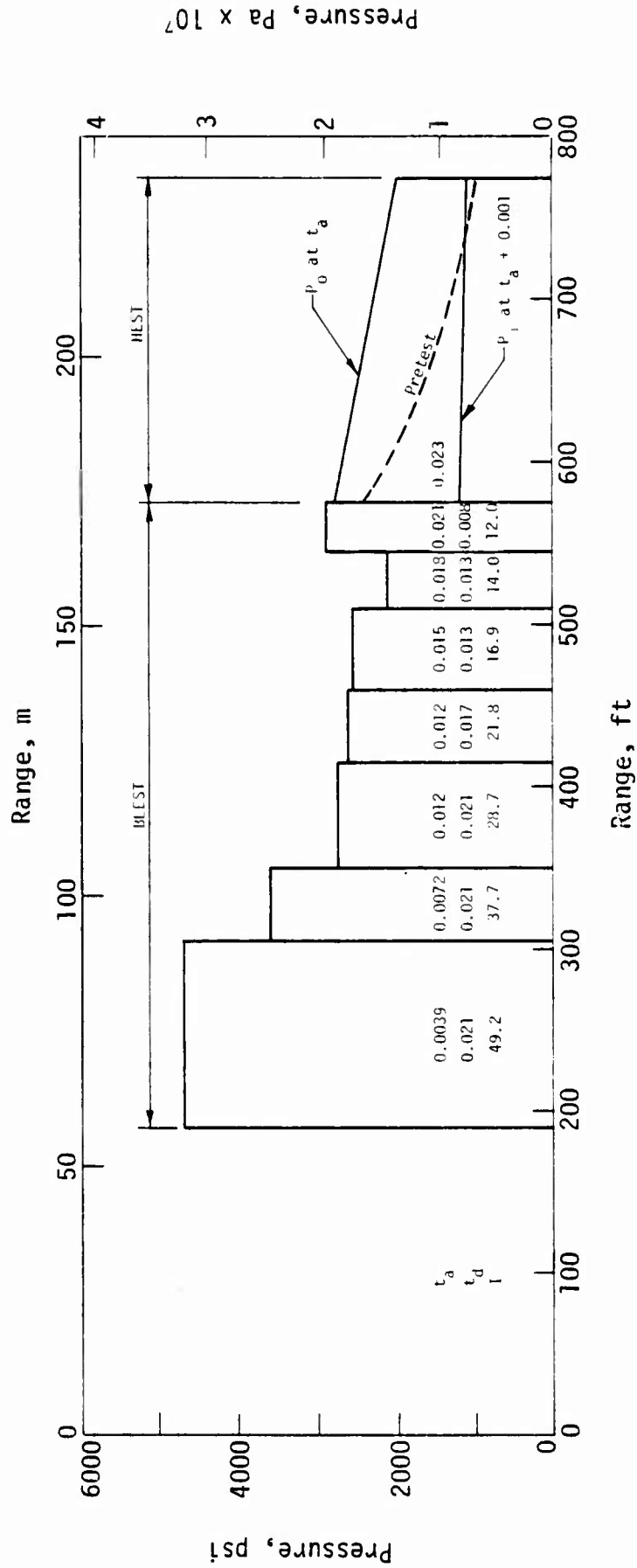
Figure 5. BLEST/HEST Peak Pressure Functions

t_a = Airblast Time-of-Arrival (sec) t_d = Duration (sec)   I = Impulse (psi-sec)

t_a = Airblast Time-of-Arrival (sec) t_d = Duration (sec)   I = Impulse (psi-sec)

13

viscosity, which causes the front of the wave to spread. To approximate the actual arrival of the wavefront, the time of the inflection point of rise to first peak was selected as the arrival time. With integrated accelerometer data (i.e., experimental data), it is sometimes difficult to separate arrival of the real signal from background noise. Therefore, contours are generally used to examine trends in the wavefront rather than the precise location. A comparison of time-of-arrival contours of first motion is shown in figure 6. The primary differences in first arrival appear to be caused by the low seismic velocities for the wet clay (8 to 16 ft) and the limestone/shale (20 to 34 ft) and the high seismic velocities for the upper limestone (16 to 20 ft) and shale (46 to 52 ft) in the calculation, as evidenced by the headwave emanating from this layer. For both the calculation and the experiment there is a headwave generated by an outrunning signal at 52 ft; this indicates good agreement in material models near this depth, although there is a delay of about 4 msec caused by the upper layers. It should be noted that the calculation did not pick up the initial upward motion associated with the headwave because of the resolving power of the mesh. The headwave was established based on interpolation between data points above and below the interfaces at which the outrunning signals occurred.

PEAK VELOCITY ATTENUATIONS

Peak vertical and horizontal velocity attenuations with depth for the pretest calculations are shown in figure 7 and in appendix A with peak velocities obtained from integrated accelerometers.

Scatter of the experimental data with range and the few data records for the upper 8 ft make evaluation of peak vertical velocity in this region difficult. Peak vertical velocities at or near the surface appear to be high for calculation HPI-3.2, but rapid attenuation down to 8 ft brings them into better agreement with depth, although they are still overpredicted when compared with the experimental data. This is partially due to the inaccurate loading of the HEST region in the pretest calculations.

Because of the extreme data scatter with range and scarcity of horizontal records, only generalities about peak horizontal velocity attenuation can be made.
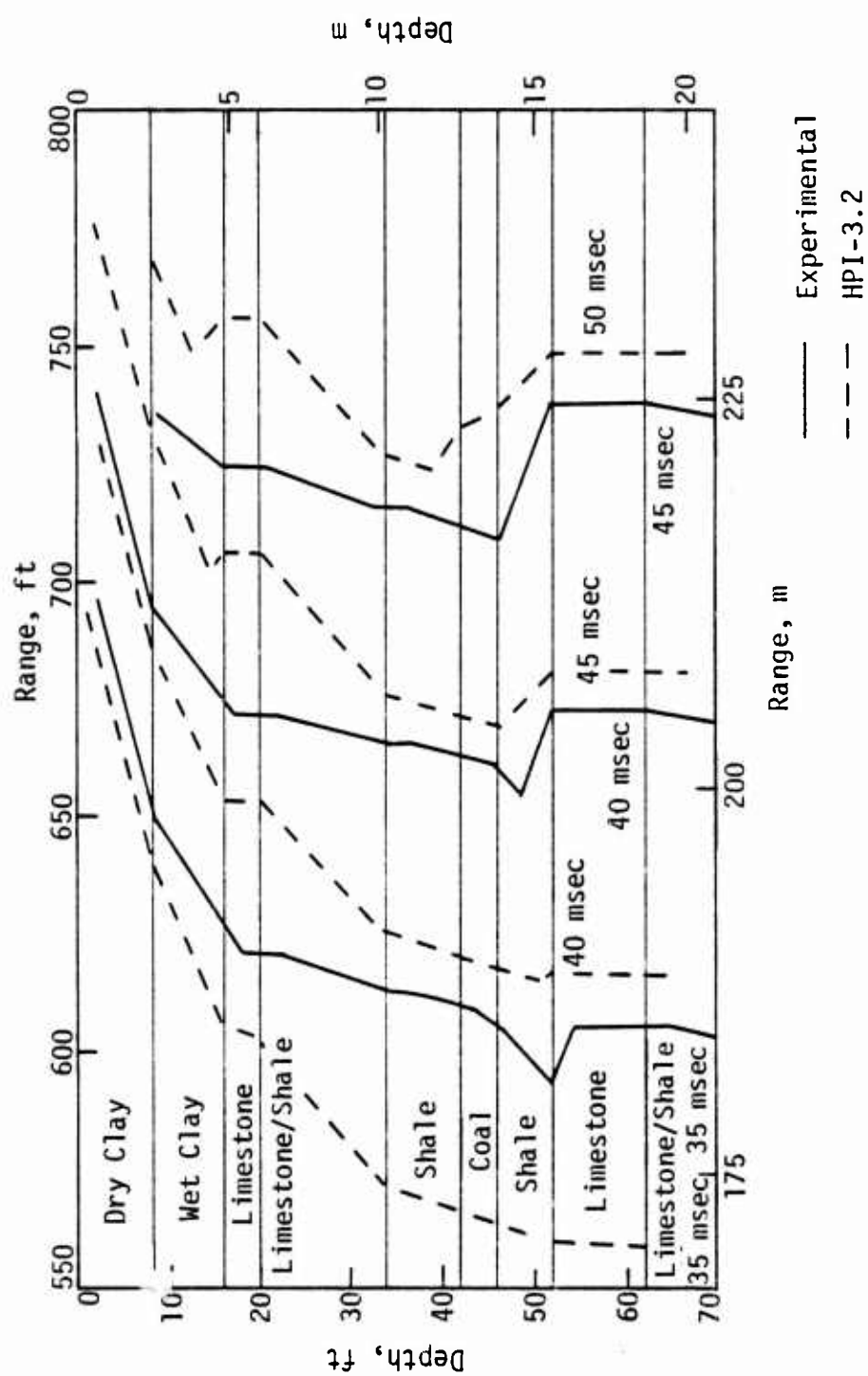
14

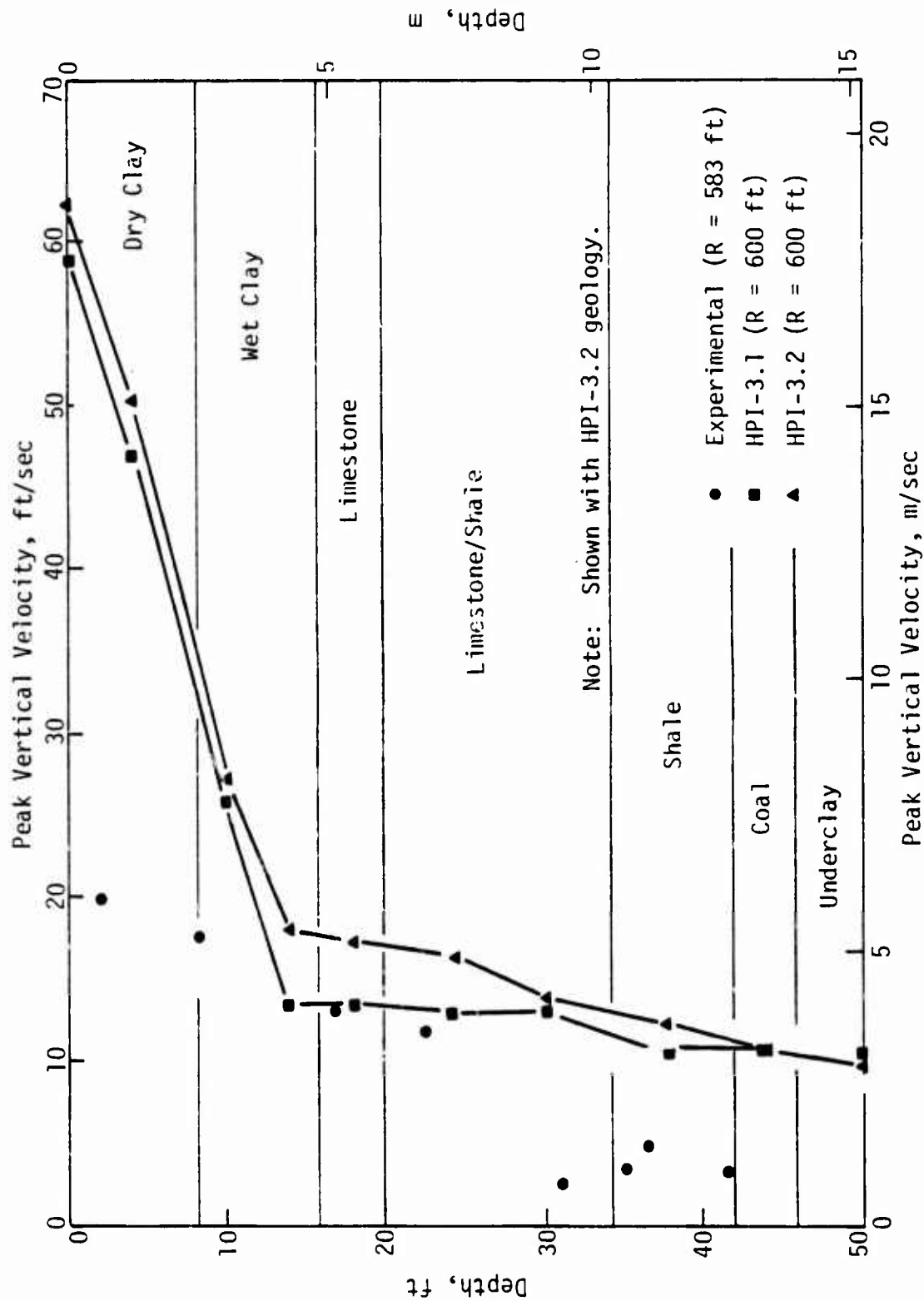Figure 6. Experimental and Calculation HPI-3.2 First-Arrival Contours

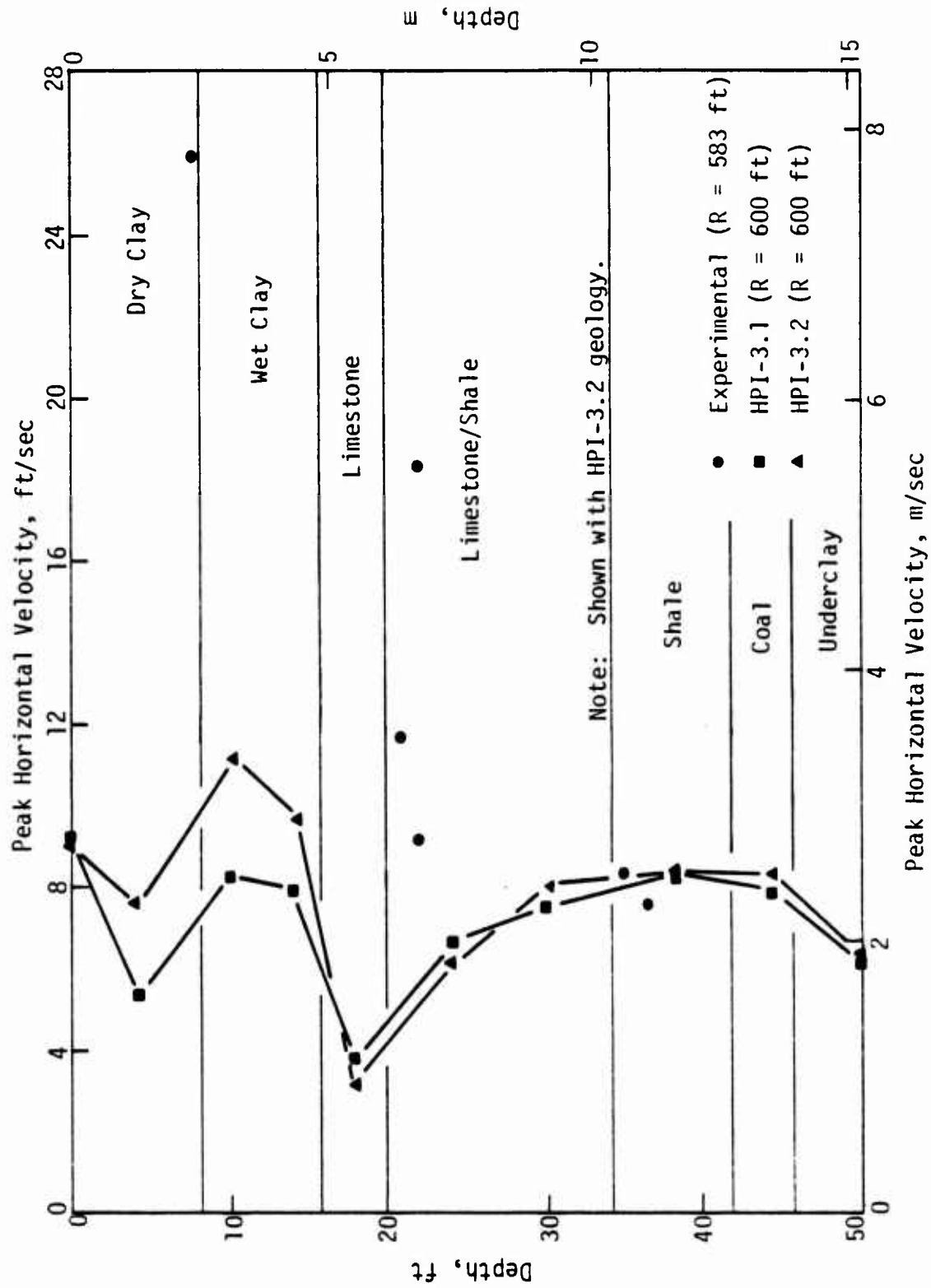Figure 7.   Peak Velocity Attenuations (1 of 2)

Figure 7. Peak Velocity Attenuations (2 of 2)

Peak horizontal velocities were approximately 50 percent lower, but they improved with range and depth and showed good agreement below 20 ft at the 725-ft range. This agreement is misleading, however, since the HEST imparted excessive impulse into this region as compared with the experimental design. Correction of the HEST loading tends to decrease associated peak horizontal velocities and cause the calculation to deviate from the experimental data. Thus, new material models which enhance horizontal motion are needed. This development is difficult and more importantly may involve problems with the elastic, ideally plastic equation-of-state in the code. Based on reference 6, more accurate horizontal velocities and improved resolution of minor wave effects can be expected from the finer mesh used in the posttest calculations, but not of sufficient magnitude to bring calculated data into agreement with the experimental data.

WAVEFORMS

Waveform comparisons for representative target points generally support the accumulative data shown by time-of-arrival contours and attenuation plots with only minor exceptions due to nonhomogeneity of the test site. The most prominent characteristic missing from the calculation and mentioned earlier is the lack of an upward velocity associated with the headwaves induced by the outrunning signal (i.e., critically refracted wave). The headwave location is defined by interpolation between contours above and below this zone. Outrunning is evidenced by the arrival of a prominent horizontal motion prior to local induced vertical motion. The upward pulse because of its short duration and relatively small magnitude cannot be detected on the waveform because of the resolution of the finite-difference mesh and the artificial viscosity parameter in the code.

6. Higgins, Cornelius J., and Rudeen, David K., *Effects of Zone Size, Aspect Ratio, and Artificial Viscosity on the Accuracy of Ground-Motion Calculations with Finite-Difference Codes*, Technical Note, Air Force Weapons Laboratory, Kirtland Air Force Base, New Mexico (in review).

18

SECTION 3
INPUT PARAMETERS FOR CALCULATION HPI-3.4

GEOLOGY

Available literature (refs. 1, 2, 3, 4, 7, 8, and 9) and the data obtained at
the June 1976 meeting were reviewed for geological layering, seismic informa-
tion, and material stress/strain properties. Presented in figure 8 are the
geologies recommended by various agencies, beginning with the pretest seismic
profile and concluding with the profile selected for calculation HPI-3.4. The
geologies are for the same datum elevation so that variation of the data can
be studied. Profile 1 is the pretest geology with seismic velocity determined
by field tests. Profile 2 is the geology used in pretest calculations HPI-3.1
and 3.2, and the velocities shown are the average propagation velocities which
resulted from the calculations, based on the shape of the hydrostat and the
pressure level experienced by the material. Profiles 3 and 4 are the geologies
at the centerline of the structure as suggested by WES in reference 7 and from
the June 1976 meeting, respectively. Profile 5 shows the boring at the CIST
test site, which is approximately 750 ft from the Event 3 site. Similarities
in the materials at the CIST site and N-3 boring were studied to determine
if CIST material properties could be used to define the same materials at
the Event 3 site. Profile 6 is the geology originally given in the HARD PAN
I Test Series report (ref. 8), and also later recommended by Capt. Pinker in
reference 9. The water table is shown at a depth of 14 ft. This was the level
of the phreatic surface as indicated by piezometric measurements made at the
test site and should not be interpreted as the boundary definition between dry

---

7. Ehrgott, John Q., *Preshot Free-Field Calculational Properties for Project
   HARD PAN I, Event 3*, U.S. Army Engineer Waterways Experiment Station, Soils
   and Pavements Laboratory, Vicksburg, Mississippi, March 1975.

8. Doran, J., *HARD PAN I Test Series and Instrumentation Plans*, AFWL-TR-75-249,
   Vol. 1, Air Force Weapons Laboratory, Kirtland Air Force Base, New Mexico,
   December 1975.

9. Pinker, Robert W., Capt., *Geology and Seismology for the HARD PAN I Test
   Site, Trading Post, Kansas*, Air Force Weapons Laboratory, Kirtland Air
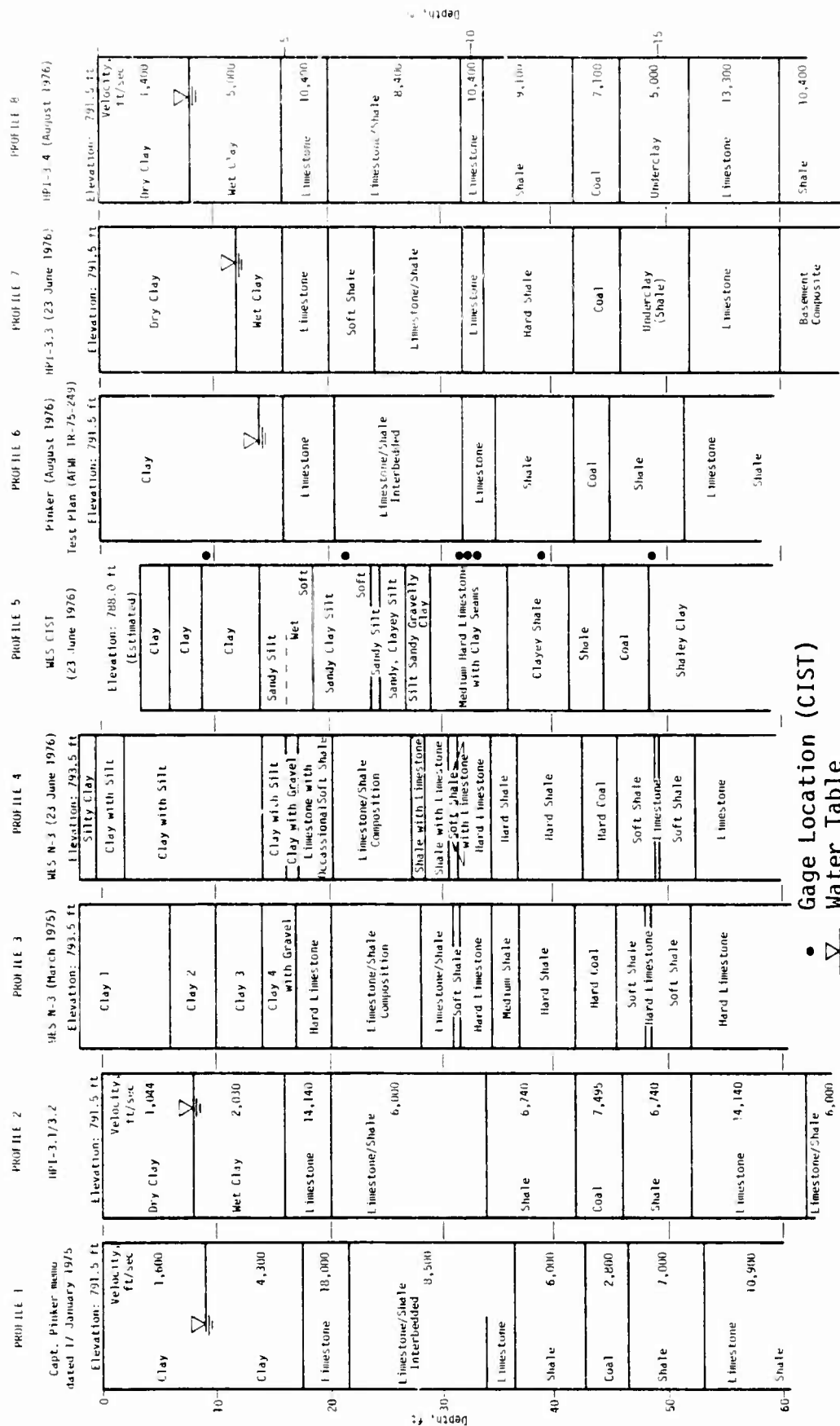   Force Base, New Mexico (in preparation).

19

Figure 8. HARD PAN I Geologies and Seismic Properties

20

and wet material. Because of capillary rise the *effective* water table (i.e., the elevation at which the material is considered to be 100 percent saturated and defined by different material properties) will have a higher elevation. Profile 7 resulted from the June 1976 meeting and was used in the first post-test calculation (HPI-3.3). Profile 8 is the geology resulting from the detailed analysis of the experimental data and consideration of profiles 1 through 7; it is believed to be the most representative geology of the site at the structure. This profile is most closely related to profiles 2 and 7, pretest geology and posttest geology, respectively. Differences between the two profiles are as follows:

(1) location of the *effective* water table, which was established by experimental first-arrival contours,

(2) removal of the soft shale at 20 to 24 ft,

(3) addition of the 2-ft-deep limestone layer at 32 to 34 ft, and

(4) elevation of basement composite to the 60-ft depth.

The seismic velocities shown in profile 8 are the velocities obtained from the experimental first-arrival contours shown in figure 9. By knowing the inclination angles of the wavefronts with the horizontal and relating to Snell's Law, the velocities for each layer were obtained by

$$\frac{\sin\alpha_1}{\sin\alpha_2} = \frac{C_1}{C_2}$$

$$\frac{\sin\alpha_2}{\sin\alpha_3} = \frac{C_2}{C_3}$$
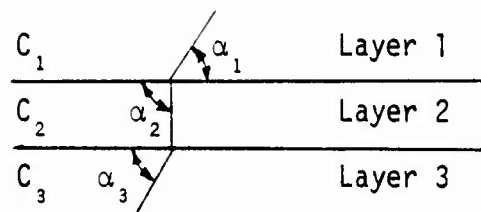
where

α_1, α_2, α_3 = inclination angle of wavefront with the horizontal in layers 1, 2, and 3, respectively

C_1, C_2, C_3 = seismic velocity in layers 1, 2, and 3, respectively

The seismic velocity for the dry clay was determined by utilizing the propagation velocity of the airblast, setting $\alpha_1 = 90°$, and graphically measuring the inclination angle (α_2) on the experimental contours. A similar procedure was used to determine the seismic velocities for the remaining layers. The velocities were later used to establish the initial slope of the hydrostat, based on the fact that first arrivals are determined by the seismic properties of
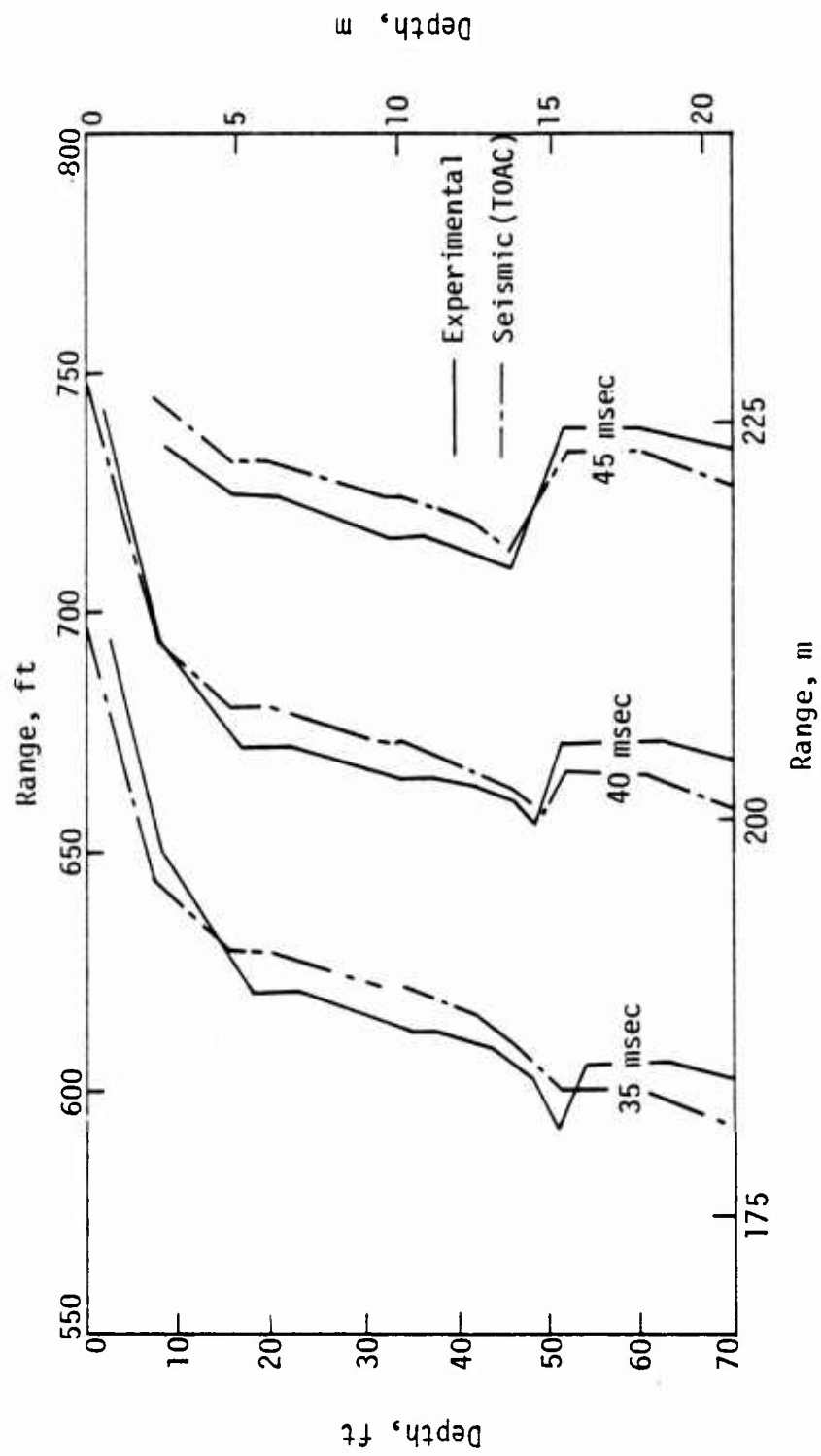
21

Figure 9. Seismic and Experimental First-Arrival Contours

the materials. If first arrivals could be calculated accurately, timing of peaks and other waveform characteristics could be analyzed better. Contours were developed by the TOAC Program[*] with experimental seismic velocities and the selected geology as input and compared with the experimental contours (fig. 9) to verify the accuracy of the seismic velocities.

MATERIAL PROPERTIES

As part of the experimental analysis, new material properties were developed from the results of the previous HARD PAN I calculations, CIST data and one-dimensional iterations, WES laboratory data, and engineering judgment. These new properties incorporated the following characteristics:

    (1)   the initial slope, *seismic toe*, of the hydrostat would correspond to the seismic velocities determined by the experimental contours of first arrivals,

    (2)   the seismic toe of the hydrostat would extend to a pressure level consistent with models from CIST 13 and CIST 14 iterations (refs. 10 and 11),

    (3)   the unloading slope of the hydrostat would correspond to the seismic velocity and agree with the initial loading slope (i.e., seismic toe),

    (4)   strain lock-up points would be consistent with previous models,

    (5)   the intermediate slope would extend from the seismic toe to the lock-up point or would be determined by 64 percent of the seismic toe (80 percent of the seismic velocity); this was based on the CIST iterations from references 10 and 11,

    (6)   materials located below the water table would have a minimum seismic velocity of 5000 ft/sec, and

    (7)   failure surfaces would be determined by laboratory results (ref. 7).

The changes made to the material models for the HPI-3.4 calculation are discussed below; the final models are presented in figures 10 through 18.

---

[*]The TOAC Program, based on Snell's Law of Refraction, calculates time-of-arrival from a point source, from which first-arrival contours can be developed. These contours are then used to develop contours for a moving source or airblast along the surface by varying the location of the point source.

10. Fedock, Joseph J., *CIST 14 Analysis and Derivation of Dynamic Properties for Site M-28, Wing VI*, Technical Note, Air Force Weapons Laboratory, Kirtland Air Force Base, New Mexico, in review (SRD).

11. Higgins, Cornelius J., *CIST 13 Analysis and Derivation of Properties for Site F-9, Wing II*, Technical Note, Air Force Weapons Laboratory, Kirtland Air Force Base, New Mexico, in review (SRD).

Dry Clay: 0 to 8 ft (fig. 10)

From experimental contours a seismic velocity between 1200 and 1400 ft/sec was indicated and the upper limit was judged to better represent the seismic properties of in-situ soil. The seismic toe was extended to a pressure level of 50 psi (determined from CIST 13 and CIST 14 iterations to be satisfactory for accurate dry-soil behavior). The intermediate slope was defined as 80 percent of the seismic velocity, and the lock-up point of 4 percent was maintained. The unloading slope was identical to the seismic loading toe of the material, and the laboratory yield surface determined by WES was used.

Wet Clay: 8 to 16 ft (fig. 11)

Seismic velocity from experimental contours resulted in a value of 4500 to 5000 ft/sec. Again the upper limit was used because the *effective* water table was determined by the analysis to be 8 ft below the surface, and materials below this point should have velocities approximately equal to that of water (i.e., 5500 ft/sec). This seismic toe extended to a pressure of 100 psi as indicated by CIST 13 and CIST 14 iterations. The 1 percent lock-up strain at 1700 psi was consistent with previous models, and the intermediate slope was established by the lock-up point and the seismic toe. The unloading slope was assumed to be identical to the seismic toe, and the laboratory yield surface was used.

Upper Limestone: 16 to 20 ft; 32 to 34 ft (fig. 12)

Because of its high-strength characteristics, the limestone was modeled as a linearly elastic material determined by a seismic velocity of 10,400 ft/sec. Laboratory testing defined a yield surface with a tension capability of 1000 psi.

Limestone/Shale Composite: 20 to 32 ft (fig. 13)

Experimental contours indicated a seismic velocity of 8400 ft/sec, which was extended to 200 psi. A lock-up strain value of 0.5 percent at 5500 psi was maintained, and the intermediate loading slope was determined from the termination point of the seismic toe and the lock-up strain. The unloading slope was assumed to be identical to the seismic toe, and the laboratory yield surface for the composite model was used with a 29-psi tension cutoff.

24

Shale: 34 to 42 ft (fig. 14)

A seismic velocity determined from the experimental contours indicated a velocity of 9100 ft/sec, and the material was modeled as linearly elastic based on the hydrostat suggested at the June 1976 meeting. Laboratory data were used to define the yield surface with a tension cutoff of 36 psi.

Coal: 42 to 46 ft (fig. 15)

A seismic toe corresponding to 7100 ft/sec and extending to 200 psi was used to define the initial slope of the hydrostat. The intermediate slope was defined by 80 percent of the seismic velocity, and the lock-up point of 0.5 percent from the June 1976 meeting was maintained. The unloading slope corresponded to the seismic toe, and laboratory data defined the yield surface. The tension cutoff was 29 psi.

Underclay: 46 to 52 ft (fig. 16)

Original contours developed from the experimental data indicated a seismic velocity of approximately 3400 ft/sec. Because the material is located below the water table, a higher velocity (5000 ft/sec) seemed more reasonable. The laboratory data for the underclay were thus reviewed and it was observed that the wet-clay hydrostat was within the bounds of the scatter for the laboratory results. Based on this, the wet-clay hydrostat was adopted for the underclay, and the yield surface was defined by WES laboratory tests. The tension cutoff was 0 psi.

Deep Limestone: 52 to 60 ft (fig. 17)

As with the shallow limestone layers, linearly elastic stress/strain properties were used with a seismic velocity and hydrostat corresponding to 13,300 ft/sec. This reflected the concern of WES that the deep limestone is more competent than the shallow limestone. The yield surface was developed from WES laboratory tests. The tension cutoff was 1000 psi.

Limestone/Shale Basement Composite: 60 ft to ∞ (fig. 18)

The material was modeled as linearly elastic with a seismic velocity of 10,400 ft/sec determined by experimental contours. The laboratory yield surface with a tension cutoff of 1000 psi was used.

25
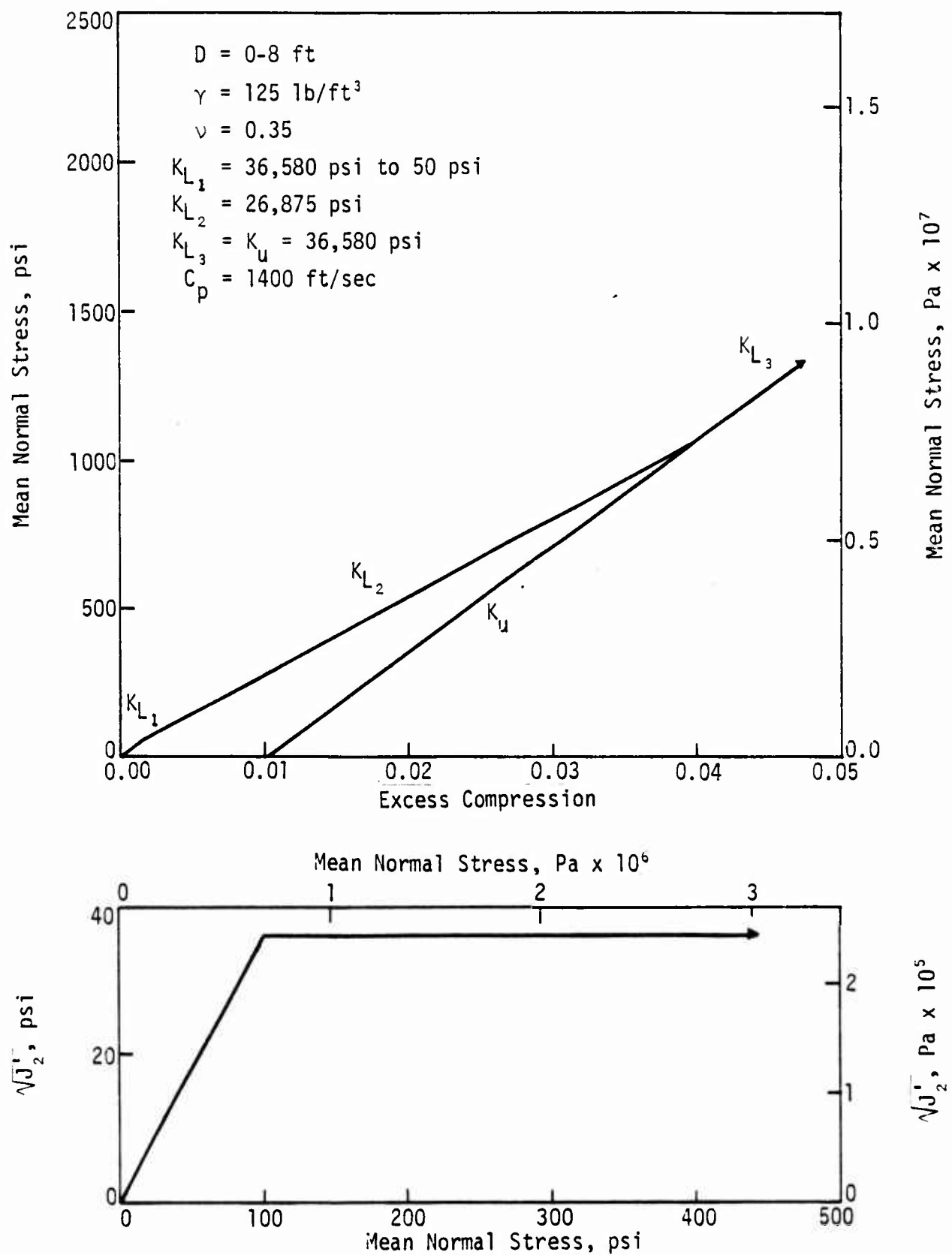
Figure 10. Material Properties of Dry Clay
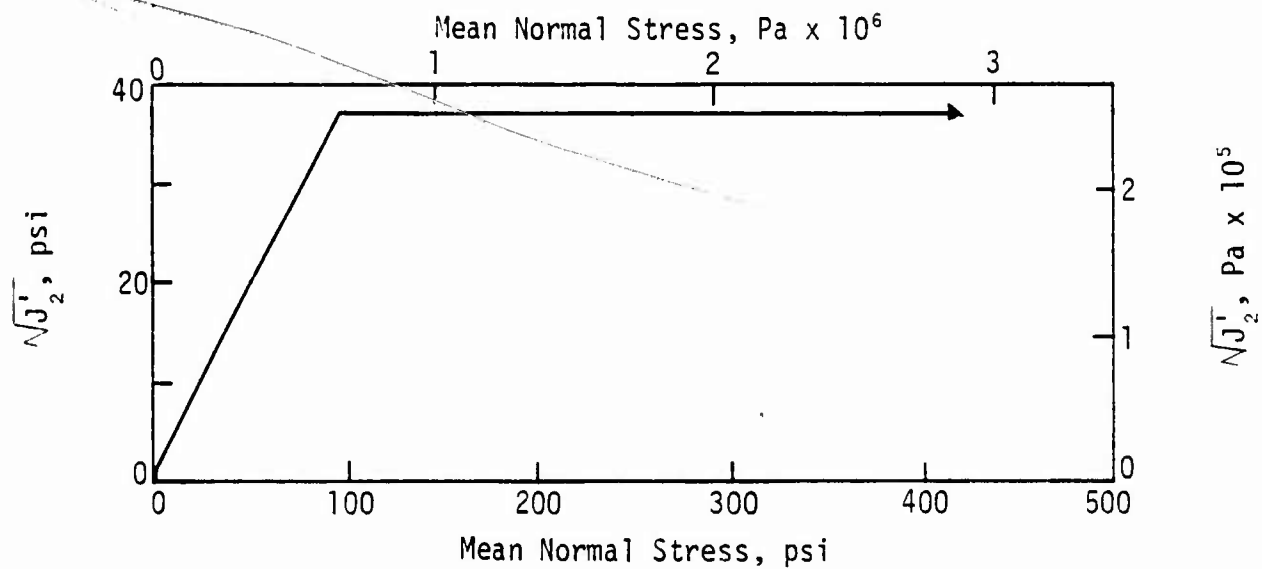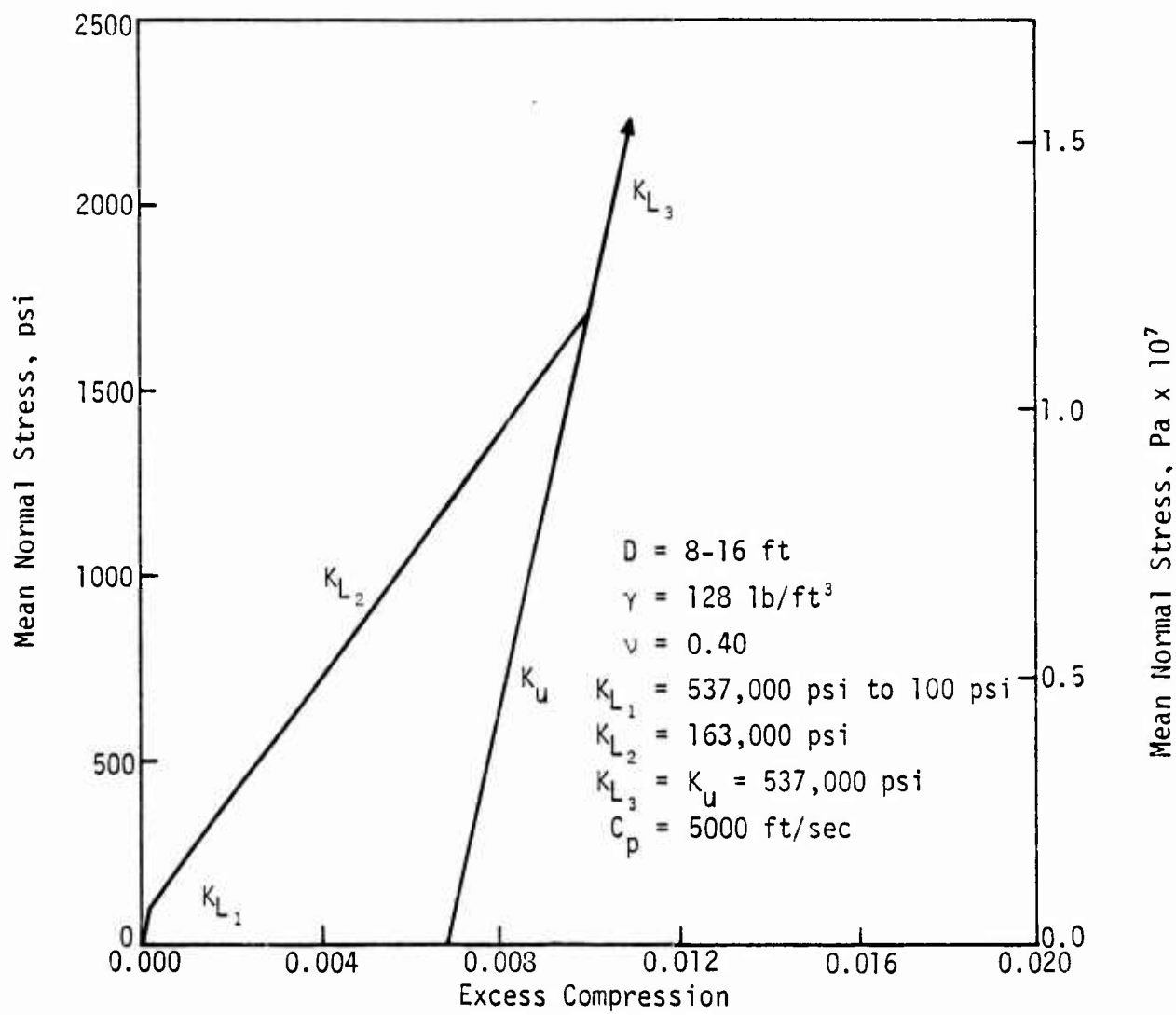
Figure 11. Material Properties of Wet Clay
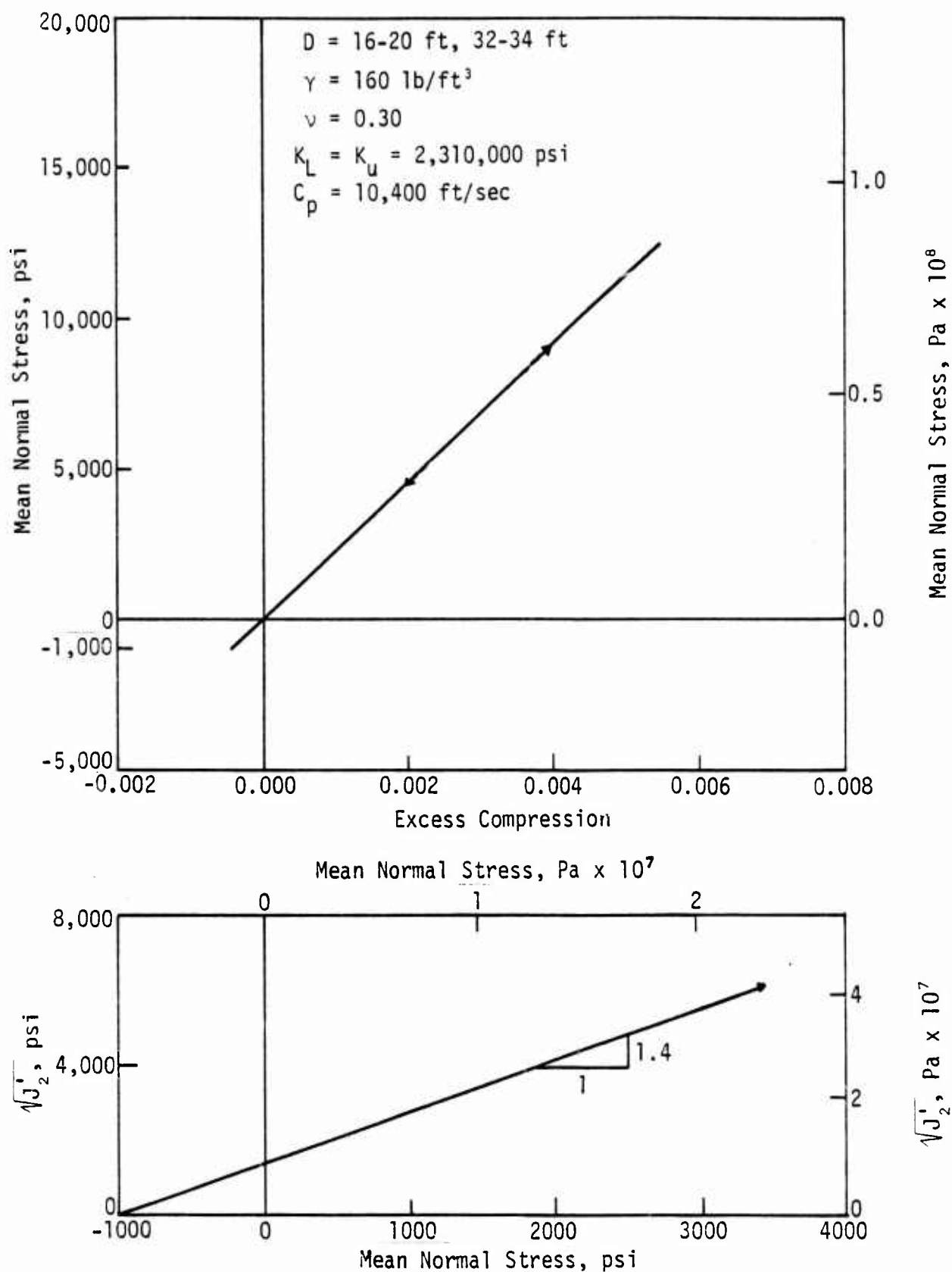
Figure 12. Material Properties of Upper Limestone

28
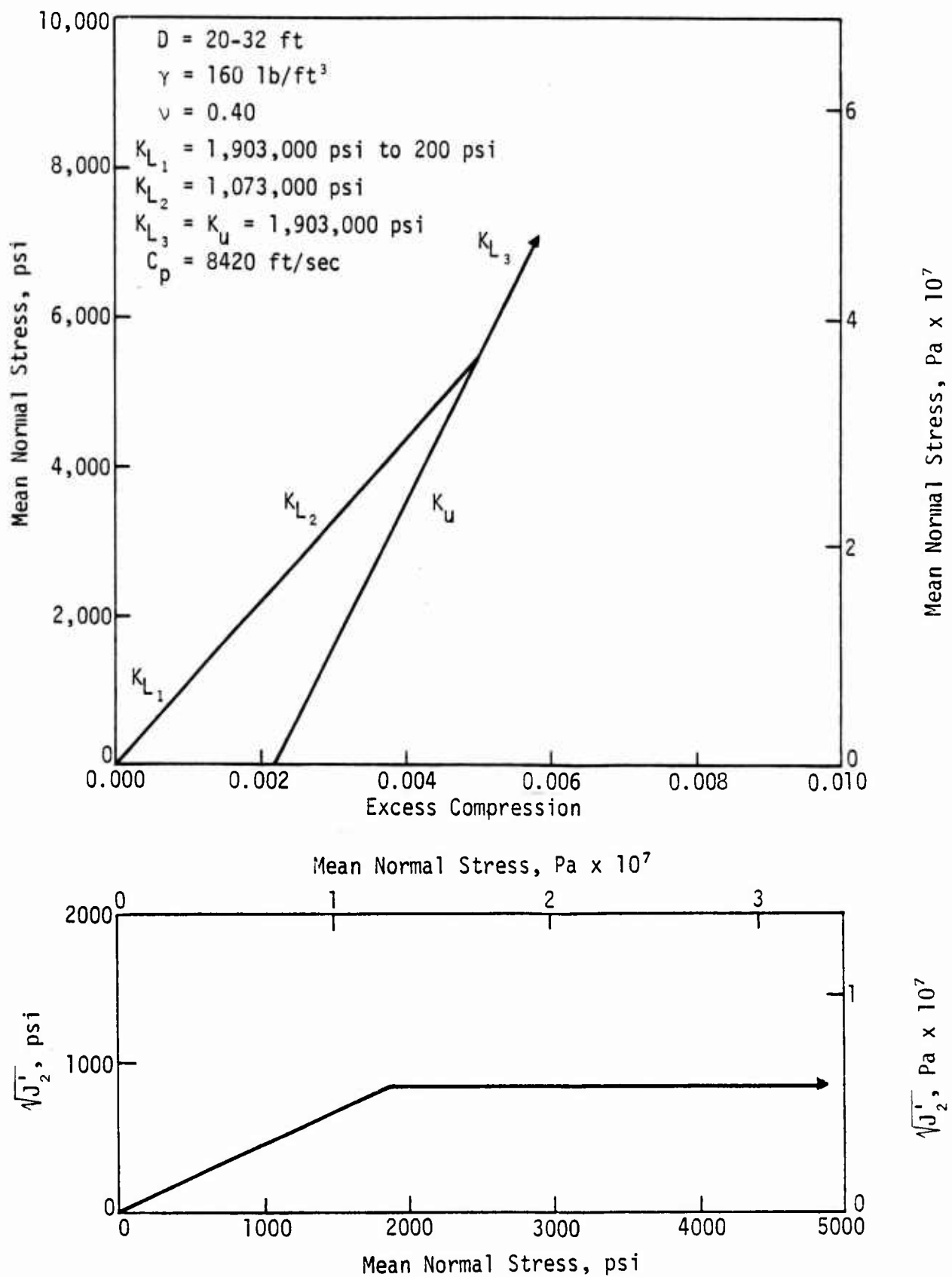
Figure 13. Material Properties of Limestone/Shale Composite

29
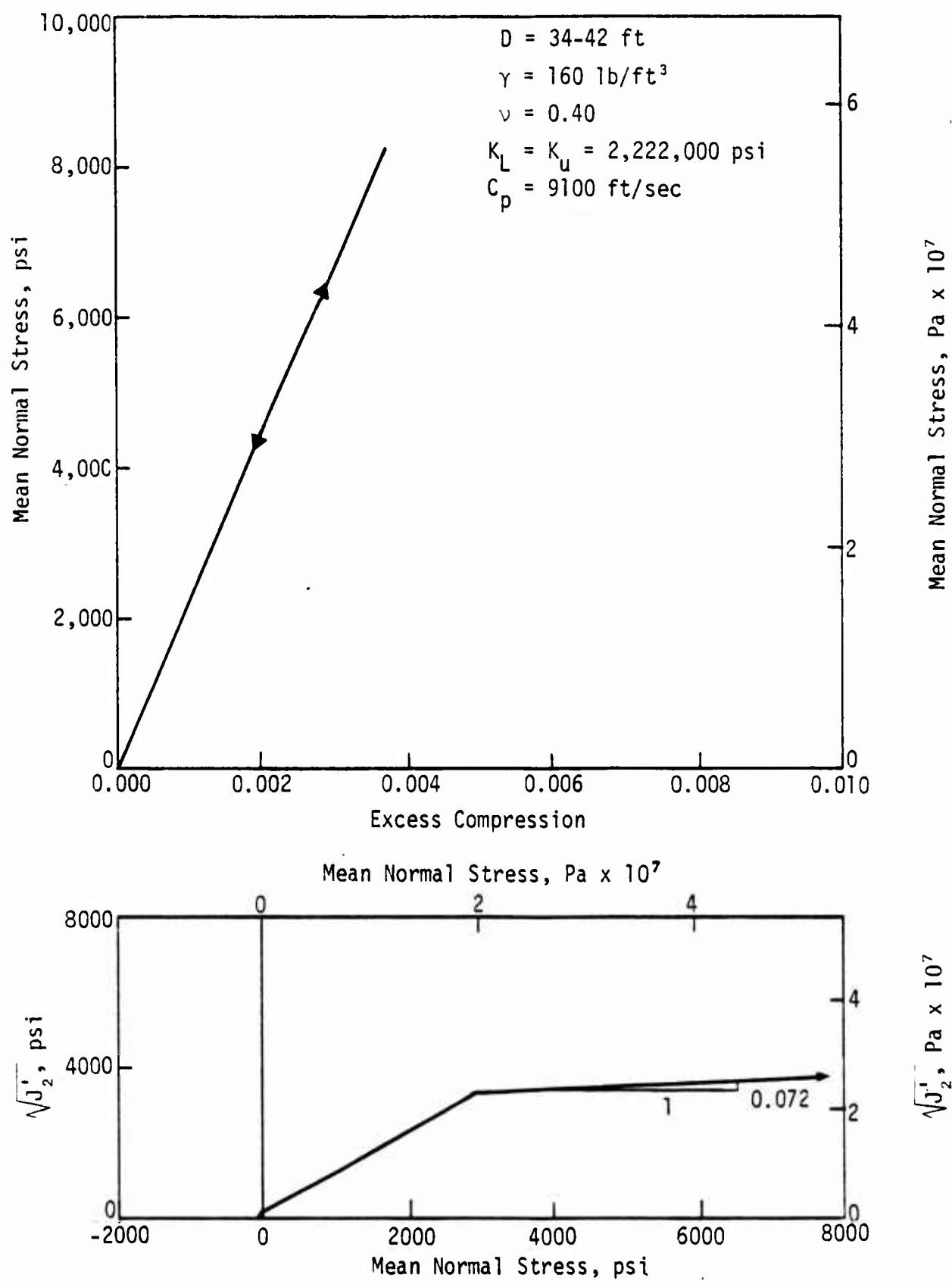
Figure 14. Material Properties of Shale
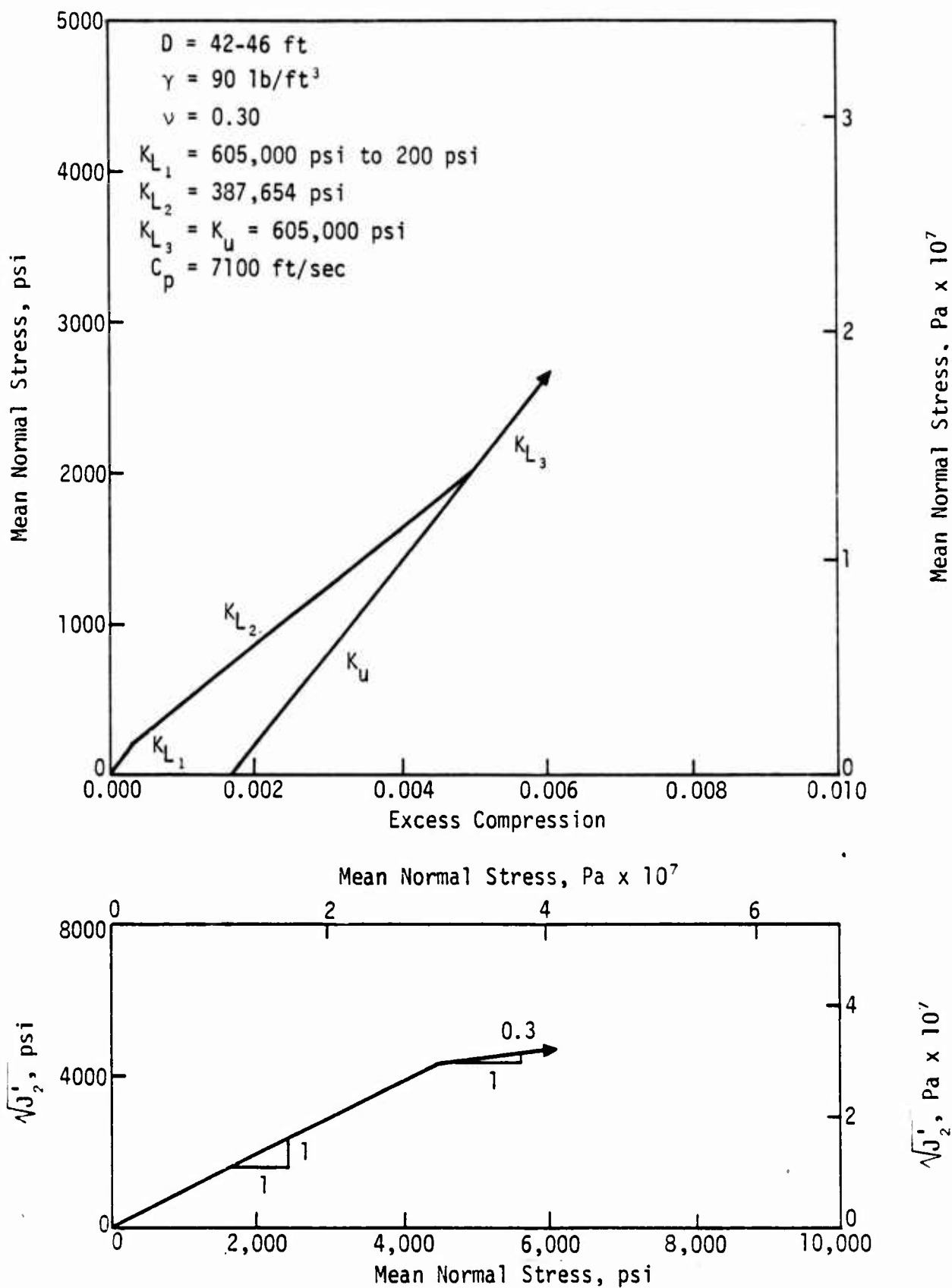
Figure 15. Material Properties of Coal

31
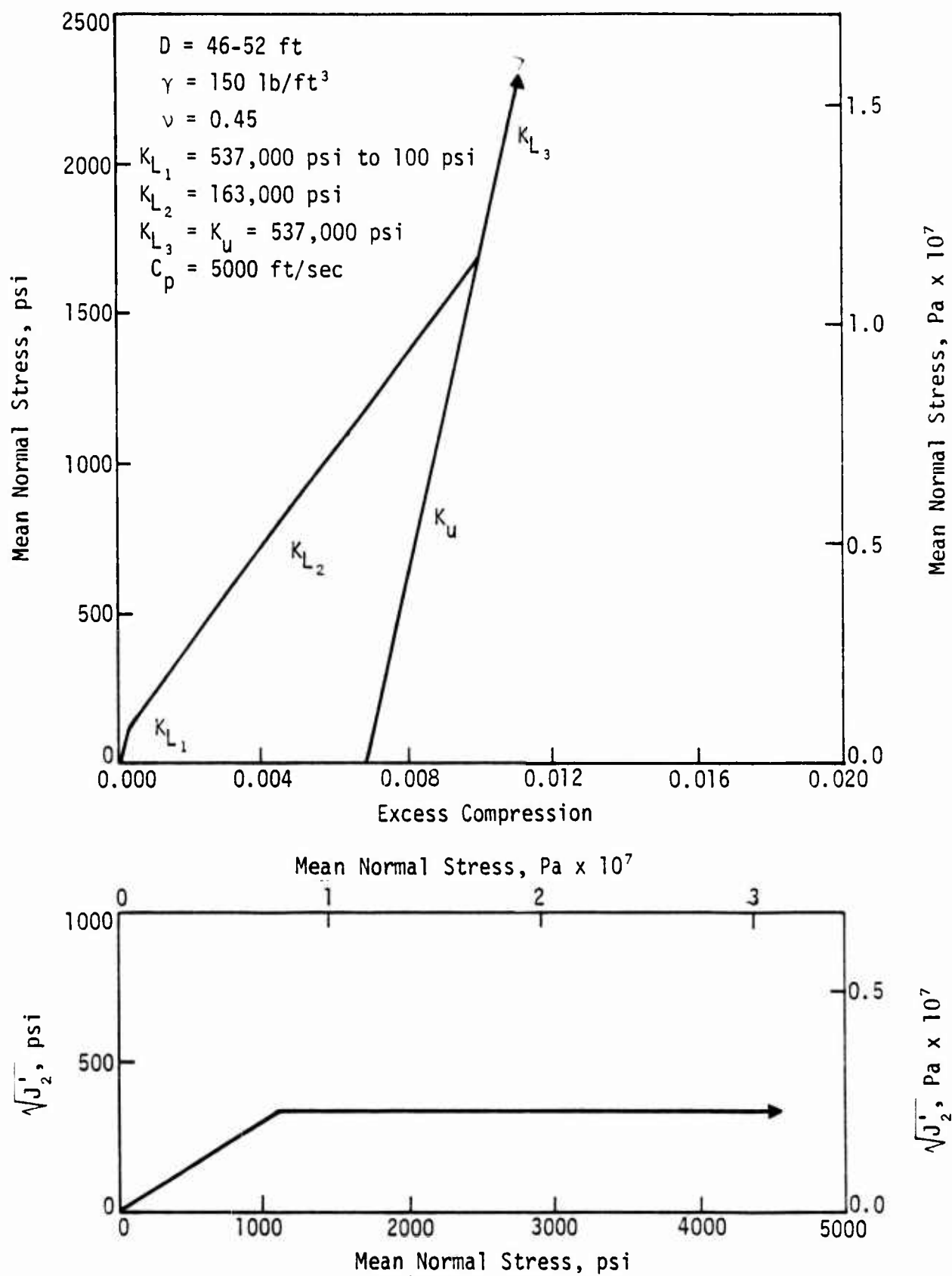
Figure 16. Material Properties of Underclay

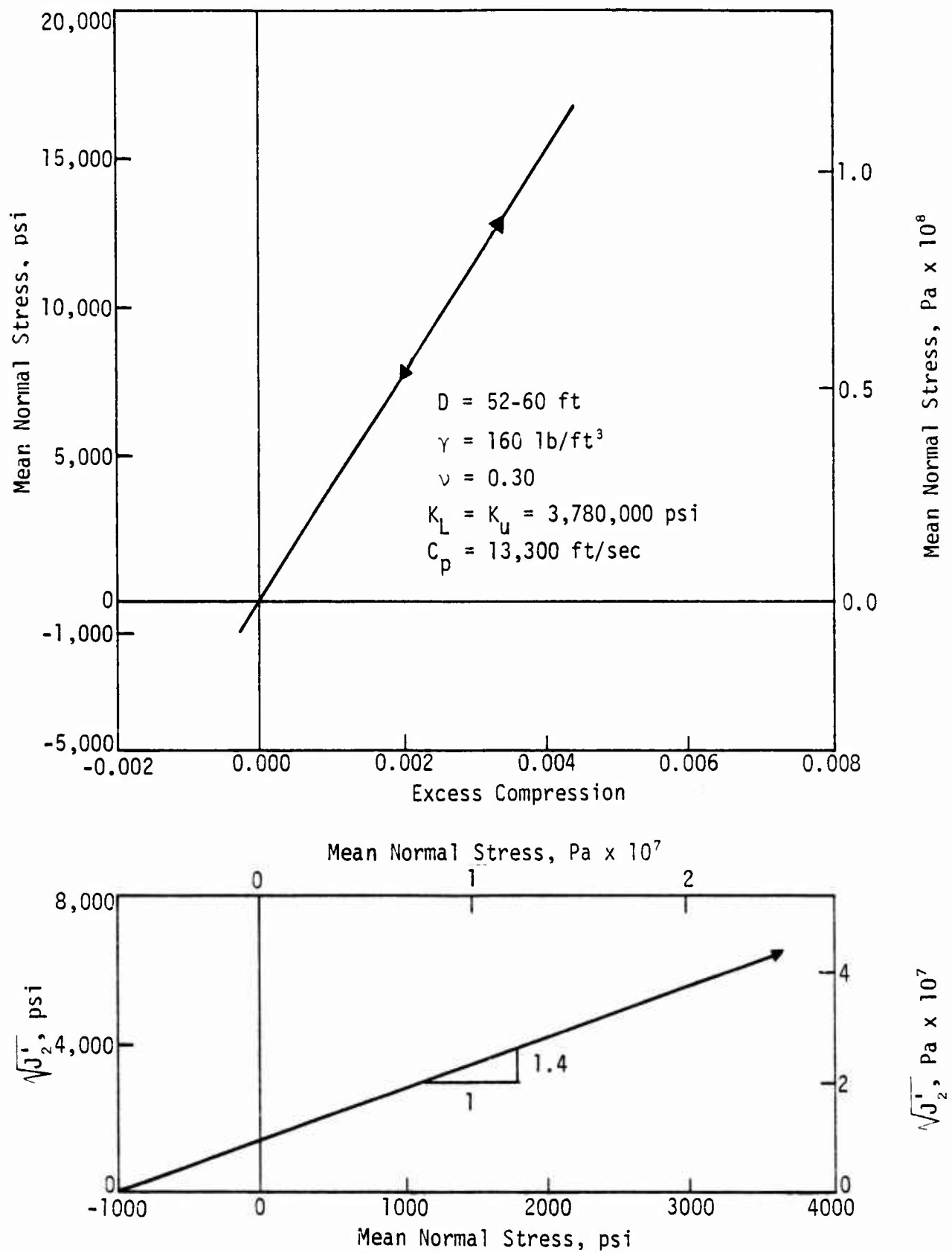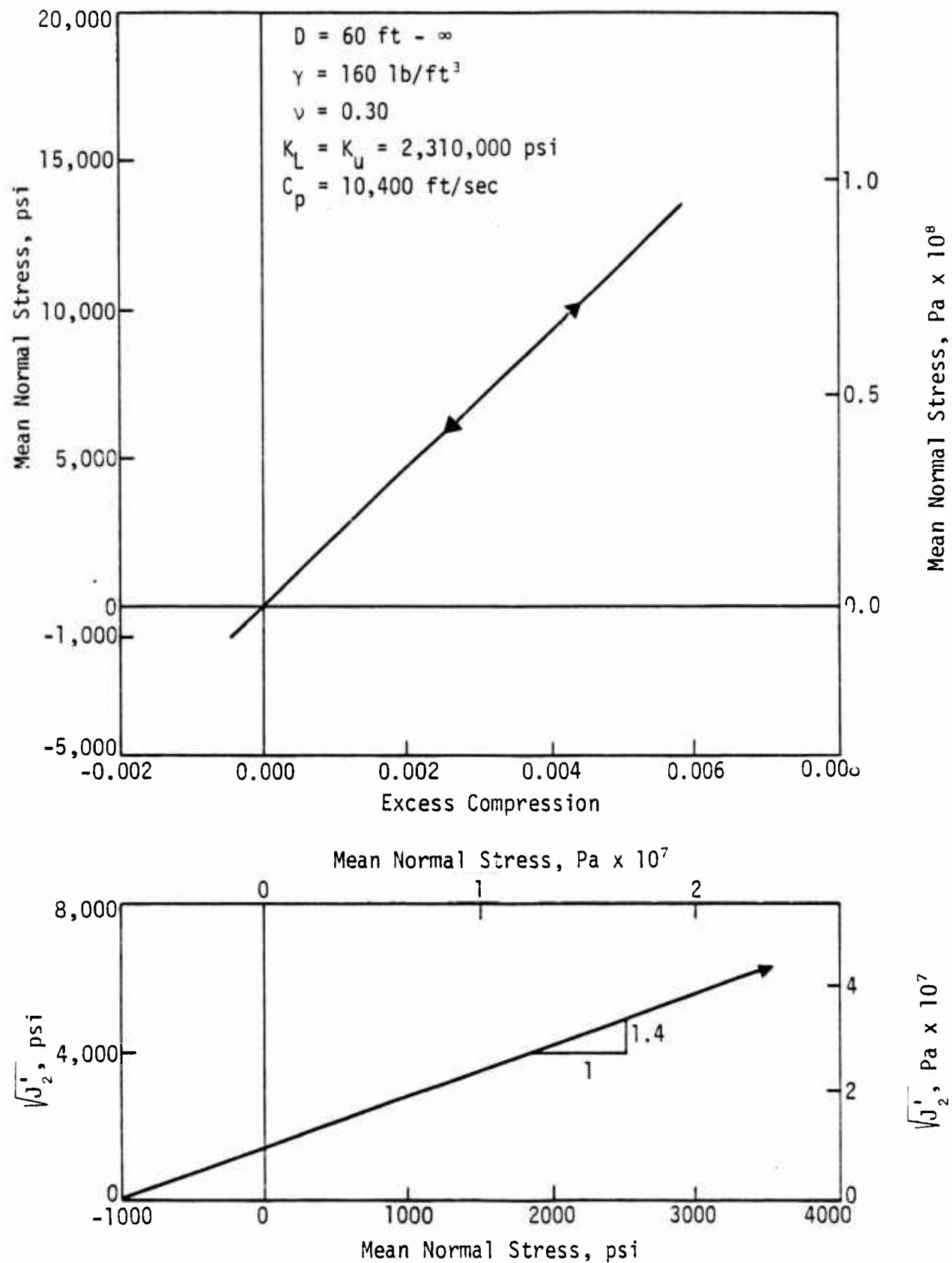Figure 17. Material Properties of Deep Limestone

33

Figure 18. Material Properties of Basement Composite

34

SECTION 4
ANALYSIS OF CALCULATION HPI-3.4

The BLEST/HEST pressure functions and propagation velocity defined by the equations and data in section 2 were used in calculation HPI-3.4. The HPI-3.4 geology is shown in figure 8, profile 8, and the material properties are given in figures 10 through 18. As a result of an investigation of the effect of zone size on calculational accuracy (ref. 6), the region of primary concern (from the 190- to the 800-ft range to a depth of 60 ft) was zoned with a finer mesh than that used in the previous calculations. Mesh size was 2.5 ft horizontally by 2 ft vertically except in the limestone layers, in which the depth was 1 ft. Outside this region, zones expanded arithmetically. From 0 to 190 ft, zones decreased horizontally from 7.5 to 2.5 ft in 38 zones at a rate of 0.135135 ft per zone; from 800 to 1000 ft, they expanded horizontally from 2.5 to 7.5 ft in 40 zones at a rate of 0.128205 ft per zone. From the 60-ft depth to the bottom of the problem area, zones expanded vertically at a rate of 0.116279 ft per zone.

FIRST-ARRIVAL CONTOURS

Contours developed from the experimental data, the HPI-3.4 data, and the TOAC Program, which calculated the time-of-arrival using the seismic velocities and geology described earlier in this report, are shown in figure 19. It can be seen that differences result from waveform interpretation and contour evaluation. Differences also result because of scatter in the experimental data; this scatter was as much as 3 msec for the same range and depth but different cross ranges. Additional differences were introduced because of the assumption of homogeneous, horizontally layered geology in the TOODY II and TOAC Codes, when the actual geology was nonhomogeneous with a 2-percent grade. The greatest factor which contributed to contour variation was the interpretation used to establish the contours through the data. Because of this a number of different contours which would fit the data adequately could be drawn. The contours shown in figure 19 are the result of several iterations of contour plotting and they reflect the best fit. It should be pointed out that the

35
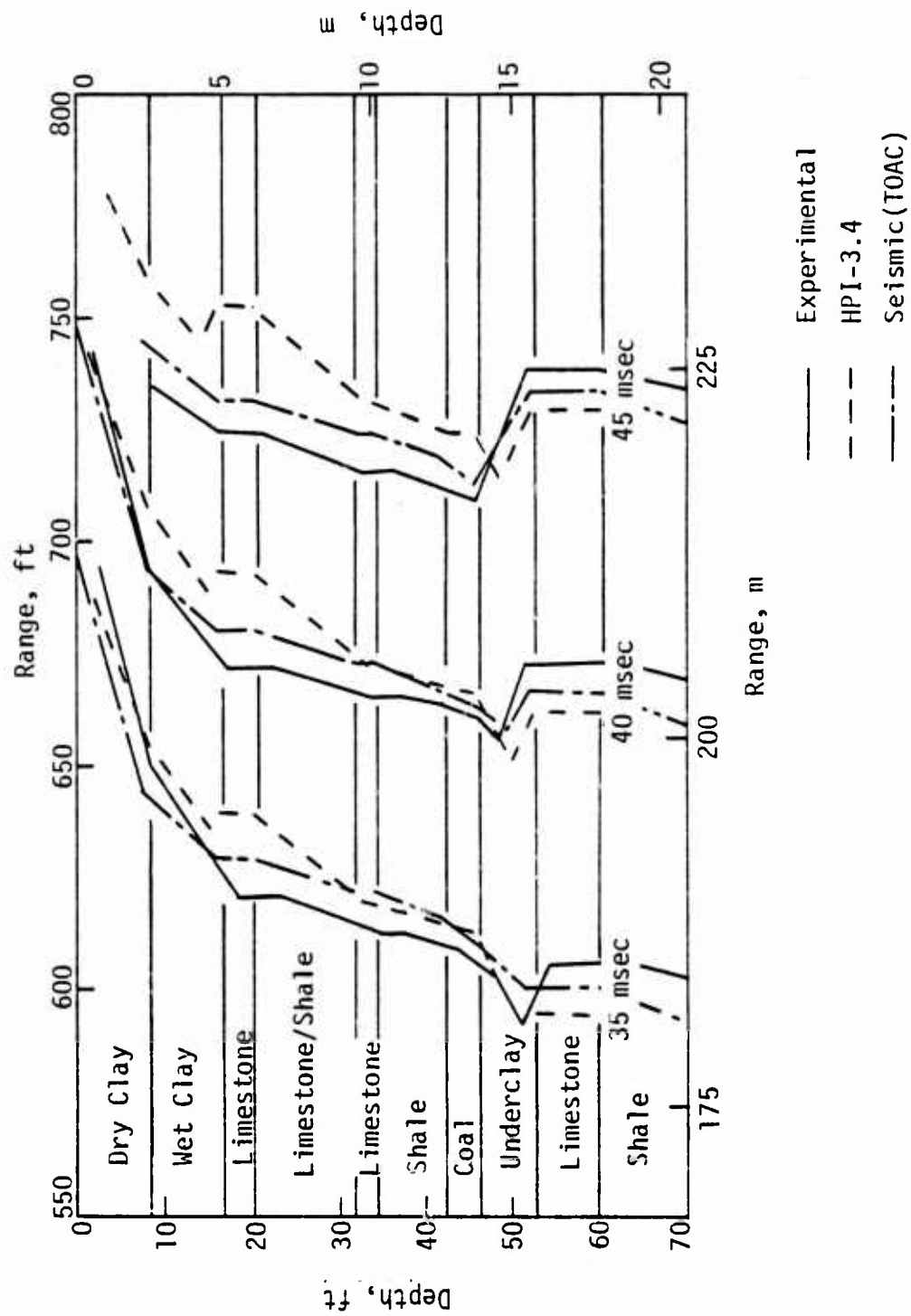
Figure 19. Seismic (TOAC), Calculation HPI-3.4, and Experimental First-Arrival Contours

headwaves emanating from the outrunning signal at 16 to 20 ft and at 52 to 60 ft were not indicated in the calculated waveforms by initial upward motion because of numerical difficulties, the resolution power of the finite-difference mesh, and the inability of the code to orthogonally transform motion.

Time contours of peak vertical velocity for the experiment and the calculation are shown in figure 20. The agreement is fairly good down to a depth of 45 ft, at which major differences occur. Timing of the calculated peak lags the experimental data; this indicates that the slope of the upper portion of the hydrostat could be increased to account for a higher propagation velocity or that the BLEST effects (i.e., outrunning phenomenon) were not accurately produced by the code. Another possible cause is that in the experiment the peak selected in the deeper materials was a result of the BLEST or upstream loading, and the peak selected in the calculation was a result of the HEST loading or locally induced. The upstream effects may have been lost in the waveform because of either timing or insufficient magnitude of the calculated upstream signal component. It is impossible at this time to determine what was in error.

Figure 21 is a contour plot of the times of peak horizontal (outward) motion for the calculation and the experiment. These contours indicate good timing between the 16- and 46-ft depth but poor timing above and below this zone. Part of the difference is due to the fact that the arrival of absolute peak was plotted, even though it may have been induced by different phenomena. The peak horizontal (outward) velocity in the experiment was generally associated with the incident wave, whereas in the calculation the peak in some instances occurred late and was due to the superposition of several waves. Also, with the dry and wet clays (0 to 16 ft), the code appears to have difficulty in transforming the completely vertical motion produced by the surface airblast to horizontal motion.

PEAK VELOCITY ATTENUATIONS

Vertical velocity attenuations versus depth for various ranges for the HPI-3.4 calculation, previous calculations, and the experiment are presented in appendix A. Analysis of these plots reveals that (1) the peak velocity at the

37
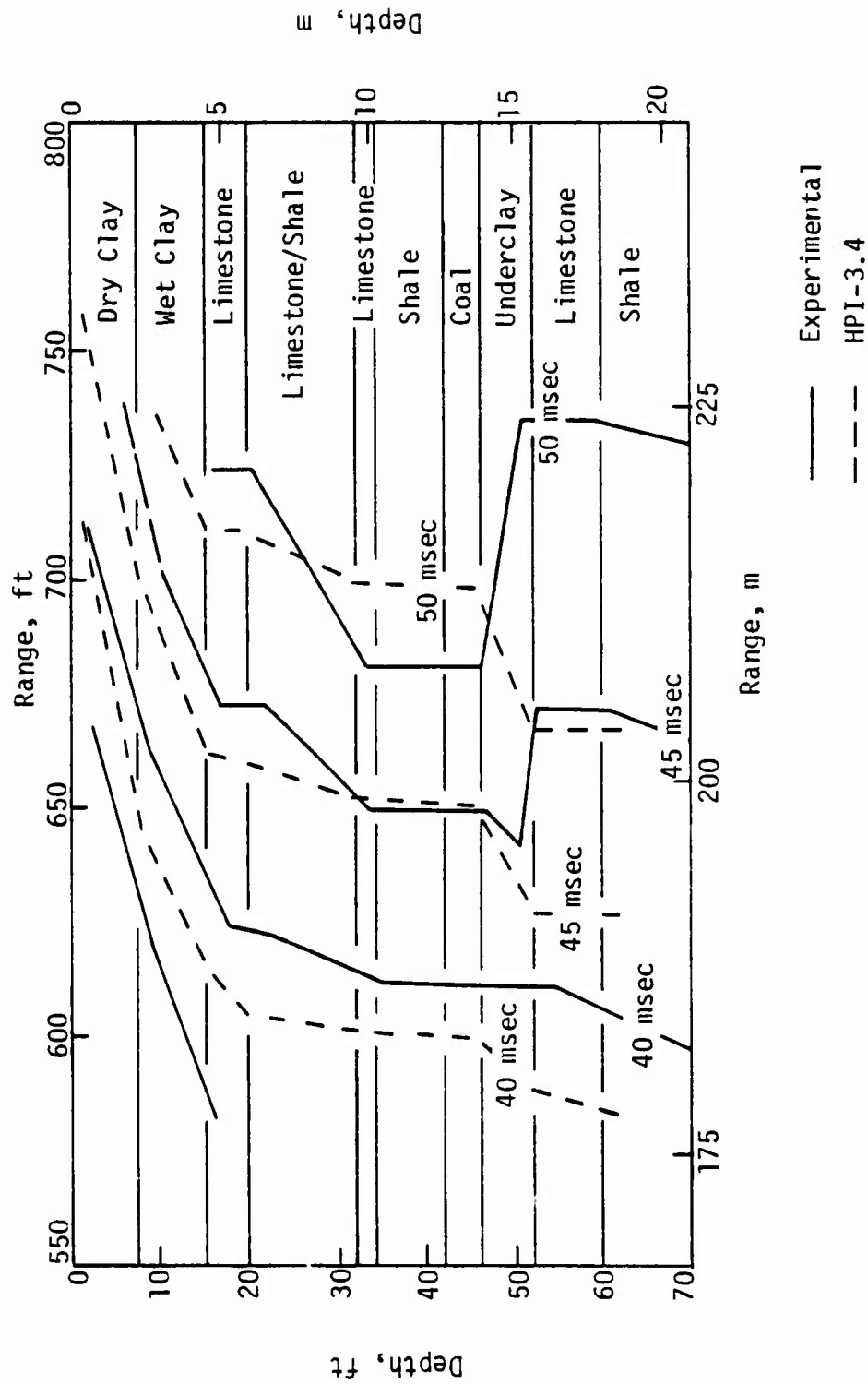
Figure 20. Calculation HPI-3.4 and Experimental Times of Peak Vertical Contours
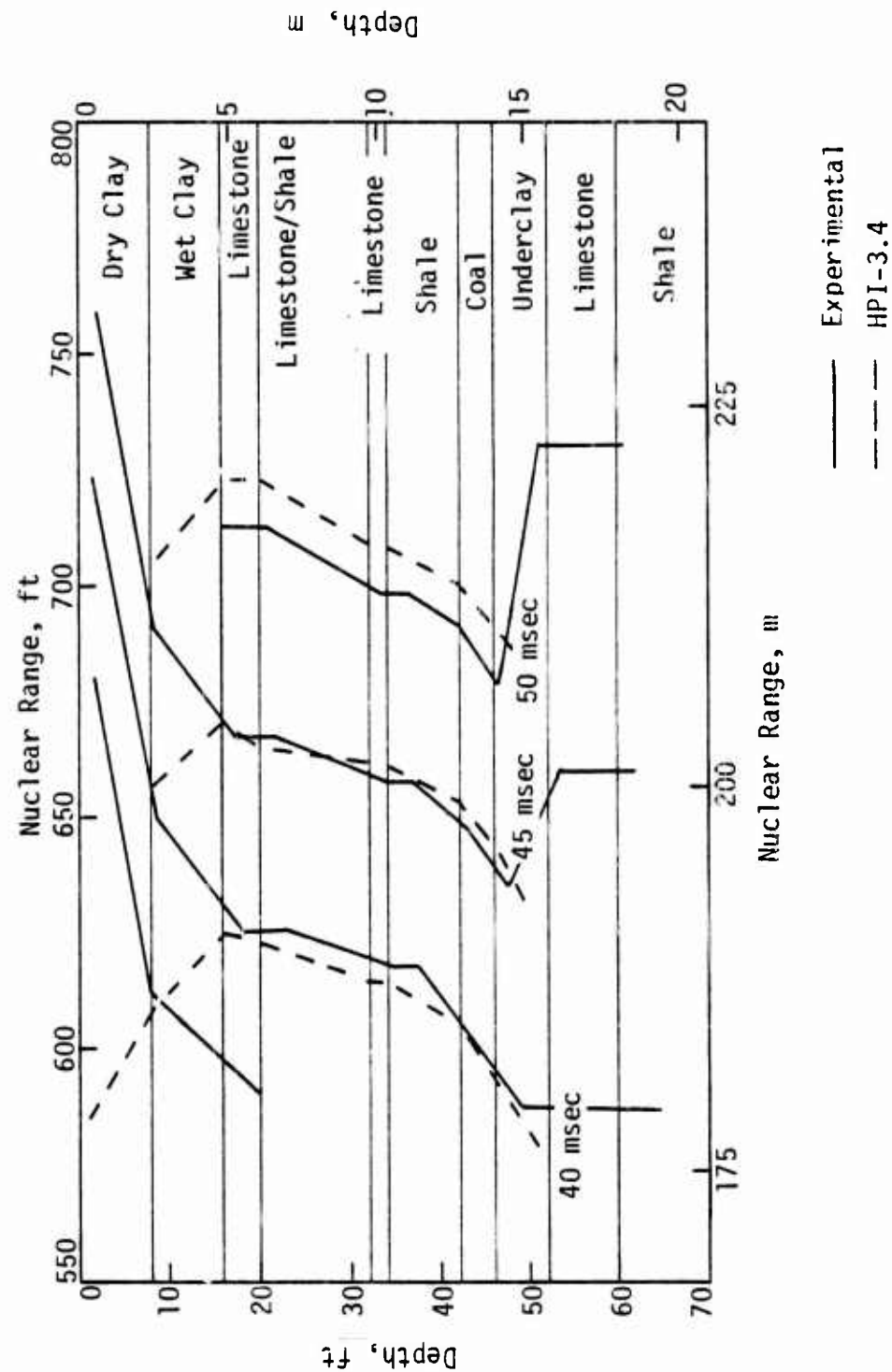
Figure 21. Calculation HPI-3.4 and Experimental Times of Peak Horizontal Contours

surface could be decreased approximately 10 to 15 ft/sec and attenuated less with depth from 0 to 16 ft, and (2) the peak velocity below 16 ft was approximately constant in the experiment, and the calculation overestimated the velocities at the 585-ft range but agreed fairly well at greater ranges.

Analysis of the peak horizontal velocity attenuations cannot give conclusive results because of the experimental data scatter, which was much greater than that for the vertical velocities. However, some very general statements can be made about the comparison of experimental and calculated data. In the near-surface materials (0 to 16 ft) the calculated horizontal motion was approximately 50 percent low, consistently, throughout the HEST region. Below the first limestone layer (16 to 20 ft) and above the deepest limestone layer (52 to 60 ft), the horizontal velocities attenuated with range too rapidly compared with the experimental velocities. At the 585-ft range the horizontal velocities were underpredicted by 30 percent, and this increased to 60 percent at the 725-ft range. As mentioned earlier, it appears that the code poorly predicts horizontal motions which result from a perfectly vertical pressure function. Whether this is due to the equation-of-state in the code, the assumption of isotropy, or poor modeling of BLEST and other upstream effects remains to be studied.

An interesting characteristic of the attenuation of both peak vertical and horizontal velocity with range for a given depth is the large peak at the 585-ft range and the roughly constant peaks for other ranges (fig. 22). The 585-ft range responds to the last BLEST impulse zone, which has a considerably larger initial impulse than the HEST (12 psi-sec as compared with 6 psi-sec for the first 8 msec of HEST). This character of the attenuation reflects both the discontinuity in the type of surface loading between the HEST and BLEST and the relatively uniform loading across the HEST. Analysis of upstream and locally induced effects remains to be studied.

WAVEFORMS

A study of the vertical and horizontal waveforms (appendix B) supports the previously mentioned points on contours and attenuations. By waveform comparisons, additional information was gained concerning the frequency content and major

40
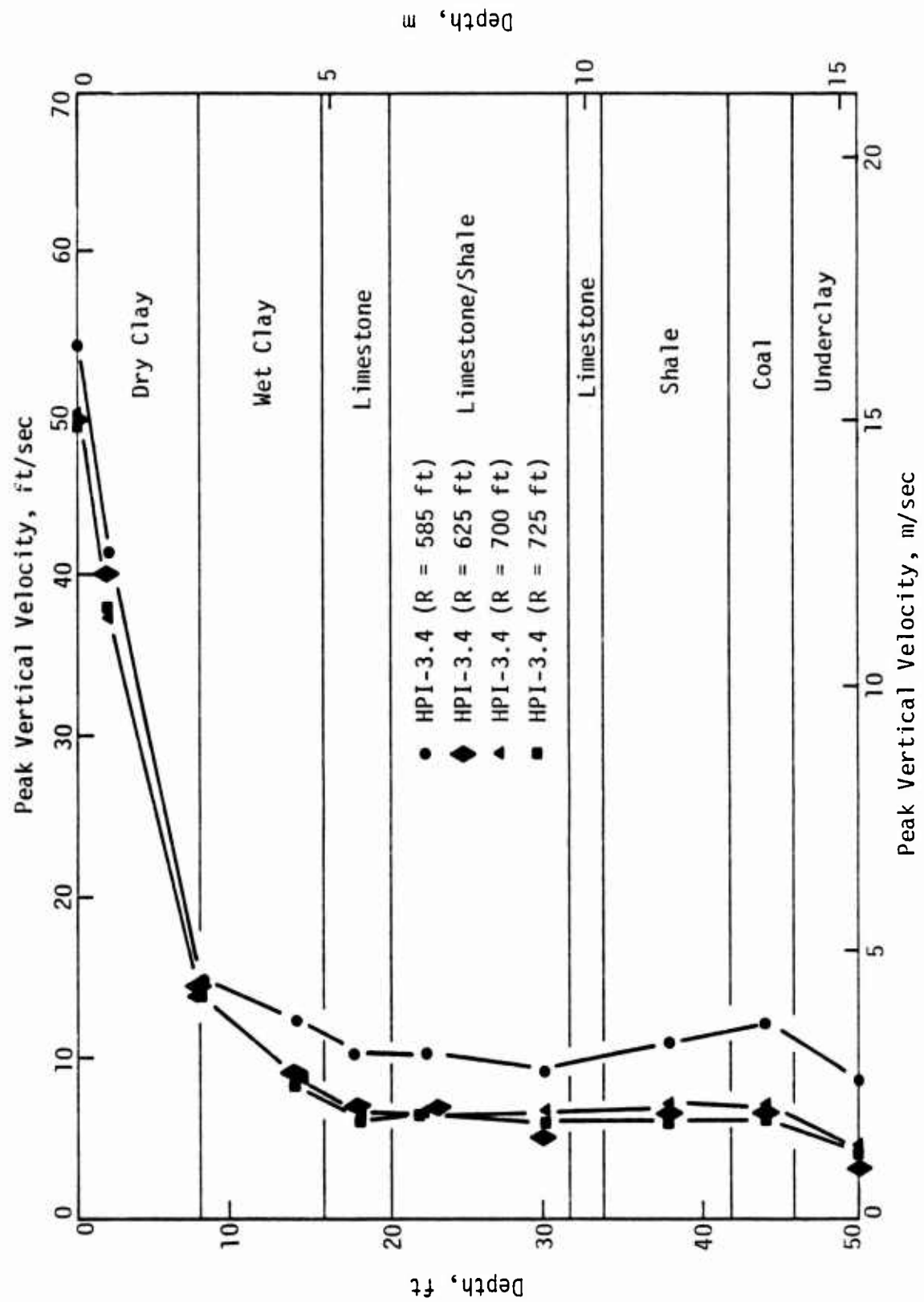
Figure 22. Calculation HPI-3.4 Peak Velocity Attenuations with Range (1 of 2)
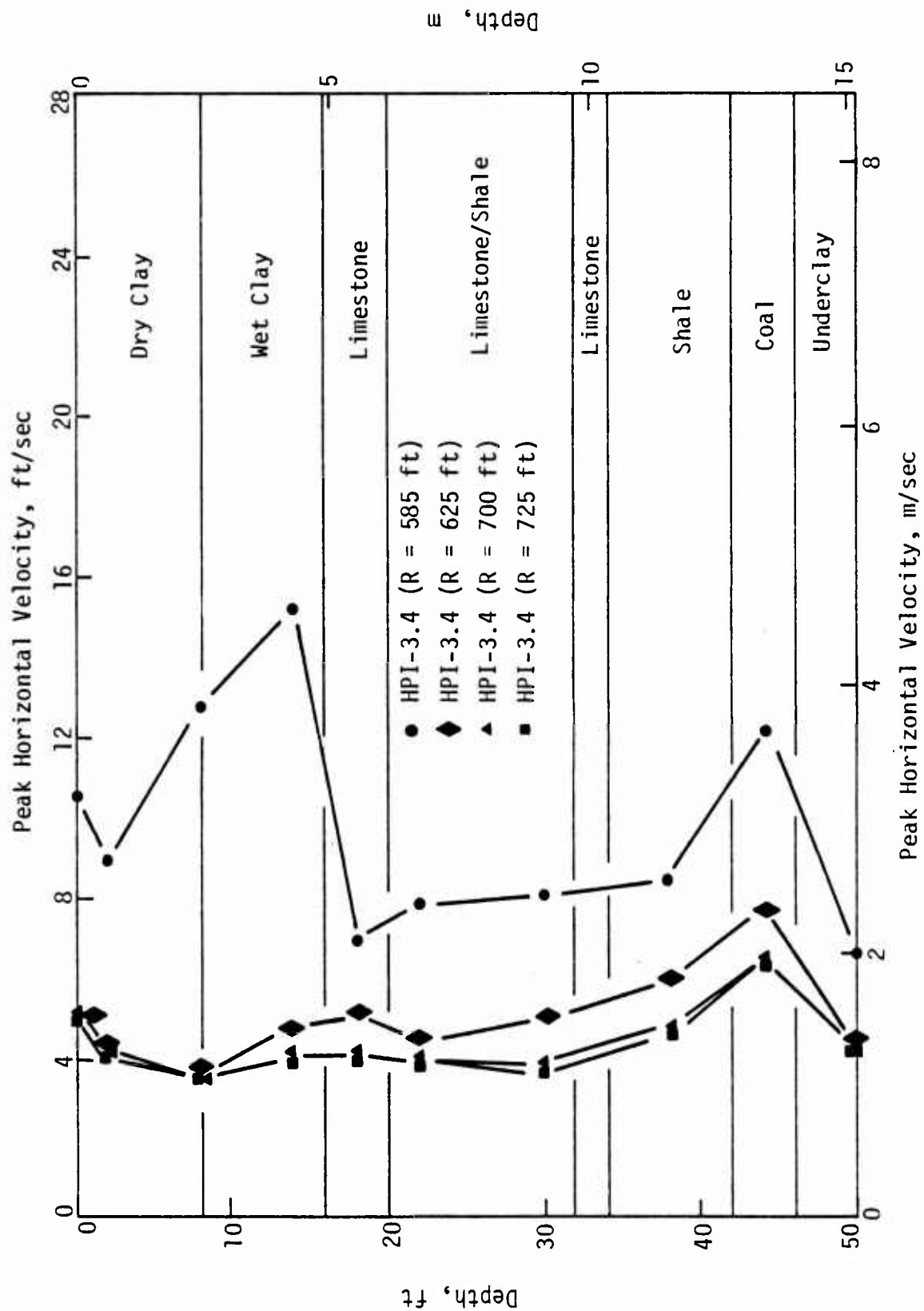
Figure 22.   Calculation HPI-3.4 Peak Velocity Attenuations with Range (2 of 2)

characteristics of the waveform. The vertical waveforms were fairly good and were greatly improved compared to the pretest results with respect to the timing of first motion, peaks, and frequency content. Because of data scatter and inconsistent comparisons of horizontal waveforms, no definitive statement can be made concerning the accuracy of the calculation. However, the horizontal waveforms from the HPI-3.4 calculation were as good as, and in some cases better than, the waveforms from the pretest calculation.

MODIFICATION FOR SMI INPUT

One of the objectives of this post-test calculation of HARD PAN I Event 3 was to generate input for the SMI3D Code, which is used to calculate structural responses. In addition to the actual data from the HPI-3.4 calculation, empirically modified data which matched the experimental data more accurately were used. Since time-of-arrival data appeared to be relatively accurate, these modifications amounted to changing the magnitude of the velocities. This was done by applying multiplication factors which were a function of depth to the entire velocity/time history. These multiplication factors were derived from trying to match peak vertical and horizontal velocities throughout the entire HEST region. For this reason, agreement was better at some ranges than at others. Figure 23 shows peak vertical and peak horizontal attenuations for the experimental, calculated, and *adjusted* calculated data.
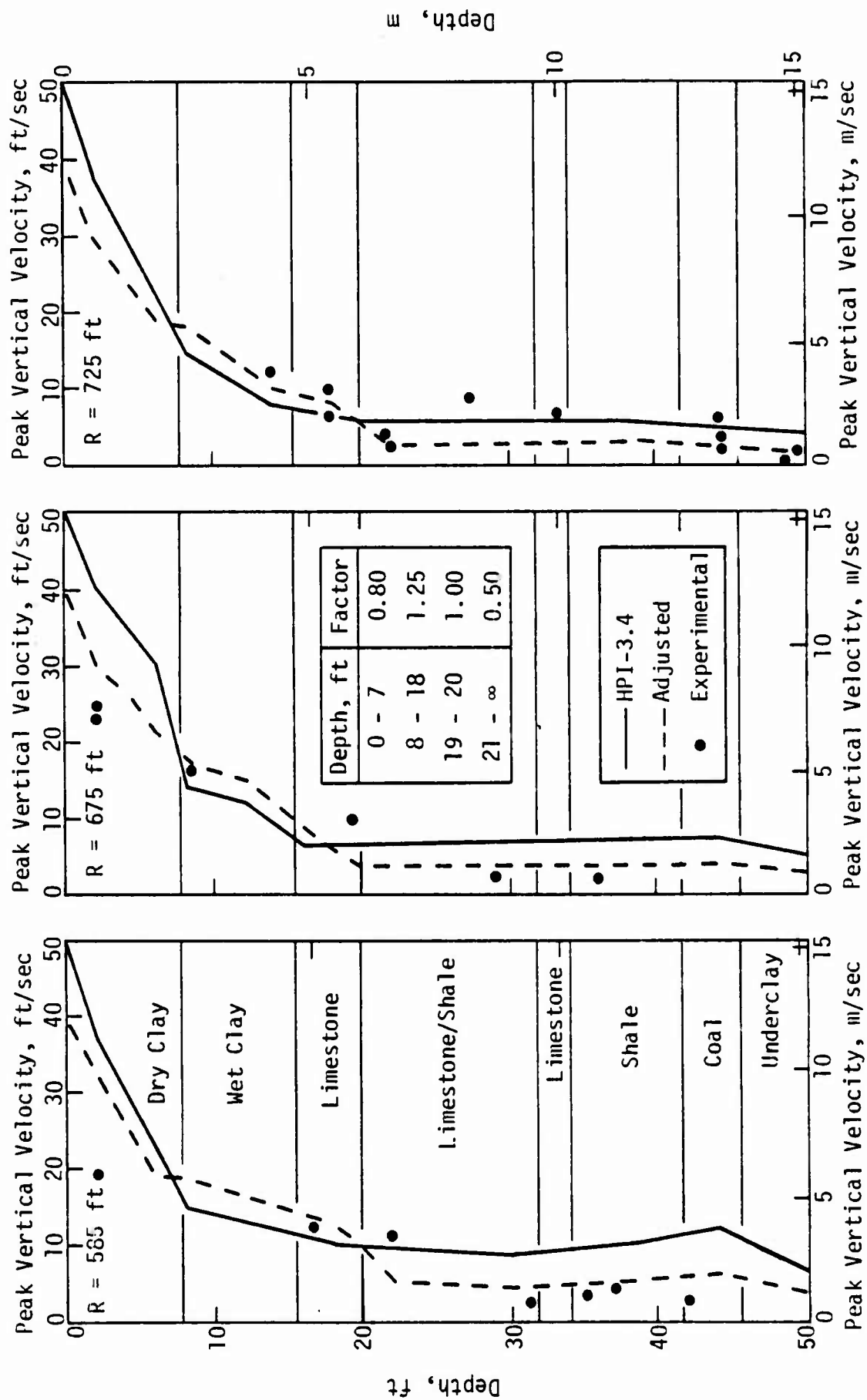
Figure 23. Peak Velocity Attenuations with SMI Adjustment Factors (1 of 2)
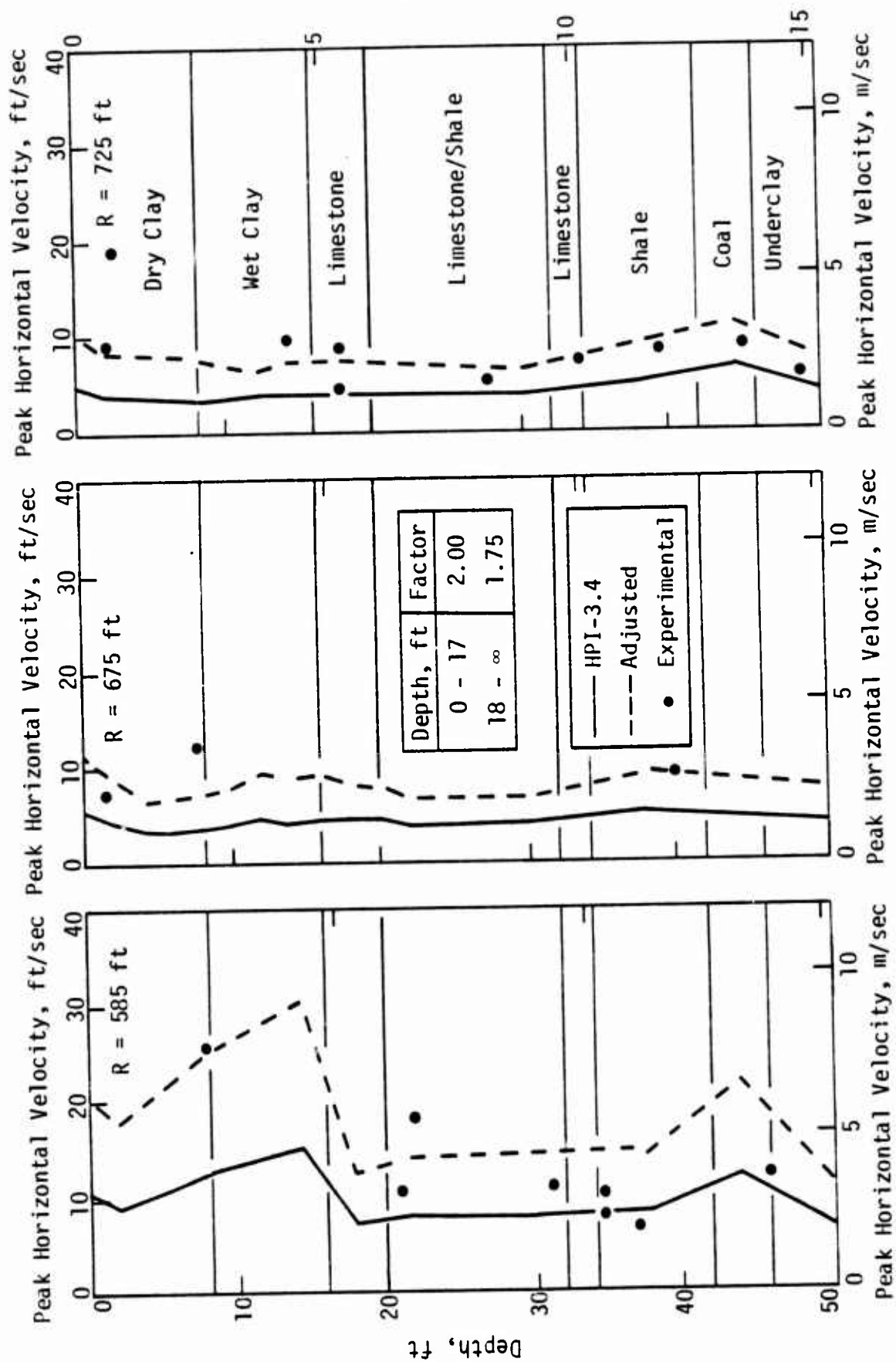
Figure 23. Peak Velocity Attenuations with SMI Adjustment Factors (2 of 2)

45

SECTION 5
CONCLUSIONS AND RECOMMENDATIONS

The BLEST pressure function used in the pretest and posttest calculations is accurately modeled based on the impulse values calculated from a limited number of experimental BLEST pressure records. However, peak vertical velocity attenuations from the HPI-3.4 calculation indicate that the BLEST pressure functions and/or the contribution of BLEST effects to the waveform are not accurately duplicated. Future research will be directed toward separation of the BLEST or upstream and HEST or locally induced effects, both in the calculated and in the experimental waveforms, to determine their significance.

A new HEST pressure function and propagation velocity were developed based on comparison of pretest pressure functions and experimental data; these were incorporated in the posttest input. Results from calculation HPI-3.4 indicate that the HEST is accurately modeled based on agreement of vertical velocity attenuations in the down-range region with the experimental data.

Contours were developed from the time of the first arrival indicated on the experimental integrated accelerometer (i.e., velocity) plots. These contours were then studied as to their applicability to each of the various geologies (fig. 8). From this study, profile 8 and the contours shown in figure 9 are recommended.

New material models were developed; these models incorporate *seismic toes* on the hydrostat corresponding to the seismic velocity determined from the experimental contours extending to a minimum pressure level of 50 psi for dry clay and as high as 200 psi for other materials. Thus, the time of first arrival in the calculation matched the time of first arrival in the experiment, and it was expected that this would aid in more accurate phasing of other ground-motion phenomena. With materials such as the limestone and basement composite, a linearly elastic hydrostat corresponding to the seismic velocity could be used. The upper portion of the hydrostat and the unloading slope correspond to the seismic velocity, and hysteresis is determined by passing the unloading curve through the lock-up point. The contour and waveform comparisons indicate that the

46

timing of first arrival is fairly accurate, especially for vertical waveforms. Calculated horizontal waveforms are in the poorest agreement with the experimental data; this may be the result of inaccurate duplication of the BLEST or upstream effects or the inability of the code to transform vertical motion to horizontal motion.

Despite isolated differences which exist between the calculated and experimental data, the HPI-3.4 calculation is a significant improvement over the pretest calculations and posttest calculation HPI-3.3. The results of this calculation indicate that both laboratory and in-situ properties are necessary for adequate in-situ modeling of soil stress/strain properties and prediction of ground-motion phenomena.

REFERENCES

1. Baird, Glenn T., Rudeen, David K., and Higgins, Cornelius J., *Pretest, Two-Dimensional, Free-Field Calculation of HARD PAN I, Event 3: Calculations HPI-3.1 and 3.2*, DE-TN-77-002, Air Force Weapons Laboratory, Kirtland Air Force Base, New Mexico (to be published).

2. Rudeen, David K., *Post-Test, Two-Dimensional, Free-Field Calculation of HARD PAN I, Event 3: Calculation HPI-3.3*, DE-TN-77-003, Air Force Weapons Laboratory, Kirtland Air Force Base, New Mexico (to be published).

3. Pinker, Robert W., Capt., *HARD PAN I-3 Geologic and Seismic Profiles*, memorandum, Air Force Weapons Laboratory, Kirtland Air Force Base, New Mexico, 17 January 1975.

4. Dzwilewski, Peter T., Lt., *Stress-Strain Relationships for Hard Pan Soils and Rocks*, DE-TN-75-022, Air Force Weapons Laboratory, Kirtland Air Force Base, New Mexico, December 1975.

5. Bertholf, L. D., and Benzley, S. E., *TOODY II - A Computer Program for Two-Dimensional Wave Propagation*, SC-RR-68-41, Sandia Laboratories, Albuquerque, New Mexico, November 1968.

6. Higgins, Cornelius J., and Rudeen, David K., *Effects of Zone Size, Aspect Ratio, and Artificial Viscosity on the Accuracy of Ground-Motion Calculations with Finite-Difference Codes*, Technical Note, Air Force Weapons Laboratory, Kirtland Air Force Base, New Mexico (in review).

7. Ehrgott, John Q., *Preshot Free-Field Calculational Properties for Project HARD PAN I, Event 3*, U.S. Army Engineer Waterways Experiment Station, Soils and Pavements Laboratory, Vicksburg, Mississippi, March 1975.

8. Doran, J., *HARD PAN I Test Series and Instrumentation Plans*, AFWL-TR-75-249, Vol. 1, Air Force Weapons Laboratory, Kirtland Air Force Base, New Mexico, December 1975.

9. Pinker, Robert W., Capt., *Geology and Seismology for the HARD PAN I Test Site, Trading Post, Kansas*, Air Force Weapons Laboratory, Kirtland Air Force Base, New Mexico (in preparation).

10. Fedock, Joseph J., *CIST 14 Analysis and Derivation of Dynamic Properties for Site M-28, Wing VI*, Technical Note, Air Force Weapons Laboratory, Kirtland Air Force Base, New Mexico, in review (SRD).

11. Higgins, Cornelius J., *CIST 13 Analysis and Derivation of Properties for Site F-9, Wing II*, Technical Note, Air Force Weapons Laboratory, Kirtland Air Force Base, New Mexico, in review (SRD).

APPENDIX A

PEAK VELOCITY ATTENUATION PLOTS

53

Depth, m

Peak Horizontal Velocity, ft/sec

Dry Clay

Wet Clay

Limestone

Limestone/Shale

Limestone

Shale

Coal

Underclay

Peak Horizontal Velocity, m/sec

Experimental (R = 696-699 ft)
HPI-3.1 (R = 700 ft)
HPI-3.2 (R = 700 ft)
HPI-3.4 (R = 700 ft)

Depth, ft

54

Peak Horizontal Velocity, ft/sec

Peak Horizontal Velocity, m/sec

Depth, m

Depth, ft

Dry Clay

Wet Clay

Limestone

Limestone/Shale

Limestone

Shale

Coal

Underclay

● Experimental (R = 725 ft)
■ HPI-3.1 (R = 725 ft)
▲ HPI-3.2 (R = 725 ft)
○ HPI-3.4 (R = 725 ft)

55

APPENDIX B
WAVEFORM PLOTS

The plots in this appendix are labeled as described in the following examples:

- Experimental Record: 8-33-2 AV #117

    8 - Range from front of HEST cavity (ft)

    33 - Cross range (ft)

    2 - Depth (ft)

    AV - Integrated accelerometer with vertical (V)
         or horizontal (H) orientation

  #117 - Gage number

- Calculated Time History: HPI-3.4 (585-2) (.8X)

    HPI-3.4 - Calculation number (Fourth calculation of
              HARD PAN I Event 3)

      585 - Range from ground zero (ft)

        2 - Depth (ft)

      .8X - SMI adjustment factor

For vertical velocity, down is positive; for horizontal velocity, away from ground zero is positive.

The calculated data are based on nuclear ground zero; the experimental data begin at the HEST region. Therefore, a distance of 575 ft must be added to the x-coordinate of the experimental data to compare equivalent range data.
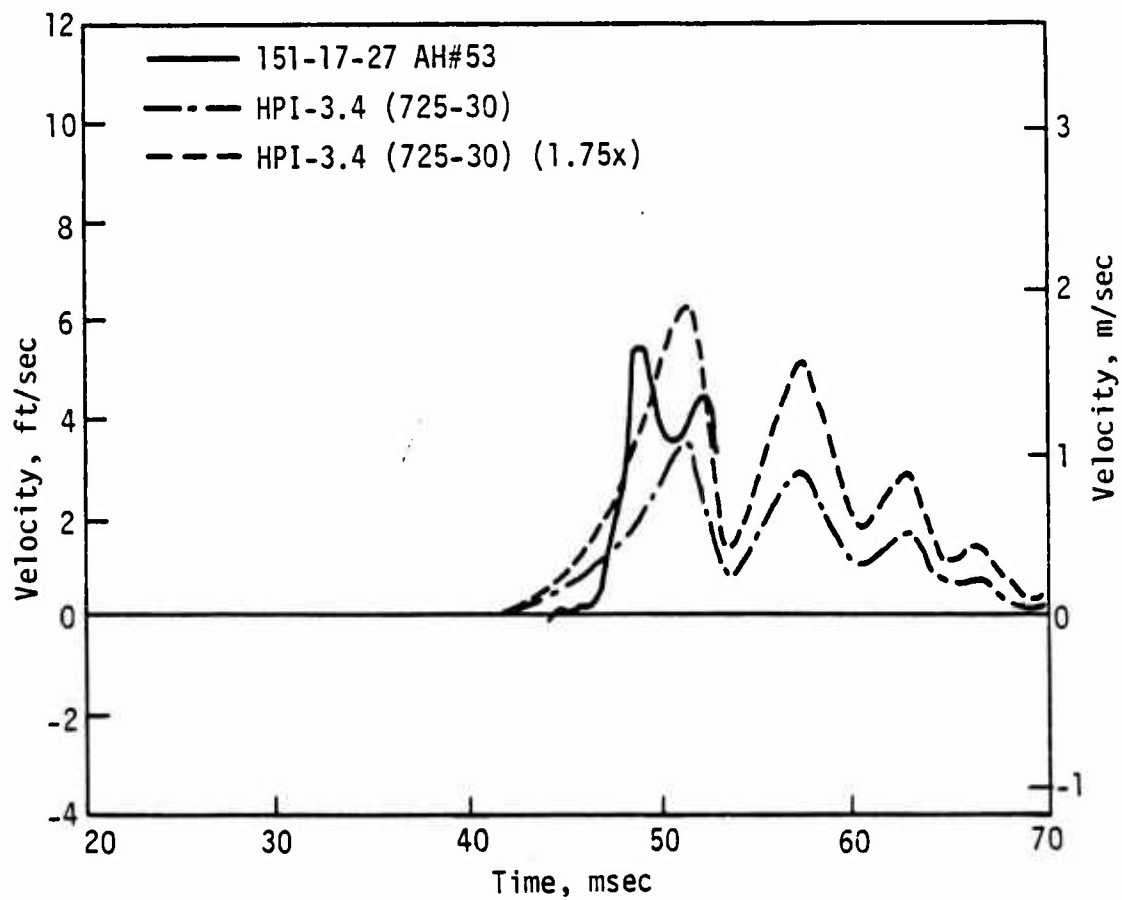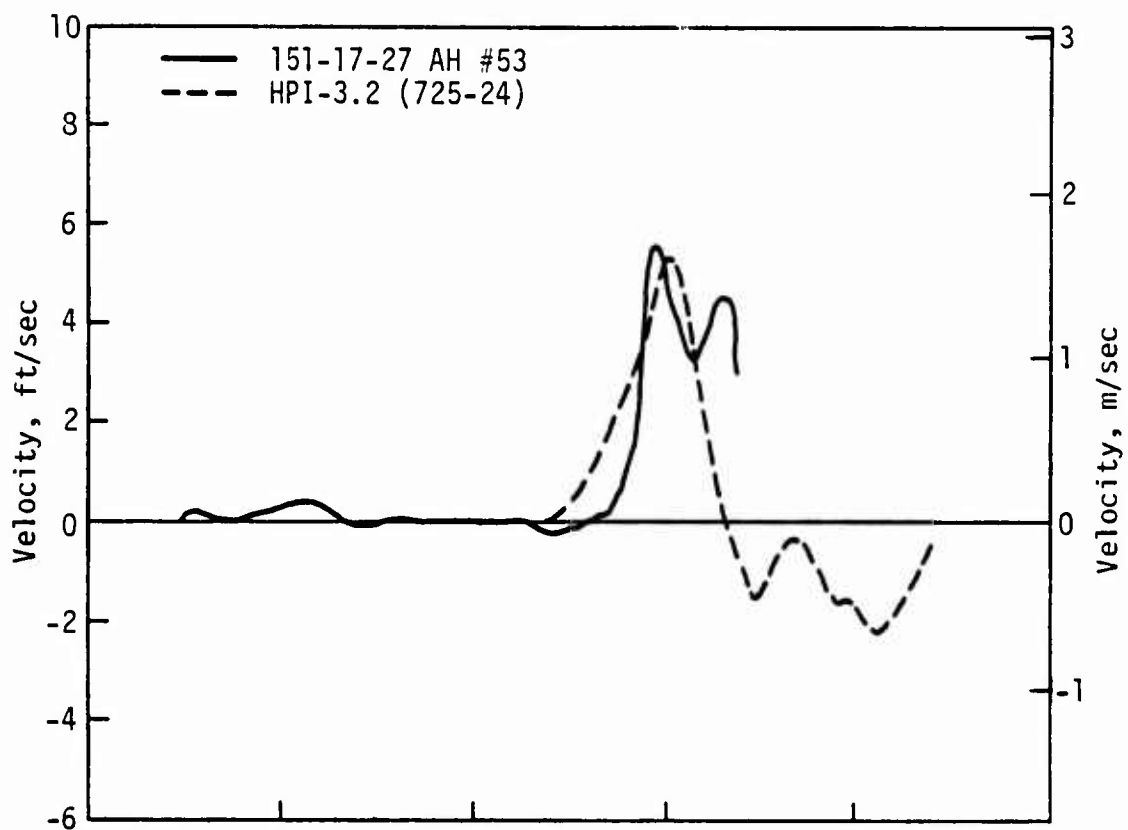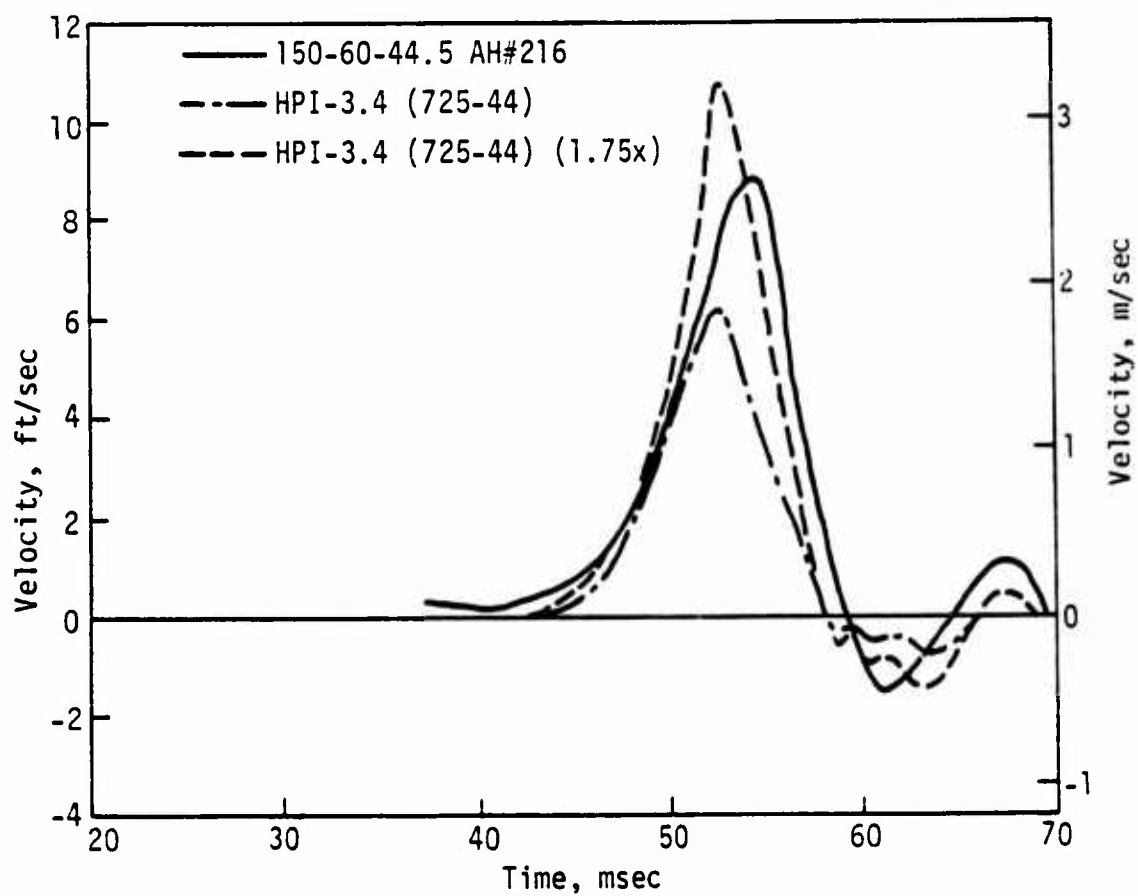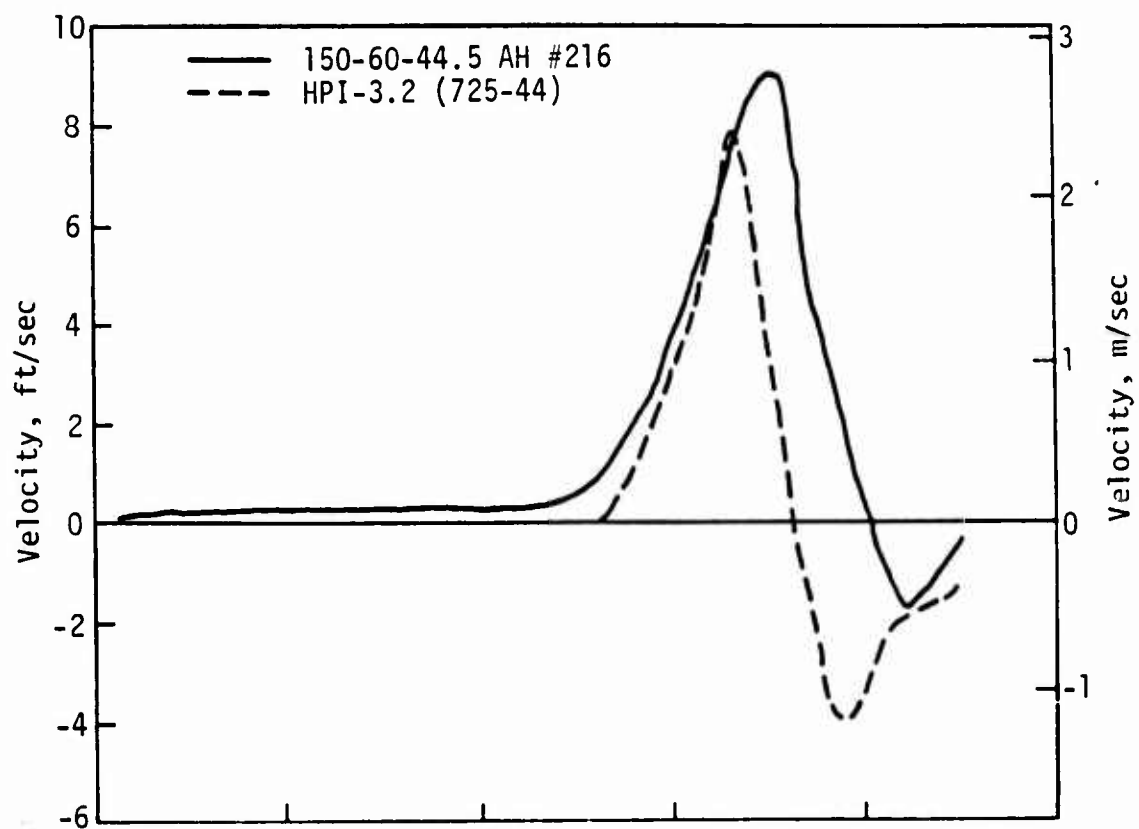
57

64
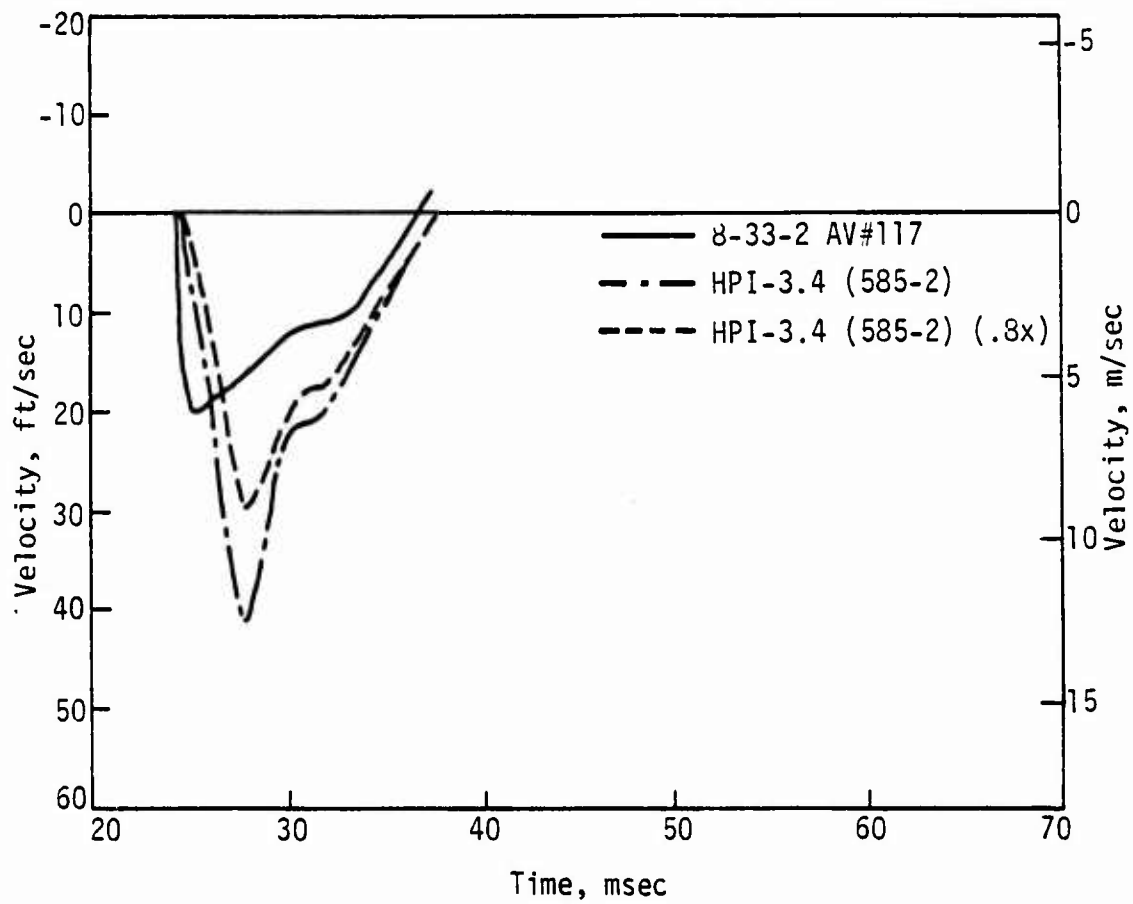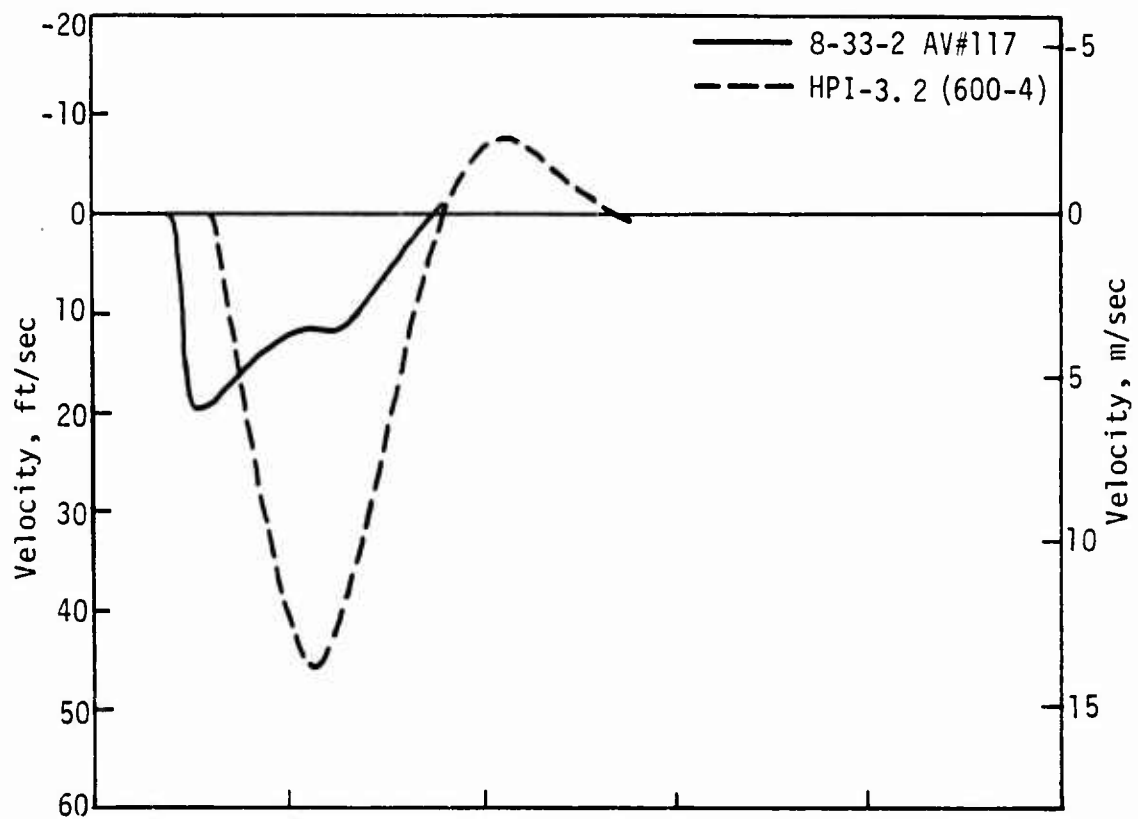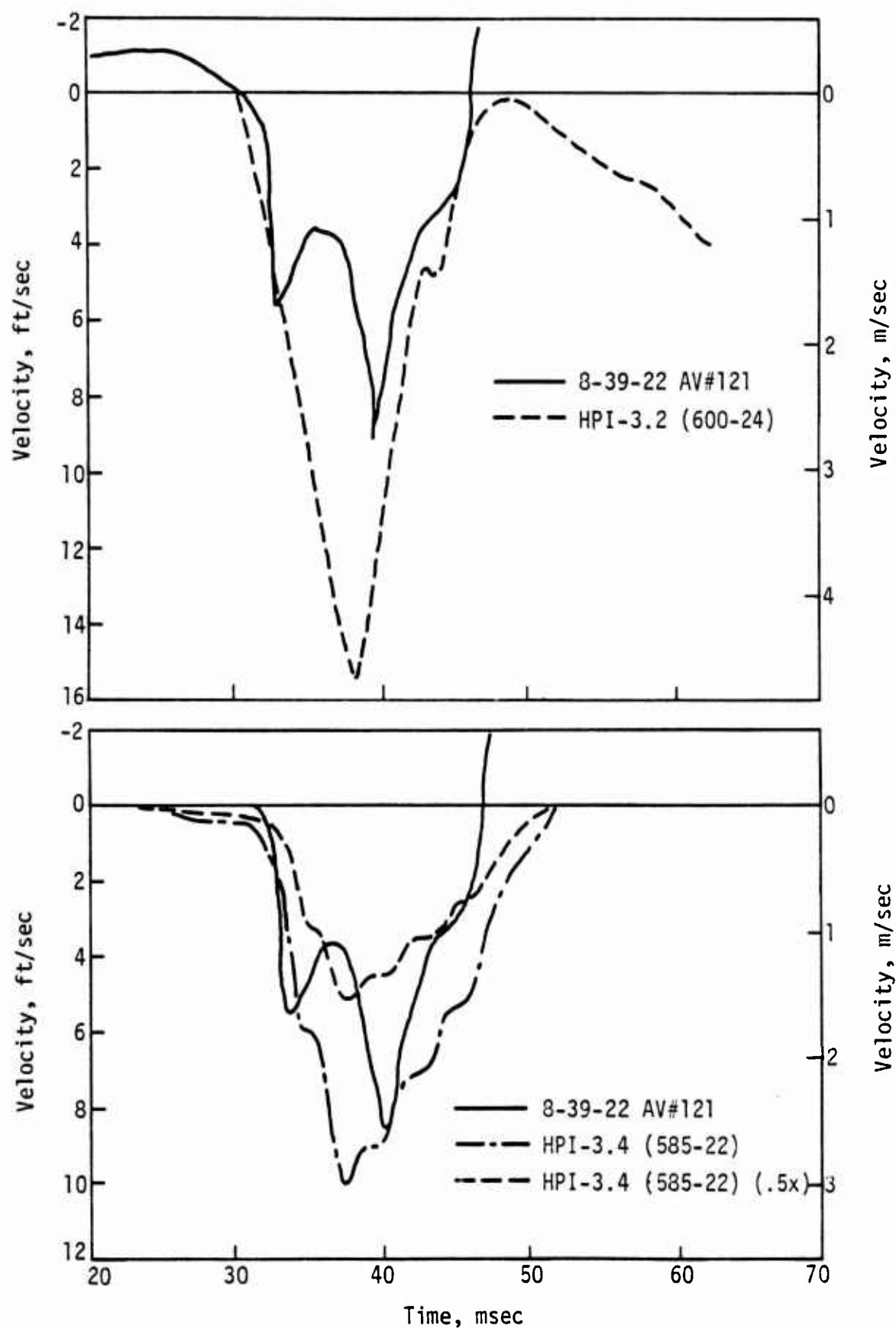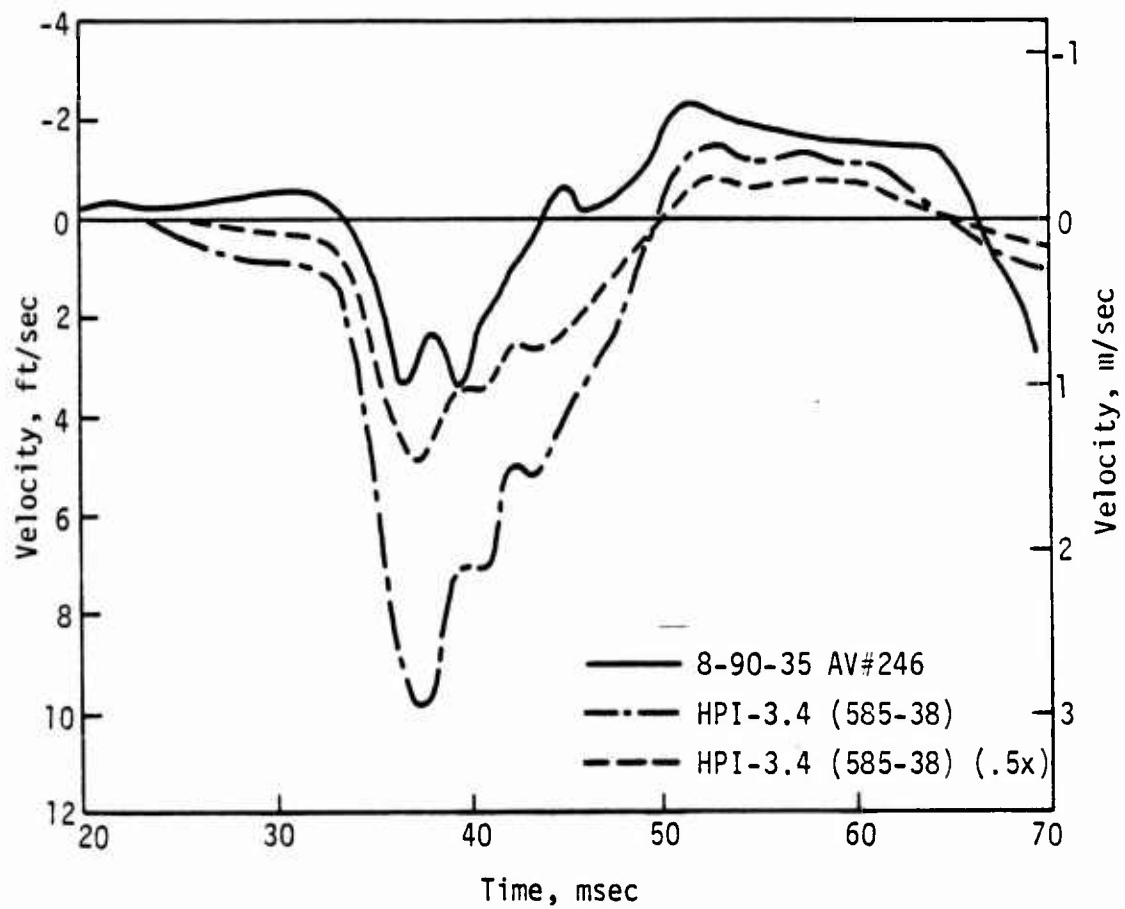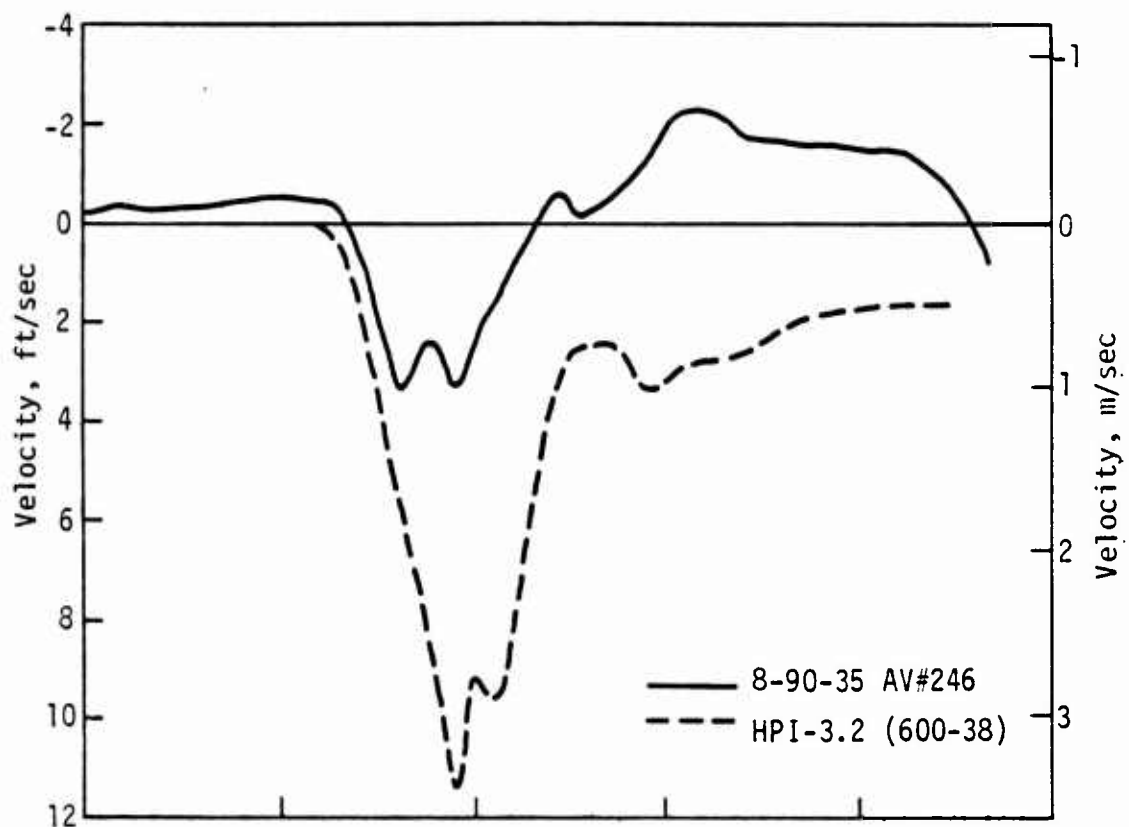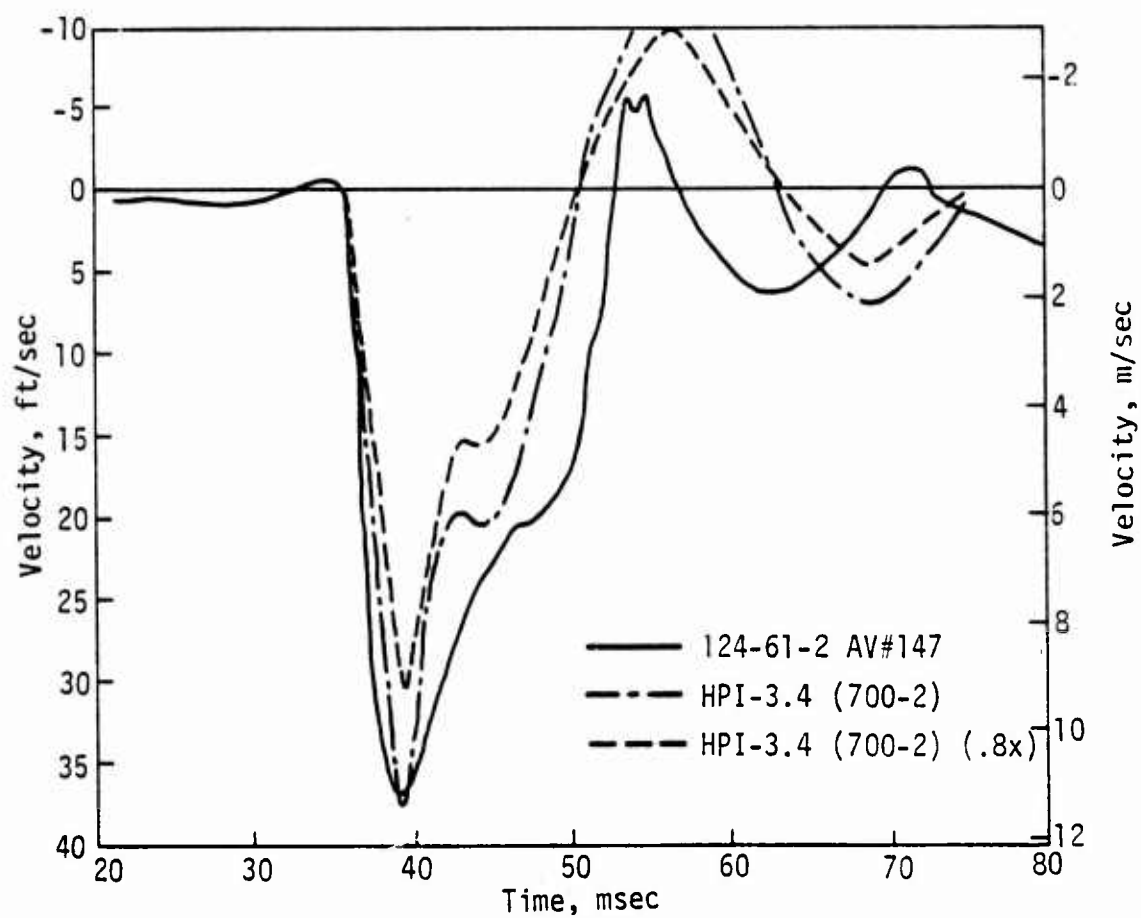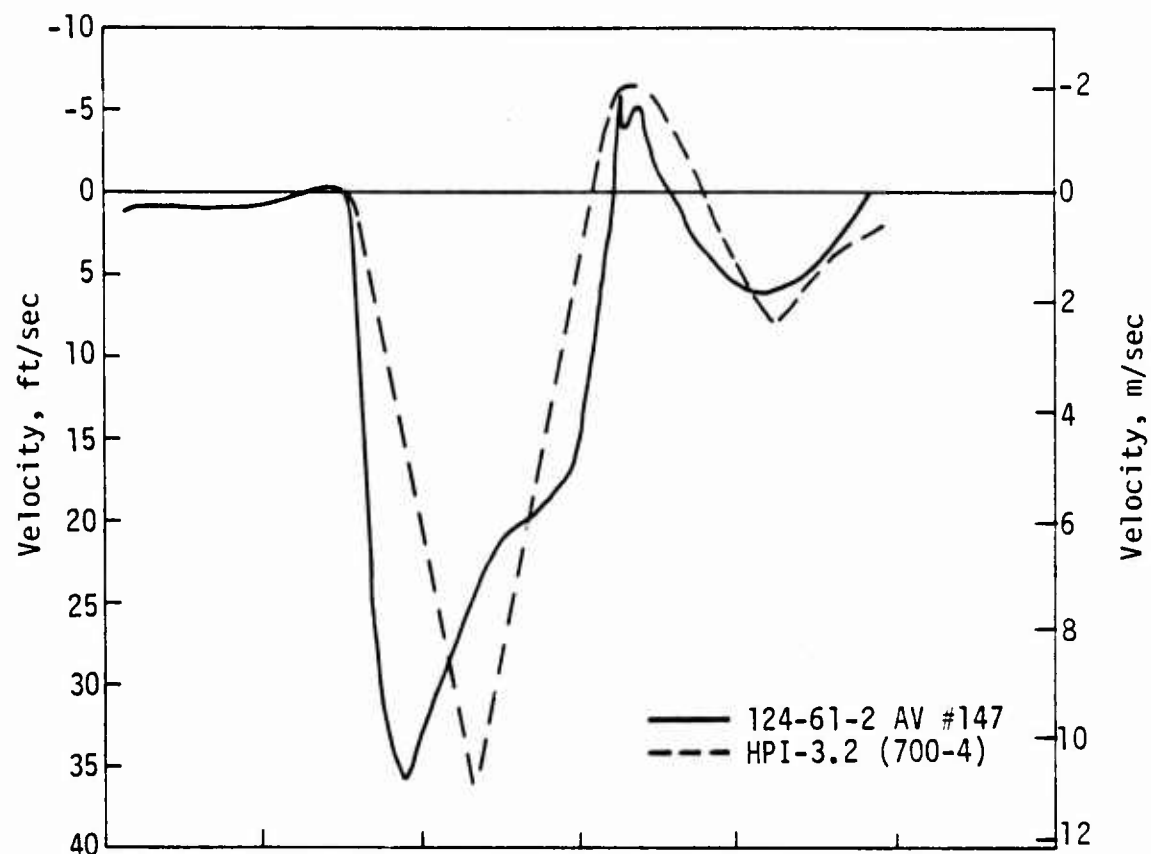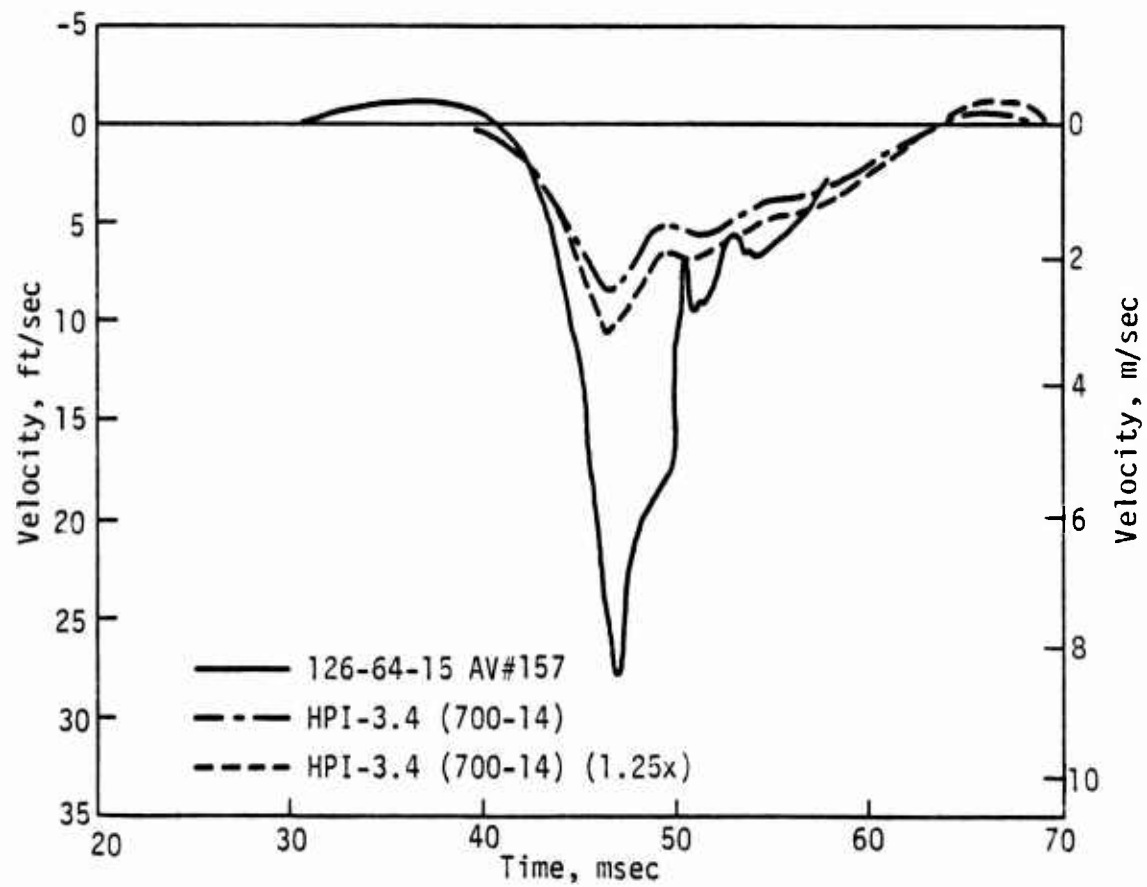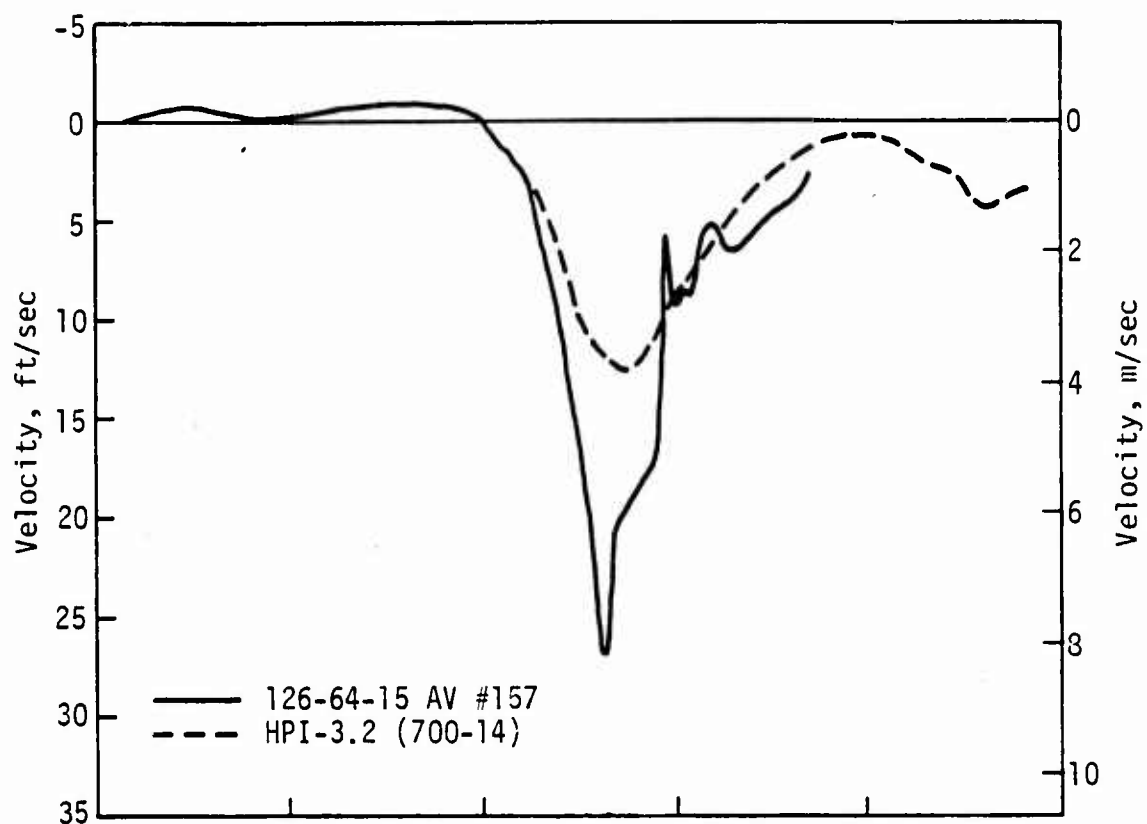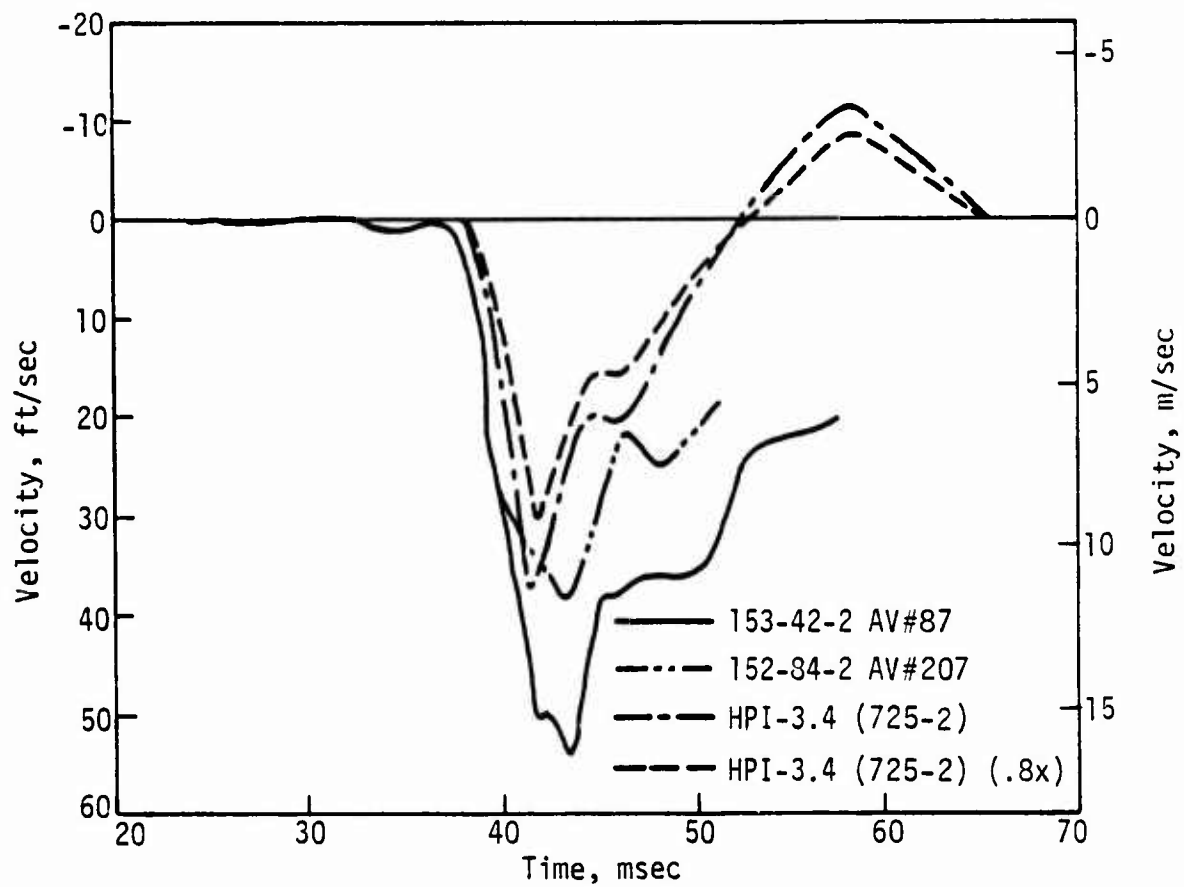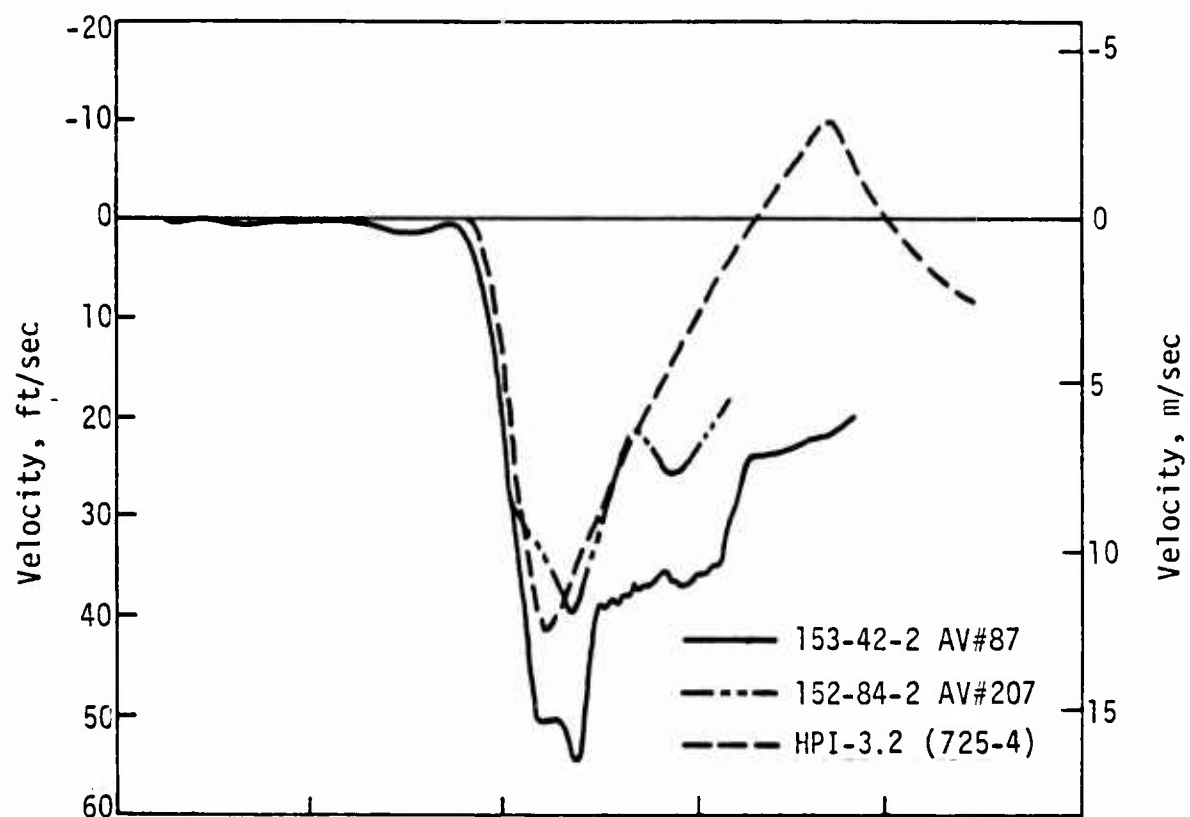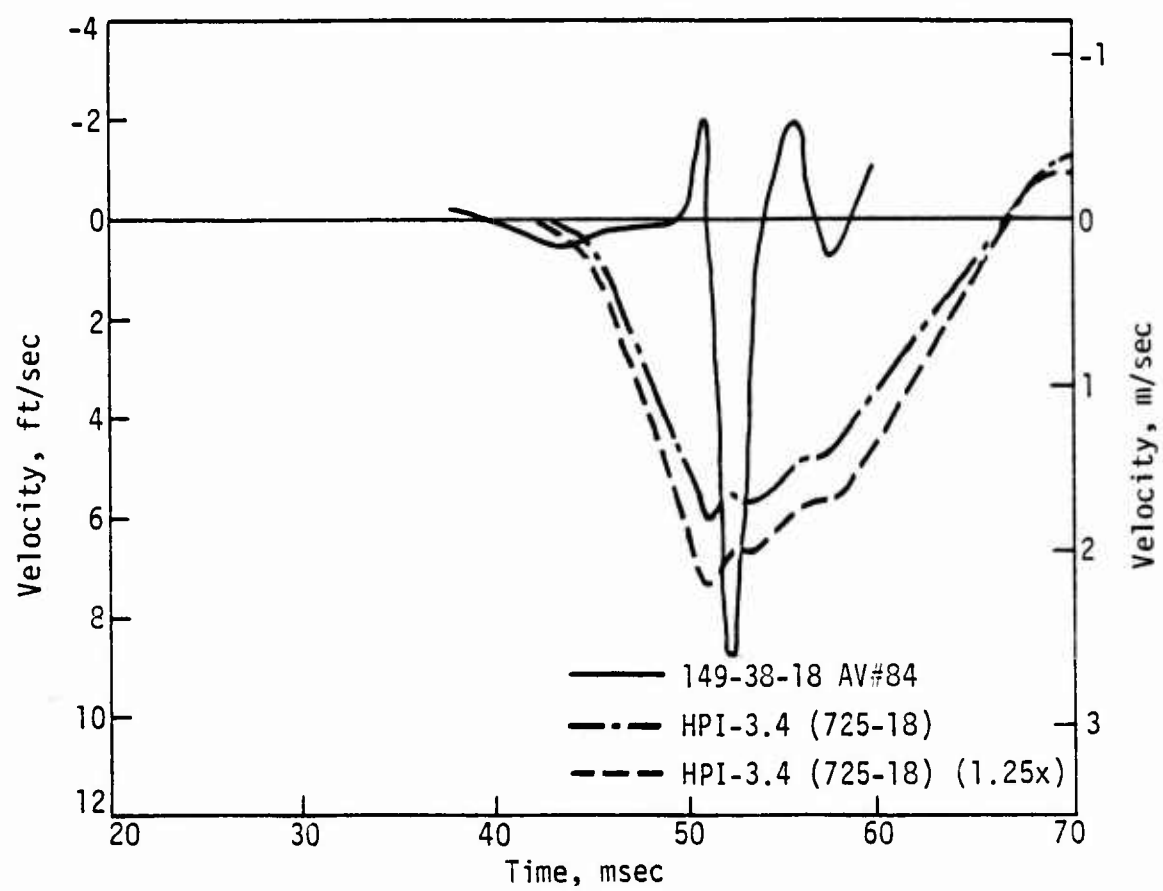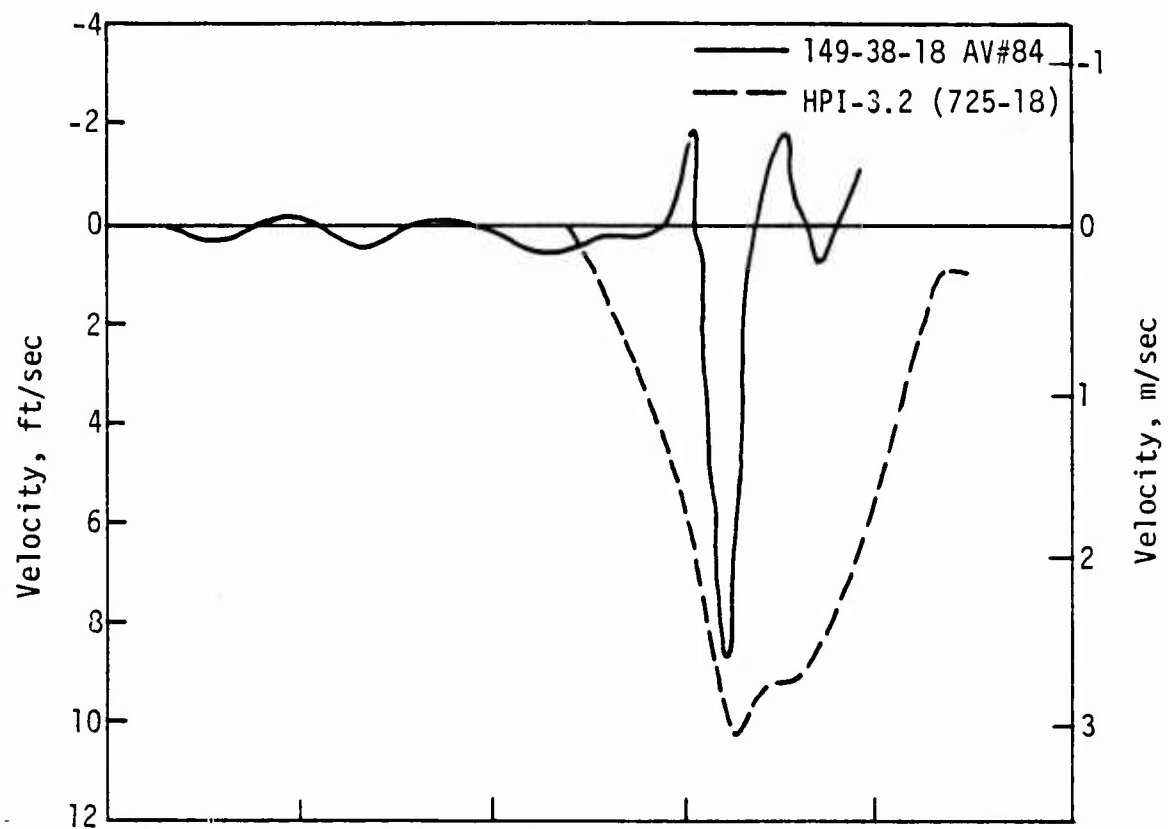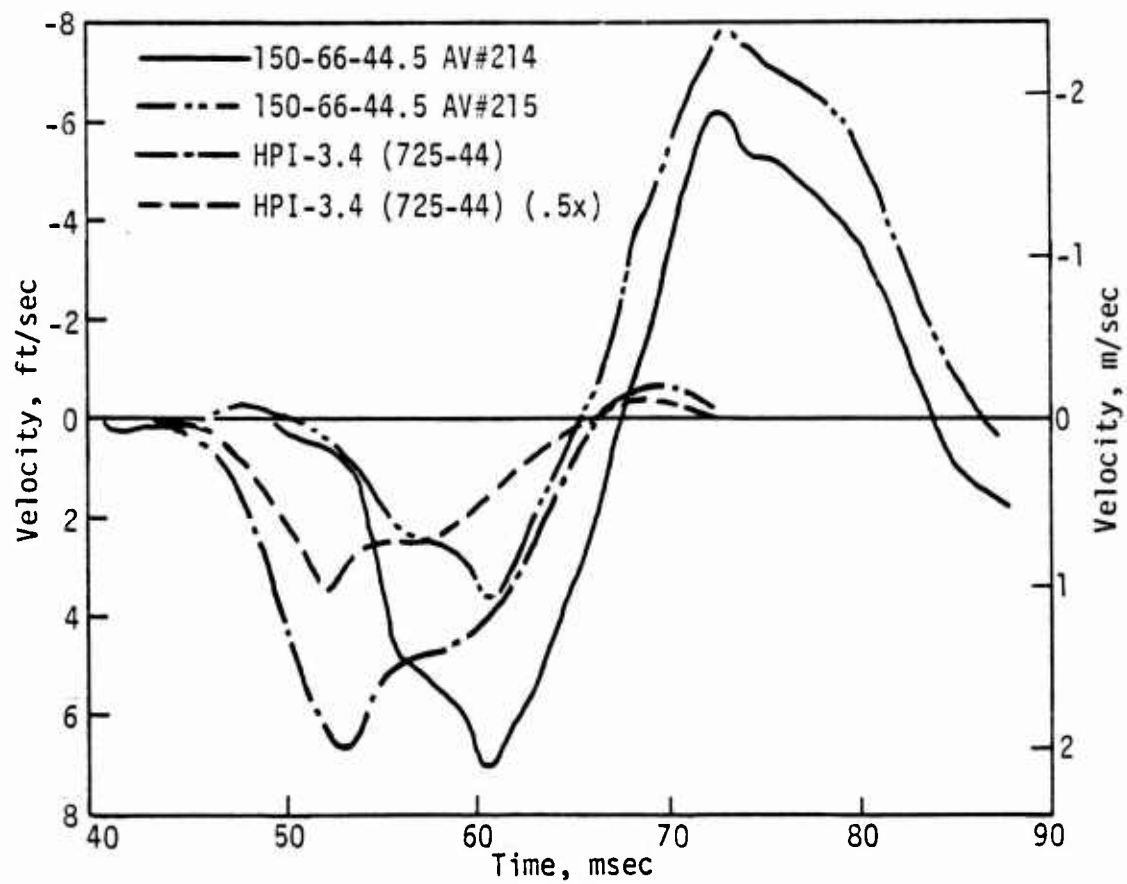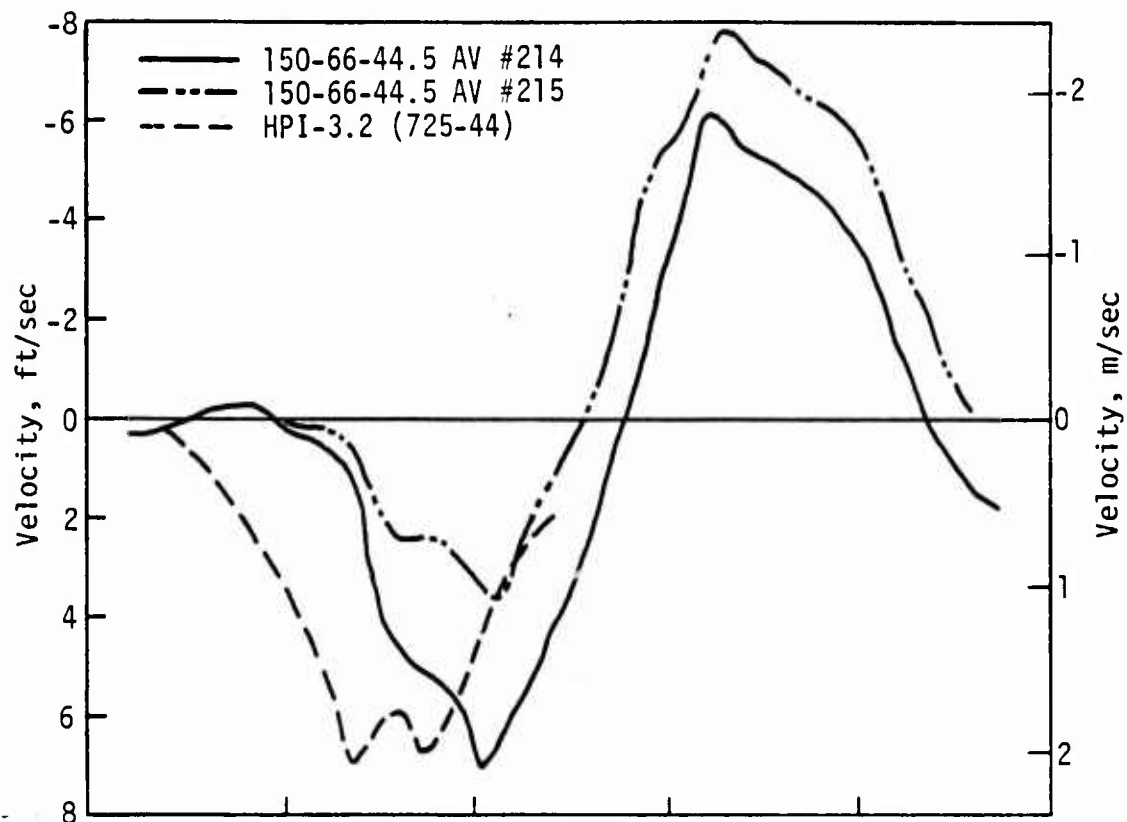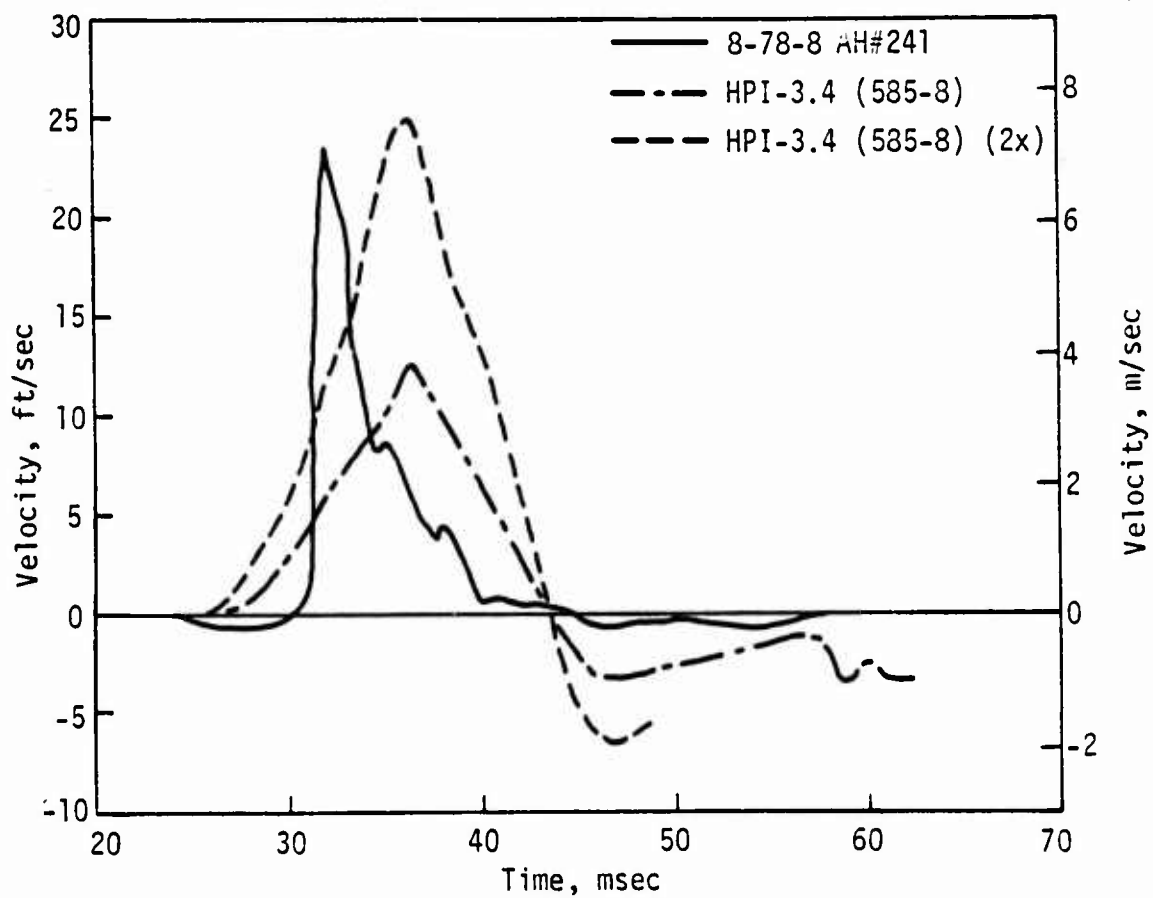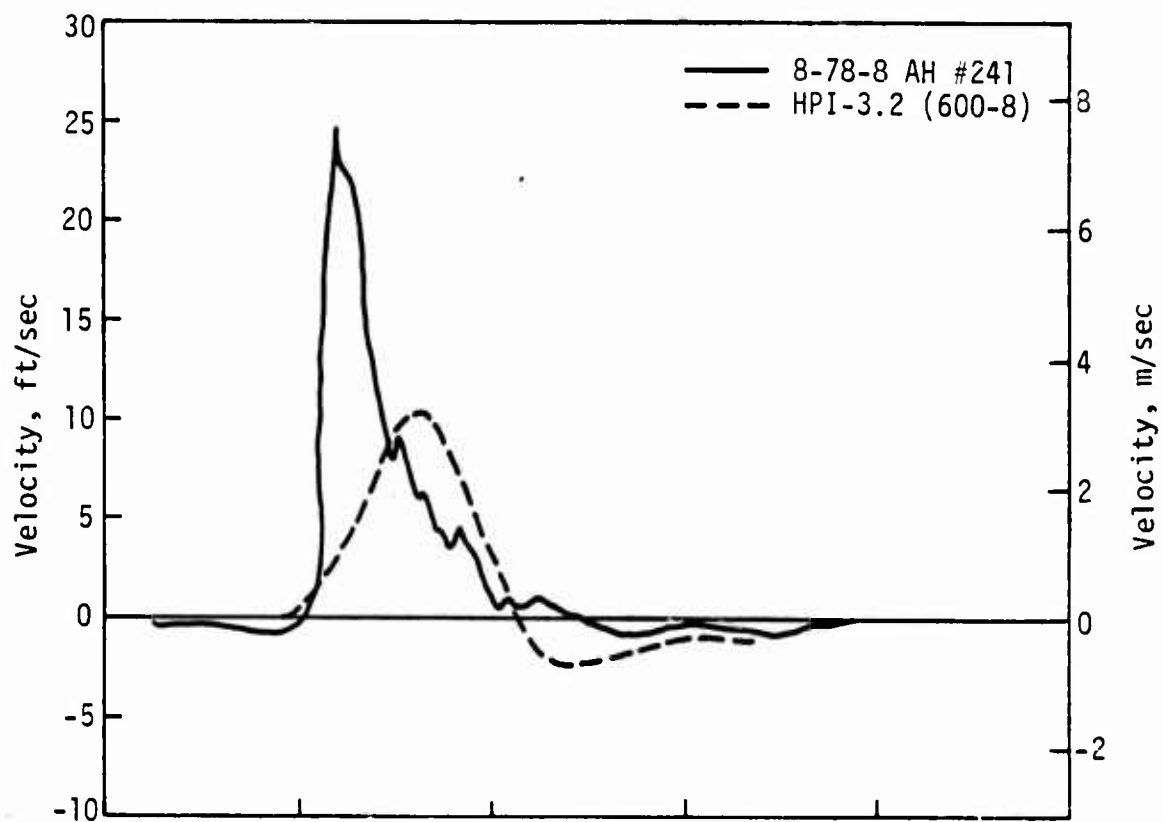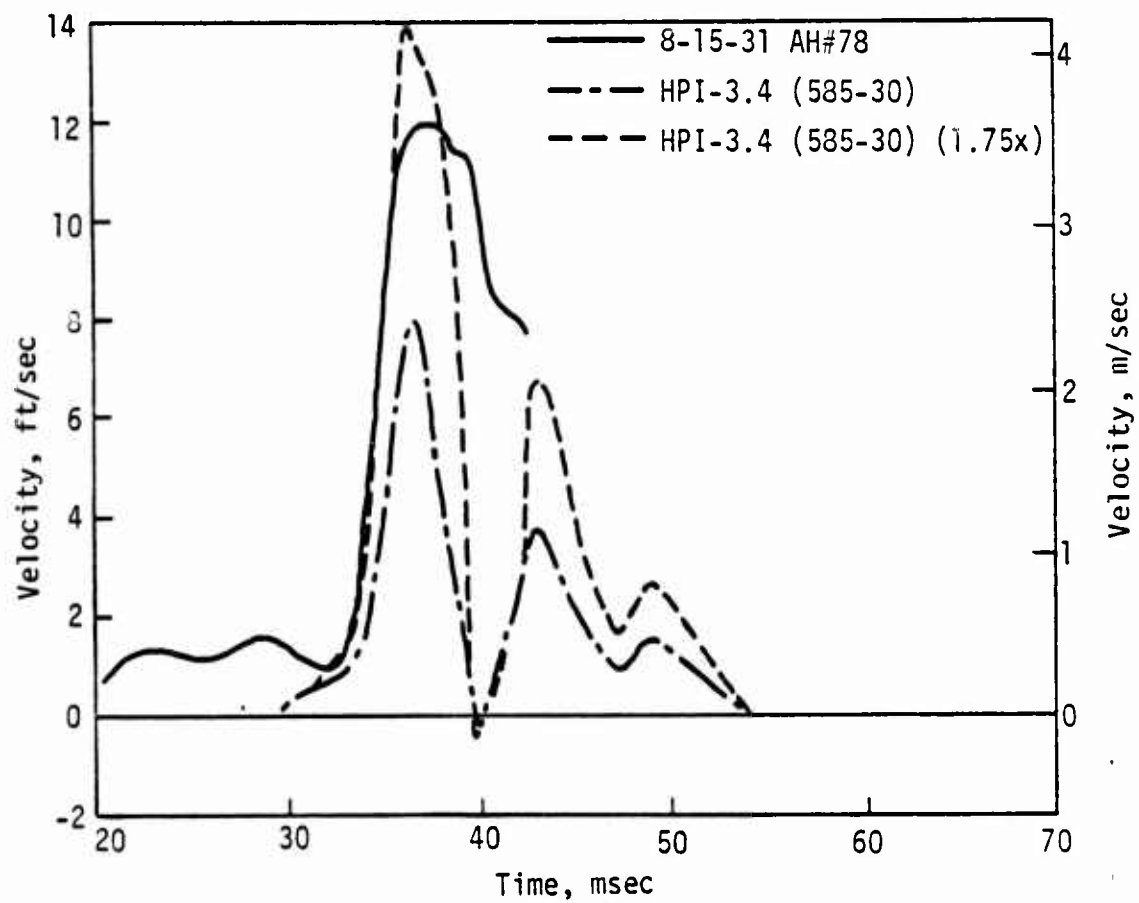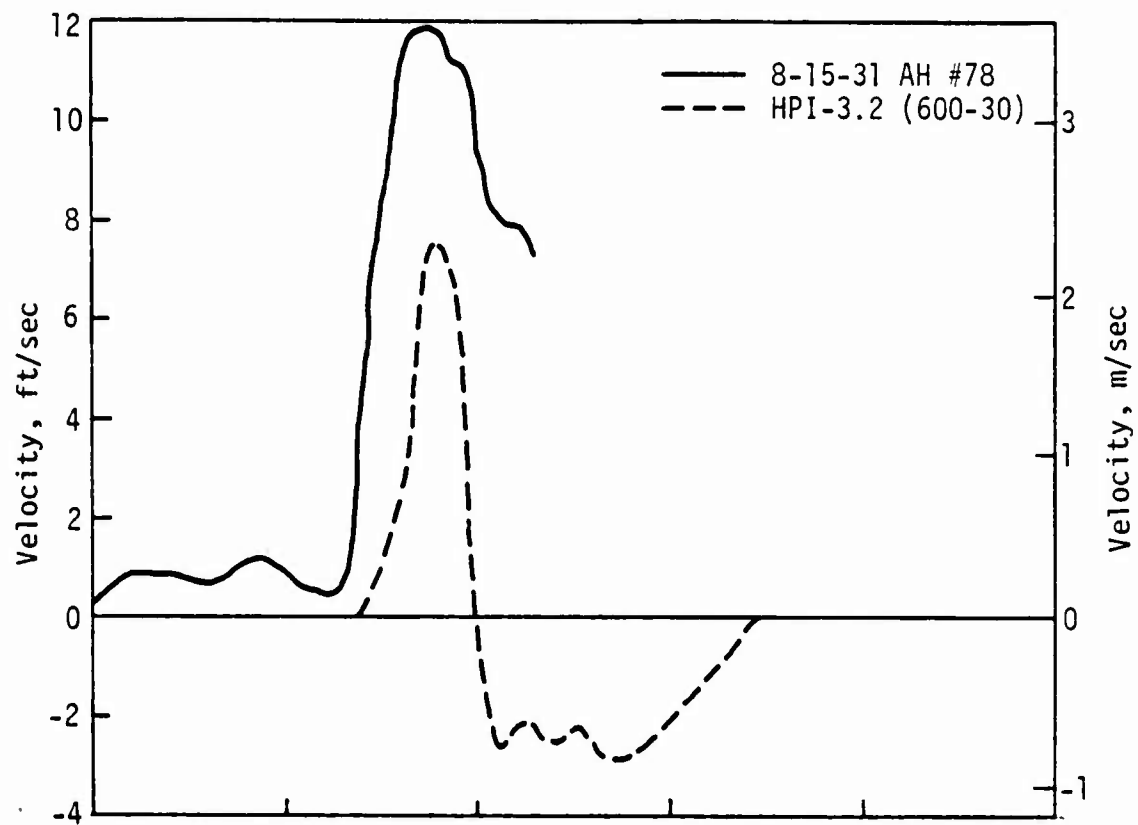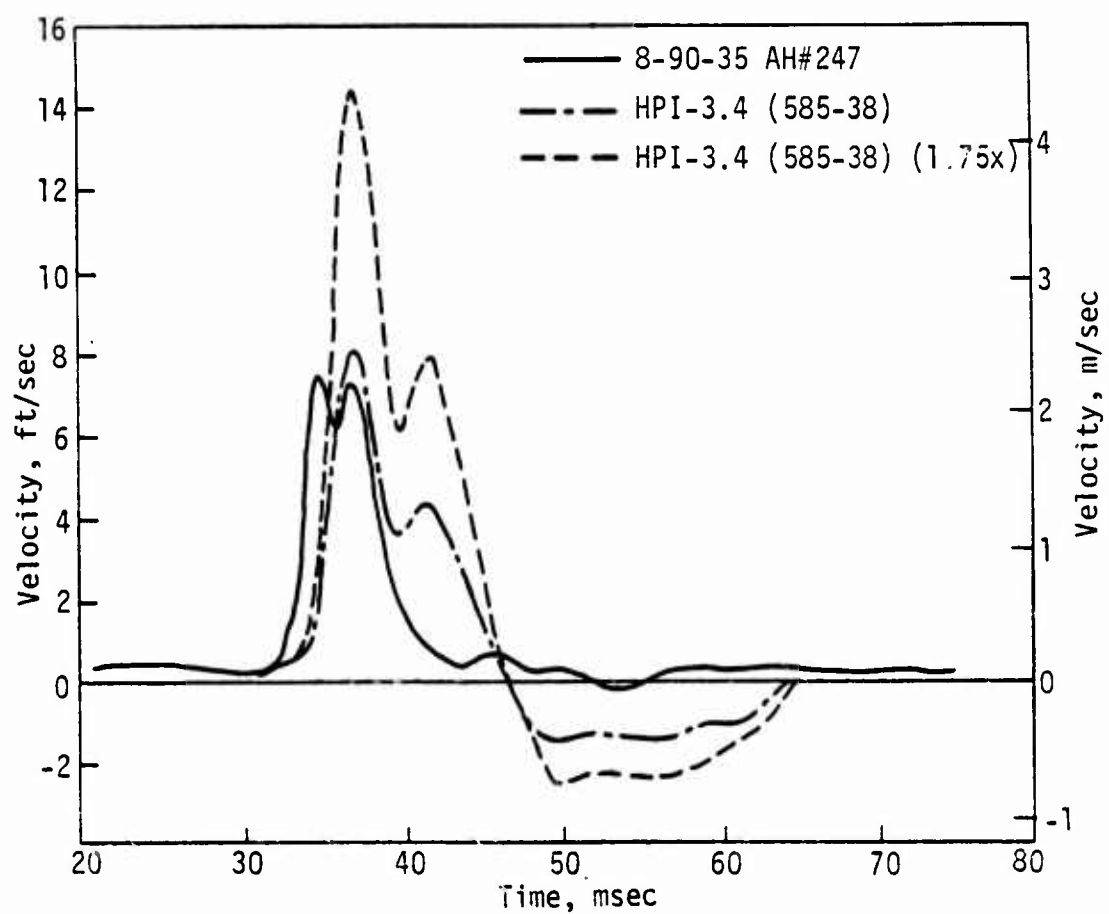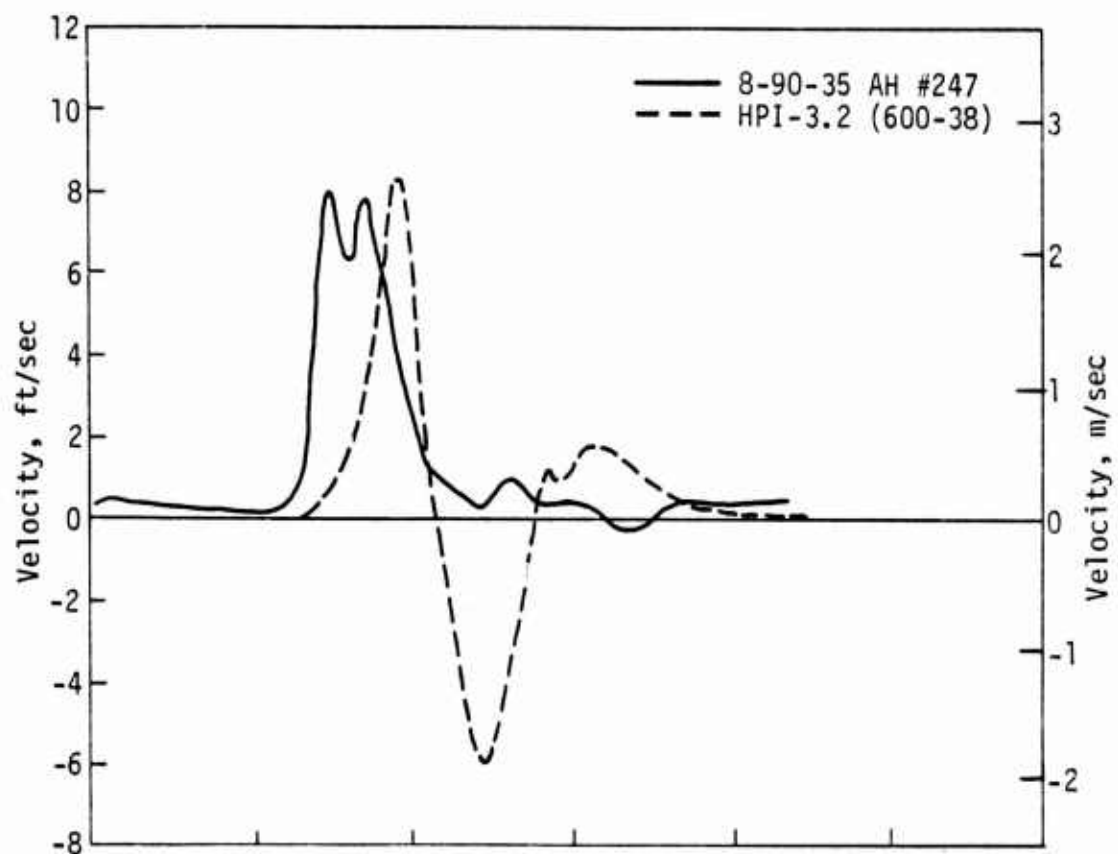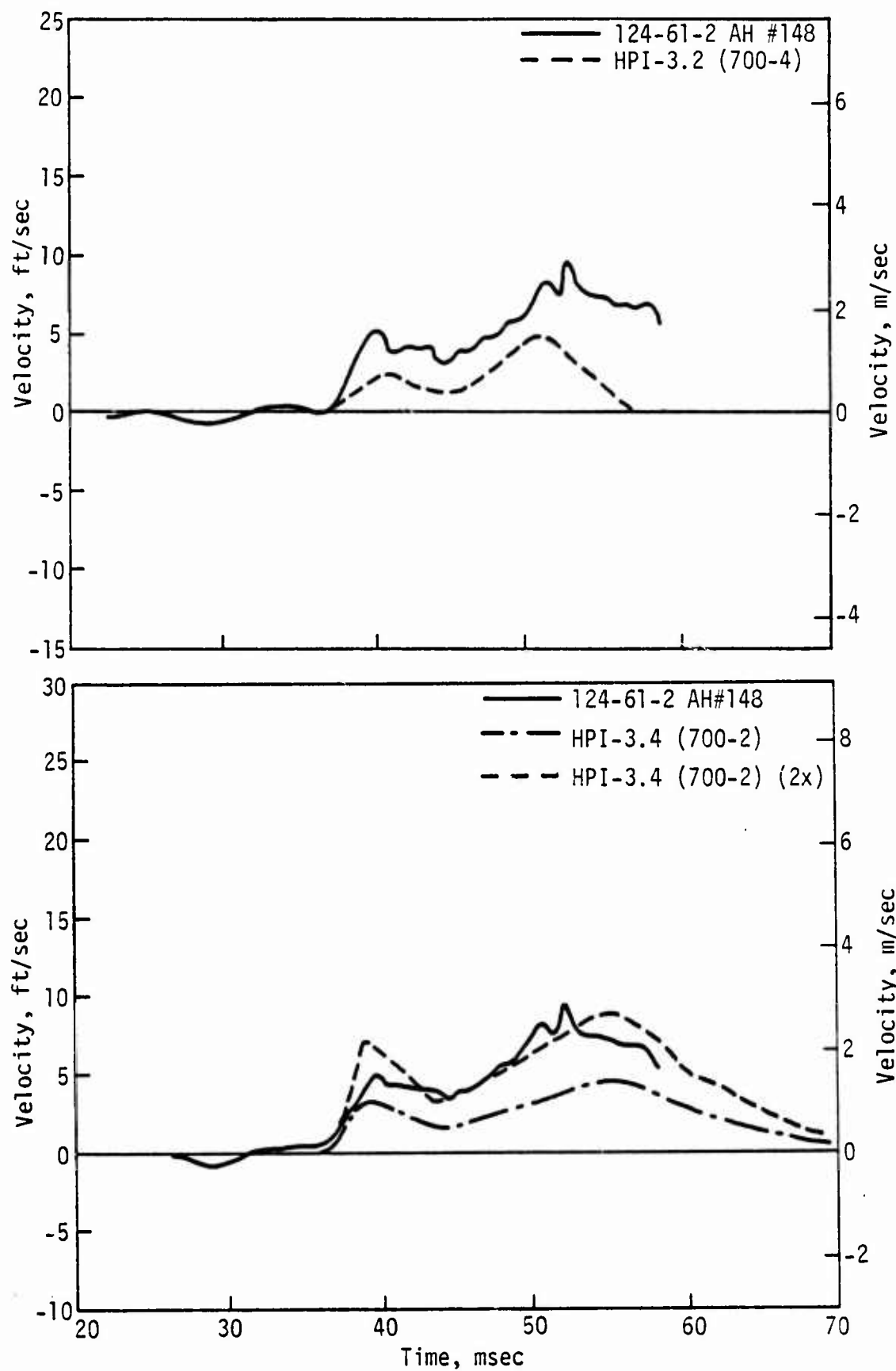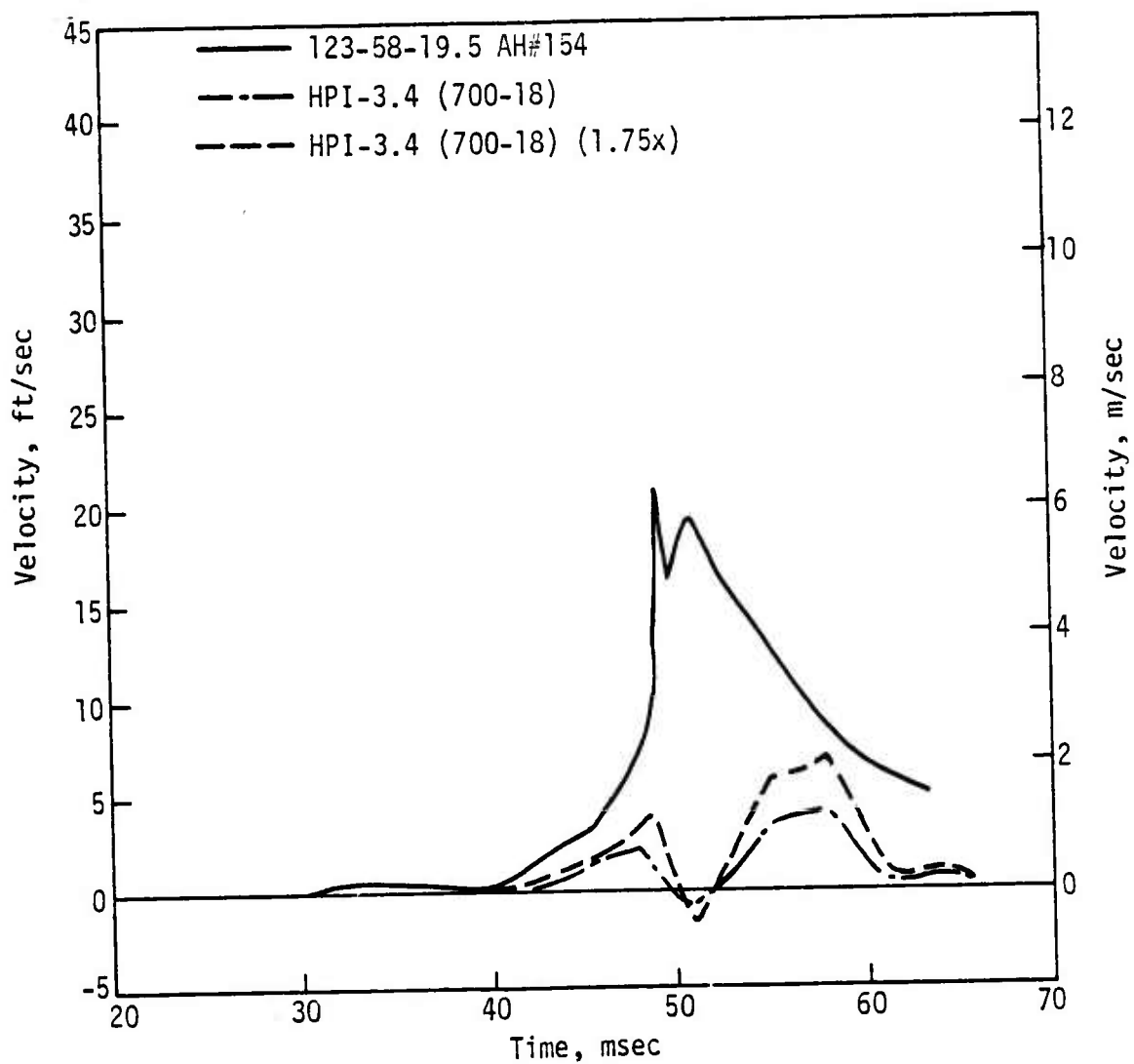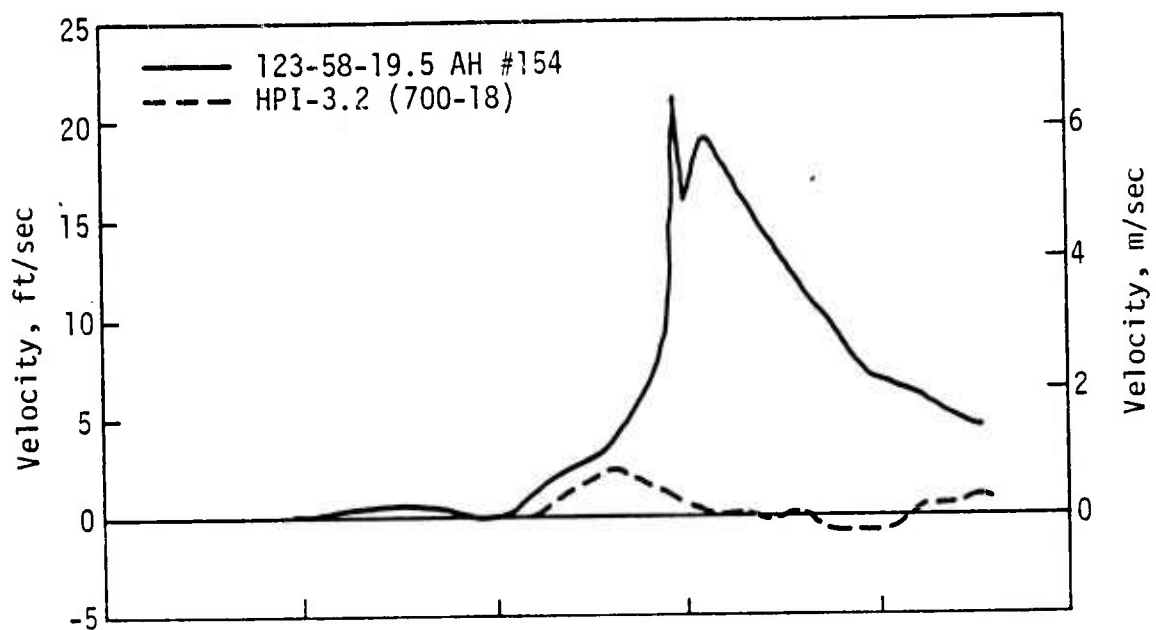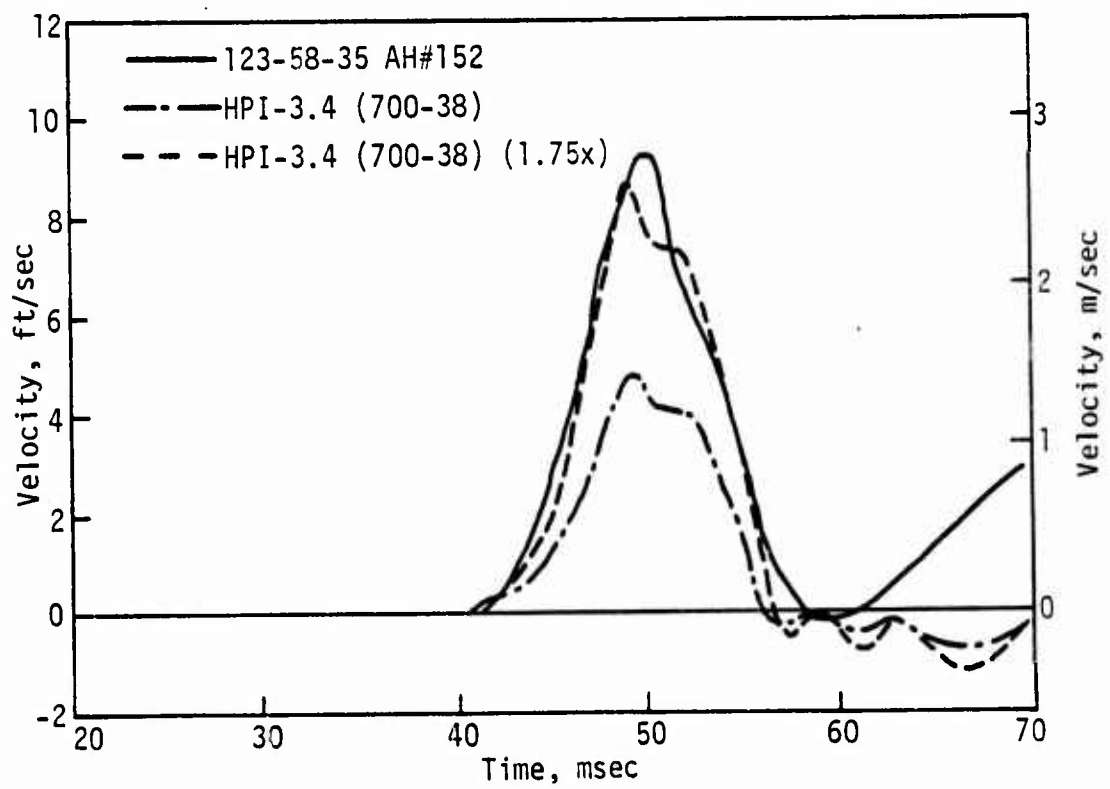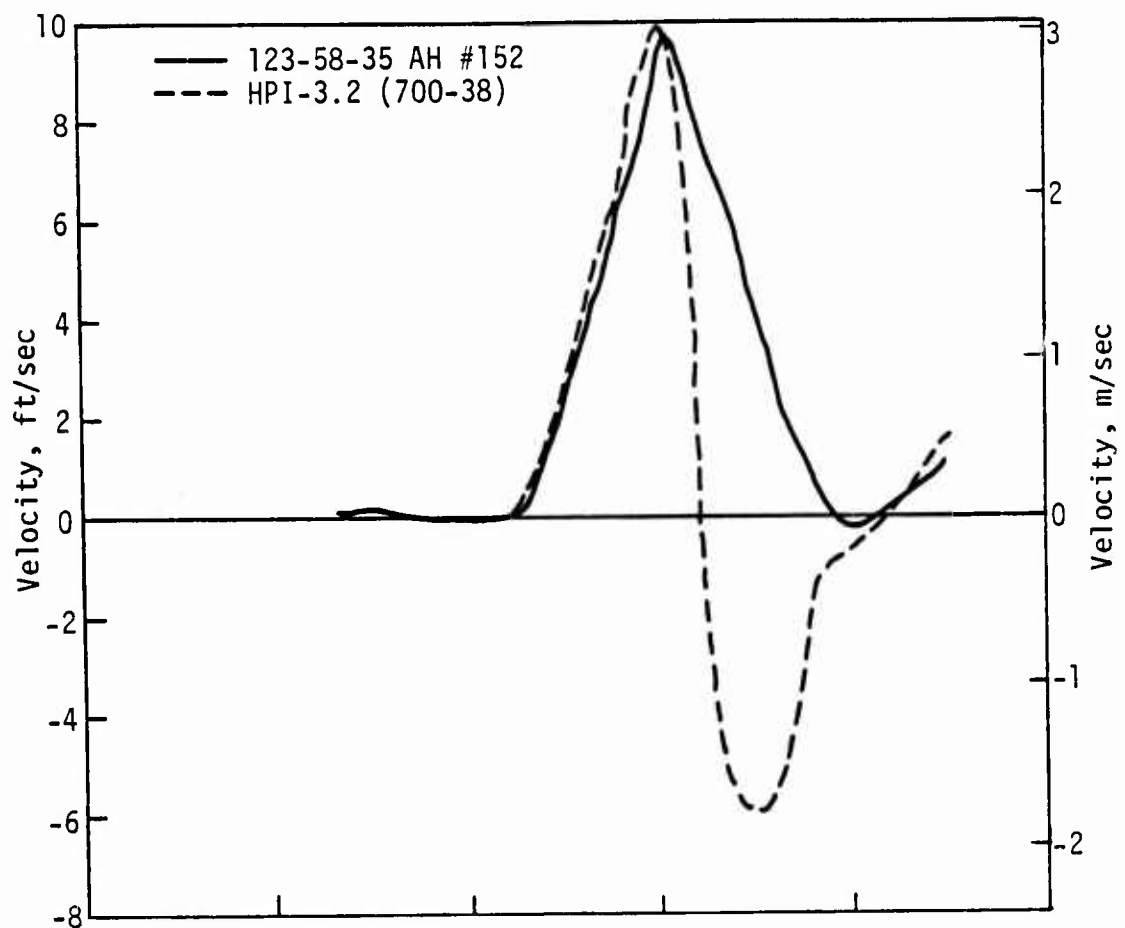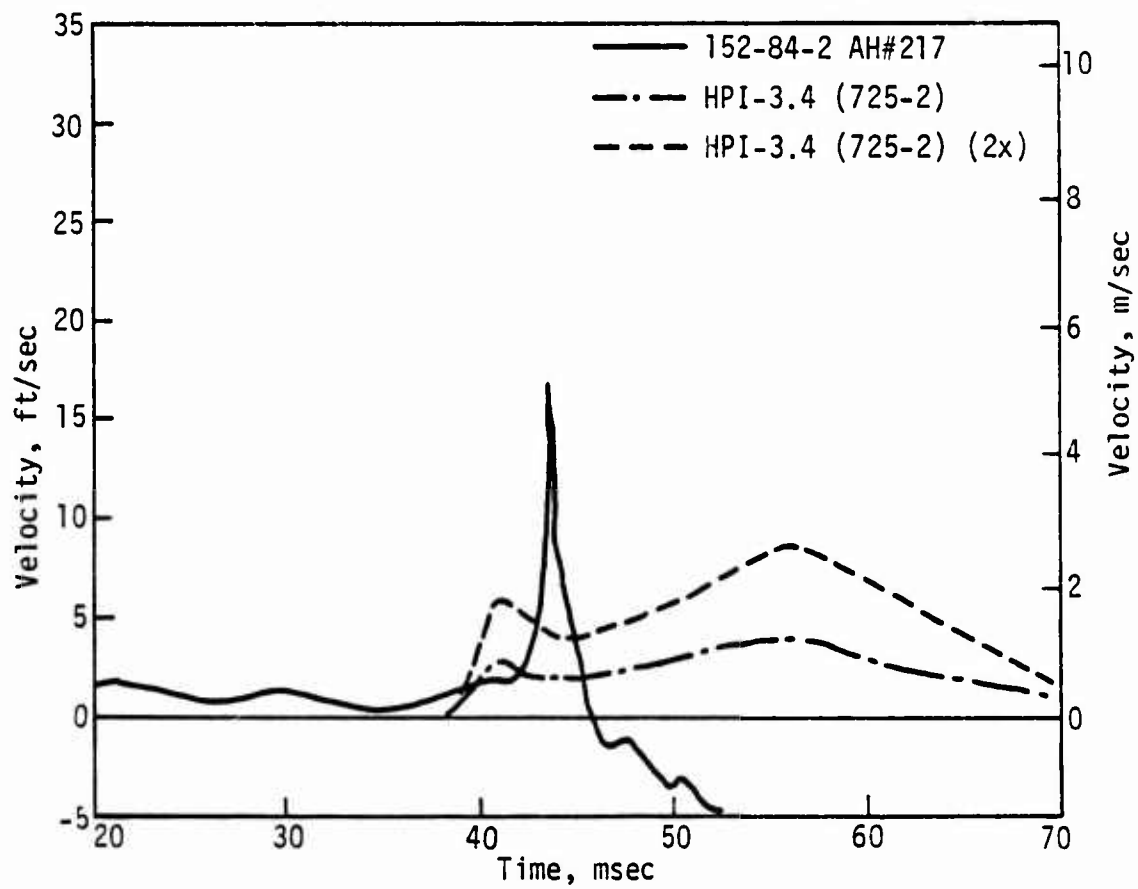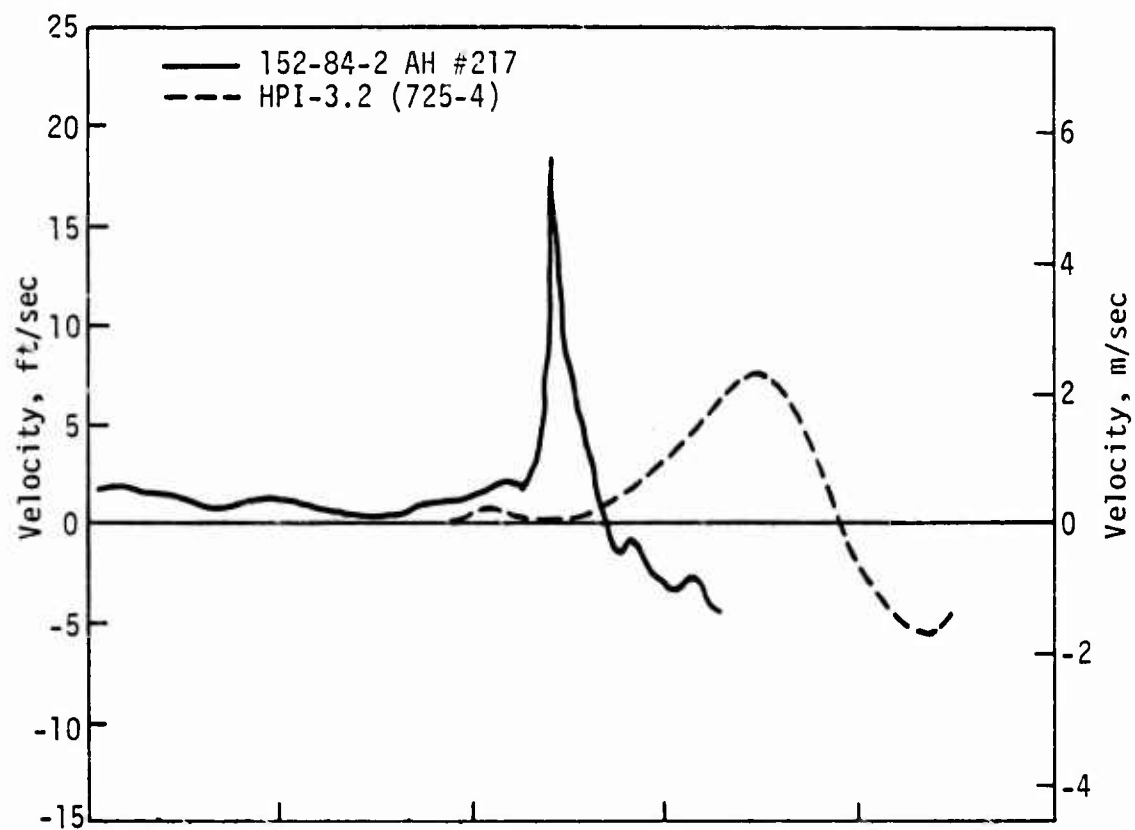
ABBREVIATIONS, ACRONYMS, AND SYMBOLS

C_p seismic velocity

D   depth

K_L loading bulk modulus

K_u unloading bulk modulus

P_o peak pressure

R   range from theoretical ground zero

t   time from detonation

t_a airblast time-of-arrival

t_d duration

α inclination angle of wavefront to horizontal

γ density

ν Poisson's ratio

DISTRIBUTION

<u>No. cys</u>

1   AUL (LDE), Maxwell AFB, AL 36112

2   DDC (TCA), Cameron Sta. Alexandria, VA 22314

5   SAMSO, PO Box 92960, WWPC, Los Angeles, CA 90009

    AFWL, Kirtland AFB, NM 87117

5   (DES/Lt James Shinn)

1   (HO/Dr. Minge)

2   (SUL)

5   Univ of New Mexico, Civ Engr Rsch Facility (Mr. D. Calhoun), Albuquerque, NM 87106

1   Official Record Copy (Lt Shinn/DES)

THIS REPORT HAS BEEN DELIMITED
AND CLEARED FOR PUBLIC RELEASE
UNDER DOD DIRECTIVE 5200.20 AND
NO RESTRICTIONS ARE IMPOSED UPON
ITS USE AND DISCLOSURE.

DISTRIBUTION STATEMENT A

APPROVED FOR PUBLIC RELEASE;
DISTRIBUTION UNLIMITED.